Environnement Canada
Centre météorologique canadien

Environment Canada
Canadian Meteorological Centre

Improvements to the Regional Deterministic Prediction System (RDPS) from version 2.0.0 to version 3.0.0

Development and Operations Divisions
Meteorological Research Division
at the Canadian Meteorological Center
of Environment Canada

P. Vaillancourt[1], L. Fillion[1], J. St-James[2], A. Patoine[2], M. Reszka[2], M. Tanguay[1], E. Lapalme[1], B. He[1], M. Lajoie[2], A. Plante[2], A. Zadra[1], R. Mctaggart-Cowan[1], C. Creese, L. Lam, A. Rahill, S. Roy and V. Thomas
1- Meteorological Research Division
2- Development and Operation divisions at the Canadian Meteorological Center (CMC) of Environment Canada (EC)

Revisions			
Version	Date	Authors	Remarks
1.0	11 May 2012	L. Fillion	First draft of data assimilation section
2.0	August 2012	P. Vaillancourt, A. Plante	First draft of modelling sections
3.0	August 2012	M. Reszka, P. Vaillancourt	First draft of evaluation of final series
4.0	September 10 2012	P. Vaillancourt N. Gagnon	Text editing
5.0	September 20 2012	J. St-James	Revision of changes to data assimilation system section and first draft of evaluation of parallel run
6.0	September 21 2012	T. Robinson	Objective scores for the parallel run period
7.0-3	October 6 2012	A.Giguère	Text and format editing, and addition of subjective evaluation of parallel run by A&P
7.4	October 11 2012	A.Giguère	Final text and format editing, publish in CMC product guide
7.5-7	November 1st to Dec. 31st 2012	N. Gagnon, A.Giguère	Add information on subjective evaluation (section 6) and dependent systems (section 7)

Table of Contents

1 Introduction

This document describes the latest modifications to the Canadian regional deterministic prediction system, hereafter referred to as RDPS version 3.0.0 or simply RDPS-300. We present modifications made to the data assimilation and model components of the RDPS in support to the operational implementation on October 03 2012, replacing the 15km-3D-Var RDPS version 2.0.0, hereafter referred to as RDPS-200. This represents the cumulative effort of many people from the analysis and modelling sections in research and development divisions, and operational sections of EC co-located at the Canadian Meteorological Center (CMC) of Environment Canada in Dorval, Québec.

The structure of the Regional Data Assimilation and Forecasting system remains the same as the REG-LAM-3D, and we summarize this structure as follows, before giving details of modifications to each of constituent parts. As shown in **Figure 1**, a global 4D-Var analysis (e.g. G206; G606 being a separate surface analysis) is routinely performed every 6 h, from which the initial conditions are produced (R206) for the REG-LAM at 10 km. In parallel to this, initial conditions for the global driving model (REG-DRIVER) named here D206 are prepared from the G206 analysis and serve in a 9-h global forecast (from 0600 to 1500 UTC) to provide the background fields for the parallel global driving analysis and for the lateral boundary conditions of the REG-LAM 10 km. A global-33km 48h D112 forecast starting at 1200 UTC is then performed and serves as the driver to the deterministic REG-LAM 10 km 48h R112 forecast (which starts from 1200 UTC initial conditions).

2 Changes to the assimilation system

Since October 20th 2010, CMC has been operating a Regional 3D-Var (3-Dimensional Variational) analysis system (REG-3D) where the deterministic REG-LAM is run at 15 km and analysis increments are produced at 100 km (T200) horizontal resolution. After 7 years of research, a 4D-Var analysis scheme is implemented as part of the new RDPS-300. The 3D-Var data assimilation system is extended to a 4D-Var scheme for the REG-LAM analysis (REG-4D) only. The REG-DRIVER analysis will continue to be produced with a 3D-Var scheme. The REG-4D shares with REG-3D the general formulation of the cost function with its background term J_b (weighting the analysis increment with prescribed error covariances) and its observation term J_o. The forecast error covariance statistics, as part of the background term J_b, have been re-computed at T180 and now include the ground temperature as a control variable.

In REG-4D, J_o measures the weighted difference between the time-evolved analysis increments (obtained from the GEM-LAM tangent-linear (LAM-TL) forecast at 100-km horizontal resolution) and the innovations at the appropriate time of the observations. The innovations are defined as the difference between observations and the short-term forecasts issued from the REG-LAM at initial time. The REG-4D is computationally more demanding as compared to REG-3D since it requires the integration of the LAM-TL for J_o and the LAM-AD for ∇J_o. One subtlety that is worth noting is the fact the LAM-TL/AD grid is an exact sub-domain of the Gaussian analysis grid (100-km horizontal

resolution). So, the communication of information (i.e., analysis increments and adjoint sensitivities) is direct; that is, no spatial interpolations in the horizontal (and vertical) are involved. Also, the REG-DRIVER provides lateral boundary conditions at each 45 minutes interval to the non-linear trajectory on which LAM-TL/AD is based within REG-4D.

After the minimization, the REG-4D analysis is obtained 3-hour *before* the synoptic time *T*. The REG-3D analysis is already available at this time. So a 3-hour REG-LAM forecast is needed to carry this REG-4D analysis up to time *T*, using the same driving conditions as the 9-hour REG-DRIVER background trajectory. This represents the REG-4D analysis at time *T*. The REG-4D analysis is no longer a simple snapshot of the atmospheric conditions at the time of the analysis. Instead, the 4D-Var approach provides a time evolution of the atmospheric conditions during the assimilation time window.

In the context of REG-4D, and its use of LAM-TL/AD, one important aspect is put on the control of the lateral boundary conditions during the minimization process. A new approach is designed where the REG-4D analysis grid extends by 30% in each direction the limited-area coverage of the REG-LAM to allow an appropriate propagation in time of analysis increments during the minimization process. **Figure 2** shows the 10 km regional model grid (dark blue) and the tangent-linear/adjoint model grid at 100 km horizontal resolution (red). As seen, in this figure, the latter extends farther than the REG-LAM 10 km resolution grid. Further technical details can be found in Tanguay et al. (2012).

Another important aspect of this implementation is that the temporal observation selection is extended so that the 4D-Var will make use of much more observations than the 3D-Var, even though we are not adding any new type of observations. The temporal resolution, within the assimilation 6-hour time window, is reduced to 15 minutes dividing the window into 24 bins. The temporal selection will allow the 4D-Var to assimilate as many observations as there are time bins. Therefore, much more asynoptic and satellite observations will be included. **Table 1** shows the average increase in assimilated observations (per observation type) for winter and summer 2011. Overall at least two times more observations is assimilated in the RDPS-300. The largest increase is for aircraft and AMSUA satellite observations (4 times more). Because of the increase in the amount of observations, 45 iterations are needed to attain convergence during the minimization process. Tests have revealed that the convergence was not sufficiently attained with only 25 iterations. The 4D-Var analyses show a much improved dynamical consistency and are accompanied by a significant improvement in the REG-LAM 10 km performance. Also, it is very important to note that the 4D-Var analyses do not fit the conventional radiosonde observations as closely as the 3D-Var analyses do.

3 Changes to the global driving model (REG-DRIVER)

The REG-DRIVER was modified to resemble as much as possible the Global Deterministic Prediction System (GDPS) that was the operational system at the time of the implementation, i.e. GDPS-220. The main modifications with respect to the previous REG-DRIVER are the increased resolution (from 720x360 to 800x600) and the activation of a so-called “masked ramp” for deep convection triggering in the tropics. This last modification was introduced in the GDPS to reduce the number of false alarms for tropical cyclones. The differences between the GDPS-220 and the new REG-DRIVER are the grid

orientation as well as the activation of additional horizontal and vertical diffusion near the numerical poles in the REG-DRIVER.

For efficiency-related reasons, the grid orientation of the REG-DRIVER must be the same as the orientation of the REG-LAM it drives. As a result the numerical poles are not collocated with the geographical poles but are situated close to the equator, one being in the warm pool region of the western Pacific, the other being in the eastern Atlantic. During the development of this REG-DRIVER, it was found that the intense convection in the warm pool region (numerical pole) coupled with the very small grid distance due to the convergence of the meridians was responsible for intense numerical noise that in some situations lead to a model crash. This noise was present only in the first few rows away from the numerical poles. Two polar filters were tested and implemented to solve this problem. One is a horizontal filter applied to the temperature. The other is a vertical filter applied to the 3 wind components. The two filters are applied at just a few rows near the computational poles and throughout the depth of the model atmosphere. Objective scores for 80 winter and summer cases have shown that these filters have no impact on the REG-DRIVER forecast over North-America but allow the successful completion of all runs which had previously crashed.

4 Changes to the limited area model (REG-LAM)

4.1 Dynamical configuration

While the size of the domain covered by the REG-LAM model has not changed, the horizontal resolution has been increased from 15 km to 10 km. The number of grid points has therefore increased from 649x672 to 996x1028. The time step has been proportionally reduced from 7.5 to 5 minutes, for a total of 12 time steps per hour. A digital filter is applied at the beginning of the 2-day forecast model integration (span and period of 3 hours) to filter out spurious gravity waves that could still be present in the analysis field. In addition, the digital filter is activated during the 9-hour forecast model integration (span and period of 1.5 hours) which serves as a a background trajectory necessary for the analysis unlike the previous version of the RDPS. No changes to the vertical discretization or resolution have been made. The number of vertical levels is 80 with a model top at 0.1hPa.

4.2 Physics configuration

The main motivations for changes in the physics configuration of the RDPS-300 were the following. Firstly, early in the project, the very first series of forecasts obtained at the increased resolution of 10 km showed significant increases in precipitation over land and water for both summer and winter seasons at all lead times. **Figure 3** and **Figure 4** compare the RDPS-200 to the preliminary 10 km RDPS in terms of 1hr precipitation rates averaged over land and over water for the summer 2008 and winter 2009 seasons at lead times up to 48 hours. This precipitation increase was a concern given that the RDPS-200 already tended to over-estimate precipitation quantities. Furthermore, precipitation scores (**Figure 5**) show an increase in the occurrence of higher rates of precipitation, i.e. > 15 mm/day.

It is very difficult to determine whether this is more realistic or not, given that we are comparing point observations to model grid values representing areas of the order of 100 km^2. However, discussions with operational meteorologists from the Analysis and Prognosis (A&P) section at CMC convinced us that this could be a concern when forecasting high impact weather.

Secondly, comparison of surface fluxes with detailed observations from a station at Lake Superior (Deacu et al., 2012) as well as comparisons with daily global analysis of surface fluxes from the Woods Hole Oceanographic Institution's "OAflux" project (Yu et al., 2008) showed that the RDPS-200 significantly over-estimates the latent heat fluxes from water bodies (**Figure 6**). Latent heat fluxes (water vapor fluxes) are important for all elements of the hydrological cycle (humidity, clouds, precipitation, etc.). As demonstrated in Deacu et al. 2012, they are critical for obtaining a realistic budget of Evaporation-Precipitation over water bodies. Furthermore, these fluxes provide fuel for the development of tropical storms as well as extra-tropical systems. Over-intensification of extra-tropical systems over the Gulf Stream region, often noted by operational meteorologists at A&P and regional EC forecast centres, could be related to the over-estimation of the latent heat fluxes in this region.

Thirdly, a long-standing problem of the RDPS has been significant warm errors in surface air temperature associated with warm air advection in winter and spring (so-called warm episodes). **Figure 9** shows a typical such situation with a warm front approaching Southern Quebec. This figure shows 2 m temperature errors as large as 9 K in the Ottawa region at a lead time of only 6 hours. **Figure 10** compares the forecast temperature profile in this region to the profile from the verifying analysis. The relatively flat or well mixed forecast profile was an indication that the origin of this problem was related to vertical mixing. Obviously, such errors in the temperature profiles lead to errors in forecasting of precipitation type, namely a well-known under-estimation of freezing rain.

In the sub-sections below, we describe the modifications made to the physics of the model, as well as their impacts, which helped to solve or reduce the severity of the three issues discussed above.

Table 2 summarizes the changes in the physics with respect to RDPS-200 while **Table 3** summarizes the changes in the physics code.

4.2.1 **Surface fluxes**

Several modifications were made that have significant impacts on surface fluxes, in particular on latent heat fluxes from water bodies. I) Deacu et al. (2012) proposed a modified formulation for the scalar roughness length (Z0T) of water inspired by the formulation in use at ECMWF. This new formulation generally results in smaller values of Z0T, which leads to reduced fluxes. II) As in the GDPS, a constant value of Z0T= 0.04 mm is now used in the tropics for water surfaces. III) The saturation specific humidity at the temperature of the ocean surface is used as a boundary condition for specific humidity when water vapour fluxes are calculated. The effect of salinity on the saturation specific humidity has been introduced as in the ECMWF system (http://www.ecmwf.int/research/ifsdocs/) according to the original formulation of Sverdrup et al. (1942). This modification also results in reduced latent heat fluxes over the oceans. IV) The Prandtl number (ratio of the vertical diffusion coefficient of momentum to the vertical diffusion coefficient for scalars, i.e. temperature and humidity) was increased from 0.85 to 1.0. Therefore, this parameter is now the same in the RDPS and GDPS.

Whereas the other modifications listed above have only indirect effects on tropospheric temperature and humidity, the change in Prandtl number directly affects both surface fluxes and tropospheric temperature and humidity.

The bottom panels of **Figure 6** show the average latent heat fluxes over winter 2011 for the new RDPS-300 (right) as well as the difference compared to RDPS-200. As can be seen by comparing to the top panels, the fluxes are significantly reduced and compare much better with the analysis. Note in particular the significant reductions (greater than 100 W/m^2) over the Gulf Stream.

Figure 7 compares the RDPS-200 to the 10 km RDPS including the modifications described in this section, in terms of 1hr precipitation rates averaged over land and over water for the summer 2008 and winter 2009 seasons at lead times up to 48 hrs. It can be seen that the precipitation is systematically reduced over water for both seasons. Over land, it is reduced for the winter season, but it is still increased for summer during daytime. Note also in **Figure 8**, compared to **Figure 5**, that no significant impacts were obtained on the bias in occurrence of precipitation rate.

4.2.2 **Deep convection**

The role of the deep convection scheme is to stabilize the atmosphere in situations of conditional instability. The triggering of this scheme is controlled by several parameters, one of which is a minimum gridscale vertical velocity (Wt) at the lifting condensation level (cloud base). Since the grid-scale vertical velocities are strongly resolution dependent, this parameter must be tuned as a function of model resolution, and is usually increased for higher resolutions. The deep convection scheme has a strong influence on the temperature and humidity profiles, on the total precipitation and its spatial distribution as well as on the probability distribution of the precipitation rate. When tuning the deep convection triggering, it is necessary to verify the impact on all these aspects and obtain the best possible "balance". The following figures show the sensitivity of these different elements to Wt and justify the final choice for the value of this parameter. Note that, as a rule of thumb, a lower Wt implies that the deep convection scheme is more easily triggered.

A linear tuning of Wt as a function of the change in resolution from 15 to 10 km suggests changing Wt from 12 cm/s (RDPS-200) to a value of 18cm/s. We explored the sensitivity of the 10 km RDPS to Wt by testing values of Wt around this control value. **Figure 14** and **Figure 15** show the sensitivity of the bias of occurrence of precipitation rate, the space- and time averaged total and convective precipitation rates as well as the upper air scores of temperature against observations from radiosondes, for a change in Wt from 18 to 12 cm/s. **Figure 16** and **Figure 17** are the same except that they show the changes when Wt is increased from 18 to 27 cm/s. Results are shown for the continental US where convection is more prevalent and where the precipitation surface observation network is the densest.

Examining **Figure 14** and **Figure 15** shows that the increased "convective activity" resulting from the reduction in Wt increases the convective precipitation at all lead times as well as the diurnal peak in total precipitation (near 2300 UTC). The occurrence of low precipitation rates increases while the occurrence of higher rates decreases (top of **Figure 14**). This may seem counter-intuitive but it can be understood because convection produces local, short-lived, intense precipitation events which once

averaged over 24 hours and over the grid scale appear as low intensity events. Finally, **Figure 15** shows that the middle and upper troposphere is warmed (deterioration).

Figure 16 and **Figure 17** show that decreasing the convective activity (by increasing Wt from 18 to 27 cm/s) has the opposite effect on all variables except for the diurnal peak in total precipitation which again increases. This last element is an interesting result in the sense that it is different from what has been obtained in the past from similar sensitivity experiments at lower resolutions (not shown). This is an indication that improving the precipitation budget and scores at this model resolution will require significant changes in both the convective and microphysical schemes.

Given our objective of not further increasing the occurrence of high precipitation rates, increasing Wt was excluded. However, decreasing its value from 18 to 12 cm/s reduces the occurrence of high precipitation rates but deteriorated the temperature profile as well as further increases the total precipitation. We therefore opted for a smaller decrease, from 18 to 15 cm/s. **Figure 18** shows an example of 1hr averaged precipitation rates for Wt=18, 15 and 12 cm/s for the south-eastern part of the RDPS domain, at 2300 UTC, near the peak in convective activity. Comparison of the three panels clearly shows what has been discussed earlier, i.e. increasing the convective activity (decreasing Wt) leads to a wider spatial distribution of less intense precipitation. Peaks around 35 mm/hr for Wt=18 cm/s are reduced to less than 10 m/hr at Wt=12 cm/s. **Figure 19** shows the NCEP (National Centers for Environmental Prediction) stage IV analysis of precipitation rate for the same domain and time period. In this specific example, very high precipitation rates (up to 90 mm/hr!) can be found that would support the more intense rates obtained with Wt=18 cm/s. However, given the coarse resolution of the model compared to convective cells, we should not aim at producing such high precipitation rates.

The deep convection scheme also allows changing Wt with time of integration. In RDPS-200, a smaller value of Wt (5 cm/s) is used for the first 6 hours of integration and then changed to 12 cm/s for the rest of the integration. This is useful because the initial conditions can be locally unconditionally unstable, leading to very high precipitation rates in the first hours of integration. In RDPS-300, we have used the same strategy except that Wt gradually increases from 5 to 15 cm/s during the first 6 hours. Note the change in behaviour of the precipitation in the first 6 hours of integration for the summer season in **Figure 7**. This gradual change in Wt leads to a more realistic time evolution (diurnal cycle) of the precipitation in the first 6 hours of integration.

4.2.3 **Vertical diffusion**

As discussed above, a longstanding problem of the RDPS has been large near-surface warm errors associated with winter warm air advection (**Figure 9** and **Figure 10)**. It was known that over-mixing in the PBL was the cause but only recently has a solution been found by introducing a hysteresis effect in the vertical diffusion scheme (McTaggart et al., 2012). This consists of introducing an asymmetry in the critical Richardson number at which there is transition between turbulence destruction and turbulence production (**Figure 11**), depending on the “direction” of the transition. Comparing the red profile to the blue profile in **Figure 10**, we see the significant improvement obtained with the hysteresis approach, namely, the more realistic surface temperature as well as the fact that the “warm nose” or peak in temperature around 850hPa is much better represented. During part of the 2012 winter, a preliminary version of the RDPS-300 including the hysteresis effect was run on a daily basis.

Meteorologists of the A&P section examined these runs relative to the operational RDPS-200 and wrote more than 10 case studies on warm episodes and freezing rain events. They noted significant impacts, generally improvements, in terms of surface temperature, precipitation type and temperature profiles accompanying warm fronts. **Figure 12** and **Figure 13** show the improvements with the hysteresis effect for two warm episode situations that occurred during winter 2012.

4.2.4 Other changes

Table 2 and **Table 3** summarize all changes in settings and code between the RDPS-200 and RDPS-300 REG-LAMs. In this section, we briefly explain the changes not already discussed in the sections above. The key "limsnodp=.TRUE." was activated as in the GDPS. The effect is to limit the snow depth to 10 cm in the calculation of heat fluxes through snow on sea and lake ice and glaciers. This has a small warming effect both over sea ice and over the frozen lakes of the Canadian Shield. The parameter "leadfrac", which represents the minimum percentage of leads (open water) in sea ice, was decreased from 3 to 2%. This has a small cooling effect over sea ice. There was an error in the formula used to determine the solar declination as a function of time. This is an important factor in determining the solar flux entering the atmosphere for a given day of the year. The consequence of this error was an under (over) estimation of the solar flux in the northern (southern) hemisphere increasingly important when approaching the poles and close to the equinox periods. The correction of this error led to a small warming of the surface and of the troposphere in the RDPS. As seen in **Table 3**, several other small modifications were made to the code included in RDPS-300 to increase the robustness of the model with no significant impact on the results. Finally, for output purposes, the algorithm used to extrapolate fields below ground, such as the sea level pressure or any field on constant pressure levels, was improved and optimized. This results in less noise in some images as can be seen in the sea level pressure maps shown in **Figure 20**.

4.2.5 Summary of impacts of model changes

As a result of the increased resolution and the modifications to the physics incorporated in the new RDPS-300, the following changes with respect to RDPS-200 have been obtained:

- decreased precipitation in winter over land and water surfaces, decreased precipitation in summer over water surfaces, increased precipitation in summer over land at the time of the diurnal peak
- increased occurrence of high precipitation rates in summer
- more realist precipitation rates in the first 6 hours of integration
- significantly reduced evaporation (latent heat fluxes) from water bodies, in particular in winter and over the Gulf Stream
- improved surface temperature and temperature profile in warm air advection situations in winter and spring
- improved forecast of precipitation types in warm air advection situations in winter and spring

- on several occasions during the winter, A&P meteorologists have noted improvements in surface temperature due to the better resolved topography (cold air channeling in valleys)

In section 4 we have focused on specific meteorological elements. Section 5 will show the overall improvements in upper air scores against the radiosonde network resultant from all the new elements of the RDPS-300, model and analysis. These scores show the positive impact of the new system on synoptic scale meteorology. The changes to the model have also contributed (not shown here) to these improved larger scale scores, namely in reduced RMS errors of temperature, winds and geopotential heights in the lower troposphere.

4.3 Geophysical fields

Whenever there is a change in the model grid, geophysical fields must be regenerated for the new grid. This was done using the same databases as for the previous operational RDPS. The method consists of using the tool called *GenPhysX* for the simple average fields (VF, GA, ME, MG, VG, J1, J2: vegetation fraction, glacier mask, topography, land-sea mask, dominant vegetation, sand and clay fraction) and the tool called *auto-genesis* for the subgrid fields (Z0, ZP, LH, Y7, Y8, Y9: roughness lengths, launching height...).

4.4 Climatological fields

A new and more realistic monthly global climatology of sea-ice thickness is implemented. This new climatology was obtained by merging three sources of data. The main source is the Global Ocean Reanalysis and Simulations Project (Mercator Ocean Quarterly Newsletter #36, January 2010, pages 15-28.) over the years 2002-2008. The second source is CMC's operational ice-ocean analysis and forecasting system for the Gulf of St-Lawrence (Smith et al 2012). The sea-ice thickness analyses from this system were time averaged over the years 2006-2011 to produce a monthly climatology for the Gulf of St-Lawrence. The third source of data is the old climatology which we continue to use over the freshwater lakes. **Figure 21** compares the old and new climatologies for the month of March. Typically, the sea-ice thickness is reduced everywhere except in the northwest portion of the Canadian Arctic archipelago. In most of the Arctic Ocean, in Hudson's Bay and in the Gulf of St-Lawrence, the ice thickness is reduced by 40 cm or more.

5 Objective evaluation of the final series

The final test series of the RDPS before the parallel run were performed for two periods in 2011: winter (20 January, 1200 UTC - 20 March, 0000 UTC) and summer (15 May, 1200 UTC - 13 July, 0000 UTC). For each period a control series was performed that was nearly identical to the current operational system, as well as an experimental series nearly identical to the RDPS parallel run currently underway. Given the analysis frequency of one every 36 hours, each final test series consists of 40

cases. The only differences between these 2011 series and the current operational and parallel runs are as follows:

- some minor differences in satellite data assimilated (dictated by the availability of data in 2011 versus the present)
- 2011 series used surface fields from the operational system (whereas the Regional operational/parallel runs include an interactive surface cycling step)
- 2011 series used G2 derivate observation files i.e. a longer cut-off time (9 hours compared to 2 hours) than in the Regional operational/parallel runs. This is an important aspect to remember when comparing the results of the final series and the parallel run. Particularly in the context of the passage from a 3D-VAR to a 4D-VAR assimilation system. Laroche et al. 2007 demonstrated that the 4D-VAR benefits more from a longer cut-off time than the 3D-VAR (see Figure 8 of this paper). Consequently, it is possible that the improvements seen in UA scores in the final series somewhat over-estimate the improvements that are obtained in the parallel run.
- 2011 series were executed every 36 hours (instead of every 6 hours as in the Regional operational/parallel runs)

It is interesting to compare at this point the number of observations assimilated by the old and new system. **Table 1** shows the observation counts for the control and experiment during both 2011 periods, first listed by observation family, followed by the totals. Not surprisingly, the observation counts in the RDPS-300 are generally higher than in the old system, especially for the families AMSU-A, AMSU-B, aircraft, GOES, profilers and SatWinds. Modest increases are also seen in AIRS, scatterometer and IASI data. Certain families show a slight decrease in observation counts in the new system, which is most likely a result of higher rejection rates during the background check due to the higher-resolution trial fields. Indeed, other tests (not shown here) demonstrate that if all the modifications of RDPS-300 are retained except the increase in the REG-DRIVER and REG-LAM horizontal resolution, the resulting observation counts do not decrease with respect to the control. Overall, noting the small differences between the 2011 series and the operational/parallel runs, RDPS-300 is expected to ingest approximately 2.3 times as much data as RDPS-200.

Objective evaluations of the new system were primarily based on forecast verification scores against radiosondes and surface stations for basic meteorological variables, and on precipitation scores against the SYNOP [1](over all of North America) and SHEF [1] (over continental USA) networks. The verification scores were computed over a number of geographic regions and averaged over all 40 members of each series. Selected plots which serve to summarize the validation results are shown in **Figure 22** to **Figure 50**. In these plots, the colors blue and red correspond to the control and

[1]The SYNOP network is the conventional North American synoptic network, which reports 12-h accumulations of precipitation at 0000 and 1200 UTC. The SHEF network is the US Standard Hydrometeorological Exchange Format network which covers most of the continental US at much higher spatial density, but reports only 24-h accumulations once a day at 1200 UTC.

experimental configurations, respectively. Regarding bias scores, the convention adopted here is to plot observation minus prediction, i.e. O-P.

5.1 Upper air scores

Figure 22 shows a comparison of mean upper air scores for the winter period at a forecast lead time of 0 hours, in other words, it demonstrates the fit of the analysis to radiosonde observations. As had been expected, generally the new analysis fits observations less well than the control. This is because the operational scheme uses 3D-Var, which only fits the analysis itself to observations, whereas the new scheme uses 4D-Var, which fits the model trajectory to observations over the entire 6-hour assimilation period. Although the 4D-Var analyses do not fit radiosondes as closely as 3D-Var analyses, the ability of the 4D-Var method to produce atmospheric features which are more consistent dynamically leads to more accurate forecasts beyond the assimilation window, as suggested by the following plots.

Continuing with the winter period, **Figure 23** to **Figure 26** show mean upper air scores over four different geographic regions (North America, Canada, Canadian Arctic and United States) at the maximum lead time (48 hours). Significant improvement is seen in all of the meteorological fields at a number of pressure levels, particularly in the mid- and lower troposphere, while a deterioration of scores occurs only at a few levels mostly confined to the stratosphere. This apparent deterioration can be traced back to the increase in resolution of the model. Based on other tests (not shown here) some improvements can be linked directly to specific modifications that have been made in the system. For example, the robust decrease in geopotential (GZ) bias, seen over North America and the United States, is mostly due to the new, higher-resolution REG-DRIVER model. It should be noted that a large fraction of the improvements is statistically significant at the 90% confidence level or higher. The results from this set of experiments are largely consistent with similar tests performed previously during the project, employing periods in the summer of 2008 and winter of 2008/2009.

Analogous to the winter period, upper air scores for the summer period are shown in **Figure 27** to **Figure 30** for the same geographic regions and at the same lead time, i.e. 48 hours. Similar comments may be made regarding these plots as for **Figure 23** to **Figure 26**. A significant improvement is evident in GZ bias and standard deviation throughout the troposphere. Likewise, standard deviations for temperature (TT), zonal wind (UU) and wind modulus (UV) are reduced in much of the mid- to lower troposphere. Regarding the dew point depression (ES), both the bias and standard deviation error are reduced somewhat below 600 hPa over North America during winter, but otherwise the impact is negligible. Deterioration seen in GZ and TT bias (and to a lesser extent, in the standard deviation) is generally limited to pressure levels above 200 hPa. Using the presence of confidence intervals as a guide, the differences between the old and new forecast systems seem to be larger in summer than in winter.

5.2 Surface scores

Spatial-mean verification scores against the surface observation network over the same regions as the upper air scores are shown in **Figure 31** to **Figure 38** for temperature and dew point depression as a function of lead time. Only forecasts launched at 0000 UTC were included in these calculations. As discussed previously in the case of upper air scores, the analysis (i.e. the 0-hour forecast) resulting from the new forecast system does not fit the observations as well as the control analysis does. This is evident in both seasons in terms of the standard deviation errors, and in winter in terms of the bias as well. At lead times 12 through 48 hours however, the new system exhibits slightly reduced standard deviation of errors for temperature and improved bias for dew point depression. However, the bias of TT in winter is deteriorated (colder nights) over Canada and the USA.

5.3 **Precipitation scores**

Precipitation is probably the most difficult field to verify given the very high variability of this field, both in space and in time, the low density of the observation network in certain areas (e.g. most of Canada) and the representativity error when comparing point observations to a finite resolution model on a grid. Furthermore, it is known that observations of snow fall accumulation contain significant errors. Our standard precipitation verification package produces scores of the bias of occurrence as well as the equitable threat score (for a rate greater than shown thresholds) on 24-h accumulations for the three periods of 0–24 h, 12–36 h and 24–48 h forecasts using two surface observation networks.. **Figure 39** to **Figure 50** show these scores for the aforementioned periods, network and for winter and summer of 2011. For the reasons stated above, we will mostly comment the bias of occurrence scores. The equitable threat scores are very sensitive to the sampling and would require confidence intervals for proper interpretation.

Figure 39 to **Figure 44** show winter scores. Given the observation errors in winter mentioned above, the only element that should be observed here is the significant relative reduction in bias of occurrence for all thresholds. This is coherent with the reduction of total precipitation in winter discussed in section 3.

Figure 45 to **Figure 50** show summer scores. The bias scores over the North American SYNOP network show varying behaviors as a function of lead time. While, day 1 (00-24-h) scores show a slight increase in occurrence of higher precipitation rates, decreases are seen for the two other accumulation periods. The following figures show the scores over the SHEF network, therefore over the USA where convection is more prevalent. As discussed in section 3, this is where we obtain increases in bias of occurrence of high precipitation rates, most noticeable for the 12-36-h accumulation period. For the shorter term day 1 forecast, we also note an improvement in the bias of occurrence for low precipitation rates.

6 Evaluation of the parallel run

The parallel run for the RDPS began on 20 June 2012 and lasted until 20 September 2012 (3 months). Objective and subjective evaluations were performed during this period. Forecast verification scores against radiosondes and surface stations for basic meteorological variables, and on precipitation scores against the SYNOP (over all of North America) and SHEF (over continental USA) networks were calculated. Here are shown selected plots which serve to summarize the results of the parallel run over the 3 month period. In these plots, the colors blue and red correspond to the operational RDPS-200 and parallel RDPS-300 configurations, respectively. Regarding bias scores, the convention adopted here is to plot observation minus prediction, i.e. O-P.

6.1 Objective evaluation

6.1.1 Upper air scores

Figure 51 shows a comparison of mean upper air scores for North America during the parallel run period at the maximum lead time (48 hours). Significant improvement is seen in all of the meteorological fields at a number of pressure levels, particularly in the mid- and lower troposphere, while a deterioration of scores occurs only at a few levels mostly confined to the stratosphere. While scores were improved most obviously in the day 2 forecasts (36 and 48 hours), smaller improvements are also obtained at day 1 (12 and 24 hours). Improvements in upper air scores are, in general, stronger in the northern and western portions of North America. Results for the other regions (not shown here) are identical to the final cases of 2011.

The parallel run occurred during the summer when RMS errors are at their lowest due to weaker synoptic patterns. However, it is encouraging to note that the day two RMS errors showed a significantly bigger difference during August (**Figure 54**), when synoptic situations were generally somewhat stronger, than in July (**Figure 53**).

While August had a record number of named tropical storms, only two such systems affected North America during the period of the parallel run – *Debby* (June 23-27) and *Isaac* (Aug. 26-31). It is therefore not possible to draw conclusions as to the relative merits of the 10 km model at handling these systems. In general, the central pressure values for those storms were not as low (deep) with the new 10 km model as those with the 15 km. Whereas scores for Debby when it was crossing Florida were not significantly different between the two models, the 10 km model scored better (except for one run) as Isaac made its approach on Louisiana (**Figure 55**).

6.1.2 Surface scores

Spatial-mean verification scores against the surface observation network over North America are shown in **Figure 52** for temperature and dew point depression as a function of lead time. Only forecasts launched at 0000 UTC were included in these calculations. As discussed previously in the

case of the development final series, the analysis (i.e. the 0-hour forecast) resulting from the new forecast system does not fit the observations as well as the control analysis. At lead times 12 through 48 hours however, the new system exhibits slightly reduced standard deviation of errors for temperature and improved bias for dew point depression.

6.1.3 **Precipitation scores**

Precipitation scores were also computed during the RDPS parallel run on 24-h accumulations for the three periods of 0–24 h, 12–36 h and 24–48 h forecasts against the North American synoptic observation and the high density U.S. SHEF networks.

Generally, there was not a lot of difference in equitable threat scores between the operational and parallel run models during the parallel run period, but the 10 km RDPS forecasts produced slightly higher precipitation amounts in the mid to high precipitation classes (10-50 mm), particularly in the 00-24 and 12-36 hour periods. This is evident in the biases as scored against both networks. Please see **Figure 56** and **Figure 57**.

6.2 **Subjective evaluation**

A subjective evaluation was done twice daily by operational meteorologists at CMC over the course of the parallel run. Mass fields and quantitative precipitation forecasts (QPF) were evaluated by comparing visually sets of images from the two different models such as **Figure 58** to **Figure 60.** Then the meteorologists had to indicate whether any of the models had performed better over specific regions **Figure 61**), of if both had performed equally good or bad. The results are displayed in **Table 4**.

When a difference in mass field forecasts was found between the two systems (about 30% of the time), a preference for the new system was expressed in a ratio of about 2:1. Differences were more frequent along the Atlantic coast than the Pacific (33 vs 27% of the time). However, when the systems differed, preference for the new system was stronger for the Pacific area (w a ratio of 3:1) than for Eastern North America and over the Atlantic (ratio of 3:2).

For precipitation forecasts, the signal was found to be neutral or slightly in favor of the new system for the ensemble of regions, similar to the findings of the objective scores. A&P meteorologists observed a noticeable increase in the details of the precipitation patterns, especially with organized mesoscale convection. Another type of evaluation was added to the usual one, involving a blind comparison of QPF fields. These were interpolated to a similar 15 km resolution grid for two different domains (covering roughly the southern Prairie provinces and the Great Lakes region), for the 24 hour forecast periods of 12 to 36 and 24 to 48 hours lead-times. They were then compared visually between them, and against the CaPA (regional deterministic precipitation analysis) system, with either model identified at random by a letter, A or B. Examples are shown in **Figure 62**. The evaluators had to indicate their preference for either model, A or B, not having knowledge of the actual sequence of equivalence of A's and B's with either the RDPS-200 or RDPS-300. Nine different evaluators were involved, from A&P, from regional forecast offices, plus two undergraduate students hired at CMC

during the summer period. The final tally of this evaluation lead to a conclusion similar to that of the A&P evaluation mentioned previously.

A subjective evaluation of surface temperatures was also done for 42 runs covering the first three weeks of August 2012, for a lead time of 24 hours, which would allow for a difference due to the change in the vertical diffusion to come into effect but without too much difference between the synoptic patterns. Although a preference was expressed more often in favor of the system in parallel, no particular pattern was detected and the total number of cases examined does not allow to conclude on the performance of the systems. The changes to the physics brought to the new system would be more visible during winter so it is not a surprise that these summer cases did not lead to any specific signal with respect to surface temperatures.

In spite of a relatively high frequency (most notably in August), storms of tropical origin did not venture often into our forecast areas, those that did were better forecast by the RDPS-300. It was found that their central pressure was less deep and their spatial extent was better defined than with the operational RDPS. In particular, RDPS-300 provided a better track forecast for tropical storm Isaac in late August and early September, a for hurricane Leslie, which affected considerably Newfoundland on September 11, 2012. On the other hand, concerning the latter, a meteorologist from the Canadian Hurricane Centre (CHC, in Dartmouth NS) commented that the higher central pressure value (less deep) was not seen as an improvement, especially to depict the storm at analysis time as "*.. storm depiction at time-zero is key to having good fields from which to derive the meteorological data used in forecast production*"[2].

7 Performance of dependent systems

Here you can find information on the adjustments made to systems that depend on the RDPS3.0.0. We describe the adaptation of UMOS, SCRIBE, the coupled model of the Gulf of St-Lawrence and the regional deterministic wave forecasting system.

7.1 UMOS

The training of the UMOS system with the new RDPS-300 has been carried out using the hindcasts (final series of forecast) for the periods of January 20th to March 20th 2011 for the winter season and May 12th to July 13th 2011 for the summer season (runs of 0000 and 1200 UTC). Additional hindcasts for the period of January 1st to April 3rd 2012 have been generated to help improve the performance of the UMOS system during the winter season (runs of 0000, 0600, 1200 and 1800 UTC). Finally, the training for the summer season has been finalized during the parallel run for all runs.

[2] Chris Fogarty, personal communication

In conclusion, for the winter season, the number of cases accumulated for training amounts to 154 cases for the 0000 UTC run, 91 for 0600 UTC, 153 for 1200 UTC and 94 for 1800 UTC. For the summer season, there are 157 cases for the 0000 UTC run, 98 for 0600 UTC, 156 for 1200 UTC and 98 for 1800 UTC. Verifications have shown that the accumulated cases ensure a stable and robust production of regression equations. Also, the performances of the UMOS forecasts in terms of bias and variance reduction of the numerical forecasts are thus maintained equivalent to the previous system.

7.2 SCRIBE

The performance of the forecasts of the meteocode as produced by the SCRIBE system was evaluated during the parallel run. The SCRIBE forecast system connected to the RDPS-300 as well as to the UMOS that make use of the RDPS-300 forecasts performed similarly to the operational system for most fields. One noticeable exception is a slight improvement in favor of the new system for the probability of precipitation.

7.3 Regional Deterministic Wave Prediction System (RDWPS)

The Regional Deterministic Wave Forecasting System (RDWPS) was modified to account for the increase in the spatial resolution of its forcing winds from the RDPS-300. All of the regional domains are now forced by the 10 km REG-LAM surface winds except the North Atlantic domain which uses a combination of wind forcing from the new 10km REG-LAM and the new 33 km REG-DRIVER models for the area not covered by the 10km resolution model. Verification during the parallel run (July-August 2012) have shown that the significant wave height forecast is improved when connected to the RDPS-300 over the large North Atlantic domain. However, over the Gulf St-Lawrence and the Great Lakes domains the signal is neutral with a slight positive bias in significant wave heights due to stronger winds from the 10 km REG-LAM.

7.4 Regional Coupled System - Gulf Of St-Lawrence (RDPS-CGSL)

The Regional Coupled System Of The Gulf Of St-Lawrence (RDPS-CGSL) was also brought to a spatial resolution of 10 km. The pseudo-analysis used to initialize the RDPS-CGSL is now also done at a 10 km resolution. The evaluation of forecast series in development showed a slight improvement for the 2m air temperature in winter 2008. However, the signal is slightly negative although not significant for the parallel run period (summer 2012). The Gulf of St-Lawrence being obviously free of sea ice during the summer the impact of the coupling of the atmosphere with the ocean is smaller compared to a winter period.

It has to be noted that the model domain was slightly reduced to limit the execution time. The grid points removed were not located where the coupled model is active (no coupling over this area). Therefore, there is no impact of this domain reduction on the Gulf of St-Lawrence area as such.

8 Availability of products

No new analysis or forecast products accompany this upgrade of the RDPS. The increase in resolution and the new 4d-VAR assimilation system are more demanding in computer resources, so to ensure the availability of most products at the same time than with the system being replaced, the data acquisition cut-off time has been shortened temporarily by 10 minutes to 1 hour 55 minutes. It was later brought back to 2 hours a few weeks after the system implementation. Ongoing code optimization combined with programmed increases in computing capacity will eventually allow us to go back to the previous cut-off time. The availability of the SCRIBE system output destined to the msc regional prediction centres will not be delayed.

9 Summary of the results

In summary, the most significant aspects of the new RDPS-300 are:

- Clear improvements in upper air scores for summer and winter seasons tested in most of the troposphere
- Clear improvements in surface temperature and temperature profile in warm air advection situations in winter and spring.
- Decreased precipitation in winter over land and water surfaces, decreased precipitation in summer over water surfaces, increased precipitation in summer over land at the time of the diurnal peak.
- Significantly reduced evaporation (latent heat fluxes) from water bodies, in particular in winter and over the Gulf Stream.
- The optimised 4D-Var can sustain a significant increase of observations in the future without increasing the computer cost.

10 Acknowledgements

We would like to thank our colleagues Stavros Antonopoulos, Maryse Beauchemin, Najat Benbouta, Martin Charron, Éric Chénard, John Cragg, Michel Desgagné, Amin Erfani, Manon Faucher, Vincent Fortin, Normand Gagnon, Stéphane Gagnon, André Giguère, Claude Girard, Sylvie Gravel, Marc Klasa, Marc Larocque, Yvan Larocque, Anne-Marie Leduc, Ron Lee, François Lemay, Jean-Francois Lemieux, Jocelyn Mailhot, Alain Malo, Jacques Montpetit, Radenko Pavlovic, Lewis Poulin, Michel Roch, Francois Roy, Guy Roy, Greg Smith, Michael Schäffer, Lubos Spacek, Ping-An Tang, Marcel Vallée, Gilles Verner, and the students Philip Mann and Patricia De Repentigny.

11 References

Daniel Deacu, Vincent Fortin, Erika Klyszejko, Christopher Spence, Peter D. Blanken, 2012: Predicting the Net Basin Supply to the Great Lakes with a Hydrometeorological Model
Journal of Hydrometeorology,doi: http://dx.doi.org/10.1175/JHM-D-11-0151.1

Fillion, L., Tanguay, M., E. Lapalme, B. Denis, M. Desgagne, V. Lee, N. Ek, Z. Liu, M. Lajoie, J.-F. Caron, C. Page, 2010: The Canadian Meteorological Center Limited-Area Regional Data Assimilation and Forecasting System. *Wea. Forecasting.* **25**, No. 6, 1645-1669.

Laroche, S., P. Gauthier, M. Tanguay, S. Pellerin, and J. Morneau, 2007: Impact of the different components of 4DVAR on the global forecast system of the Meteorological Service of Canada. *Mon. Wea. Rev.*, **135,** 2355–2364

R. McTaggart-Cowan et al., 2012: Boundary Layer Turbulent Hysteresis in NWP, in preparation.

Mercator Ocean Quarterly Newsletter #36, January 2010, pages 15-28. (online)

Smith, G.C., F. Roy and B. Brasnett : Evaluation of an Operational Ice-Ocean Analysis and Forecasting System for the Gulf of St. Lawrence. QJRMS, accepted.

Sverdrup, H. U., Johnson, M. W. and Fleming, R. H. (1942). The Oceans: Their Physics, Chemistry and General Biology . Prentice Hall, 1087 pp.

Tanguay, M., L. Fillion, E. Lapalme, M. Lajoie, 2012: Four-Dimensional Variational Data Assimilation for the Canadian Regional Deterministic Prediction System. Submitted to *Mon. Wea. Rev*., **140**, No. 5, 1517-1538.

Yu, L., X. Jin, and R. A. Weller, 2008: Multidecade Global Flux Datasets from the Objectively Analyzed Air-sea Fluxes (OAFlux) Project: Latent and sensible heat fluxes, ocean evaporation, and related surface meteorological variables. Woods Hole Oceanographic Institution, OAFlux Project Technical Report. OA-2008-01, 64pp. Woods Hole. Massachusetts.

12 Tables

Table 1 : Number of observations assimilated in the control (RDPS-200) and experimental systems during the periods (left) 20 January 2011, 12Z - 20 March 2011, 00Z and (right) 15 May 2011, 12Z - 13 July 2011, 00Z subdivided by observation type

	Control	RDPS 3.0.0
amsua	29987	123762 (+313%)
amsub	5135	10149 (+98%)
aircraft	10584	42660 (+303%)
goes	1118	4005 (+258%)
pr	673	4044 (+501%)
sfc	4740	4677
sw	3361	7469 (+122%)
ua	13339	13181
airs	16868	19127 (+13%)
ssmis	1438	1422
sc	2494	2860 (+15%)
gps-ro	3921	3841
iasi	9540	11057 (+16%)
Total	103198	248254 (+141%)

	Control	RDPS 3.0.0
amsua	30229	115192 (+281%)
amsub	7116	13116 (+84%)
aircraft	12913	57077 (+342%)
goes	1003	4023 (+301%)
pr	652	3961 (+508%)
sfc	5233	5175
sw	4134	10003 (+142%)
ua	13716	13570
airs	25988	31109 (+20%)
ssmis	1461	1455
sc	2419	2788 (+15%)
gps-ro	4195	4128
iasi	12796	16775 (+31%)
Total	121855	278372 (+128%)

Table 2 : Summary of changes to model physics

	RDPS 2.0.0	**RDPS 3.0.0**
Scalar surface roughness length over water in extra-tropics	Z0T=Z0M=Charnock formulation	Z0T=Deacu et al. 2012 formulation (Z0TRDPS-300=.TRUE.)
Scalar surface roughness length over water in tropics	Z0T=Z0M=Charnock formulation	Z0T=4.e-5m (Z0TLAT = 25., 30.)
Prandtl number	Beta2=0.85	Beta2=1.0
Ocean salinity effect on boundary condition for specific humidity	non-existent	qsat_salty=.TRUE.
Deep convection threshold vertical velocity at LCL (cm/s)	Kfctrig4=48,48,0.05,0.12 sudden change from .05 to 0.12 cm/s after 48 timesteps (3hrs)	Kfctrig4=0,72,0.05,0.15 gradual change from .05 to 0.15 cm/s over 72 timesteps (3hrs)
Hysteresis	non-existent	PBL_RICRIT = 0.15,2.
Limit snow depth to 10cm for heat conduction through sea ice and glaciers	Limsnodp=.false.	Limsnodp=.TRUE.
Minimum lead fraction in sea ice	Leadfrac=3%	Leadfrac=2%
Wind gust diagnostics	inactive	active
Algorithm for « under ground » extrapolation of output fields, e.g. Sea level pressure ...	Out3_zund=2500,2000,1500	Out3_lieb_levels= 5000., 4900.,4800. … 100.

Table 3 : Summary of the modifications to the GEM model physics code

Modified subroutines	Scheme	Justification
Moistke.ftn turbul.ftn options.cdk phy_ini.ftn phy_namelist.cdk phy_opt.cdk phybus.cdk	Vertical diffusion	New hysteresis option Bugfixes
Cccmarad.ftn raddriv.ftn swtran.ftn cldifm.ftn nocld.cdk	Radiation	Increased robustness and bugfixes
Suncos1.ftn	Radiation	Bugfix to solar declination
Water.ftn	Surface	New option for scalar surface roughness length New option for salinity effect
Diasurf2.ftn flxsurf3.ftn stabfunc3.cdk glaciers1.ftn	Surface	Code clean up and bugfixes
hines_flux.ftn90	Non orographic gravity wave drag	Smoothing of the tendency profile near model lid

Table 4: Summary of the subjective evaluation by CMC's "Analysis and prognosis" operational section. Letter o, O, p, P, indicate a preference (O, P: strong preference) for one model over the other. "e" (E) indicate if they are alike and good (very good) and X indicates they are different and neither is good.

Région / Region	**Aucune préférence/ No preference**	**Préférence pour / Preference for SRPD-200 (Op.)**	**Préférence pour / Preference for SRPD-300 (Par)**	**Préférence dans un rapport de / Preference ratio:**
Champs de masse / Mass fields GZ500 + PNM / SLP				
Pacifique / Pacific	e : 25.3% E : 47.0% X : 0.5% 72.8%	O : 0.0% o : 6.7% 6.7%	P : 0.7% p : 19.7% 20.4%	**P > O ≈ 3:1 (20.4/6.7)**
Amérique du Nord / North America	e : 27.0% E : 41.6% X : 0.5% 69.1%	O : 0.1% o : 9.4% 9.5%	P : 0.9% p : 20.5% 21.4%	**P > O ≈ 2:1 (21.4/9.5)**
Atlantique / Atlantic	e : 23.7% E : 42.4% X : 0.8% 66.9%	O : 0.5% o : 12.9% 13.4%	P : 1.1% p : 18.7% 19.8%	**P > O ≈ 3:2 (19.8/13.4)**
Arctique / Arctic	e : 28.6% E : 42.7% X : 0.2% 70.5%	O : 0.1% o : 8.9% 9.0%	P : 0.5% p : 19.0% 19.5%	**P > O ≈ 2:1 (19.5/9.0)**
Toutes régions / All regions: GZ500 + PNM/SLP	e : 26.1% E : 43.4% X : 0.5% 70.0%	O : 0.2% o : 9.5% 9.7%	P : 0.8% p : 19.5% 20.3%	**P > O ≈ 2:1 (20.3/9.7)**
GZ500 seulement / only	e : 24.8% E : 45.7% X : 0.4% 70.9%	O : 0.2% o : 9.8% 10.0%	P : 0.7% p : 18.5% 19.2%	**P > O ≈ 2:1 (19.2/10.0)**
PNM / SLP seulement / only	e : 27.5% E : 41.1% X : 0.6% 69.2%	O : 0.1% o : 9.2% 9.3%	P : 0.9% p : 20.5% 21.4%	**P > O ≈ 2:1 (21.4/9.3)**
QPP / QPF				
Toutes régions / All regions:	e : 31.0% E : 21.4% X : 4.2% 56.6%	O : 2.0% o : 18.9% 20.9%	P : 1.3% p : 21.2% 22.5%	**P ≈ O ≈ 1:1 (20.3/9.7)**

13 Figures

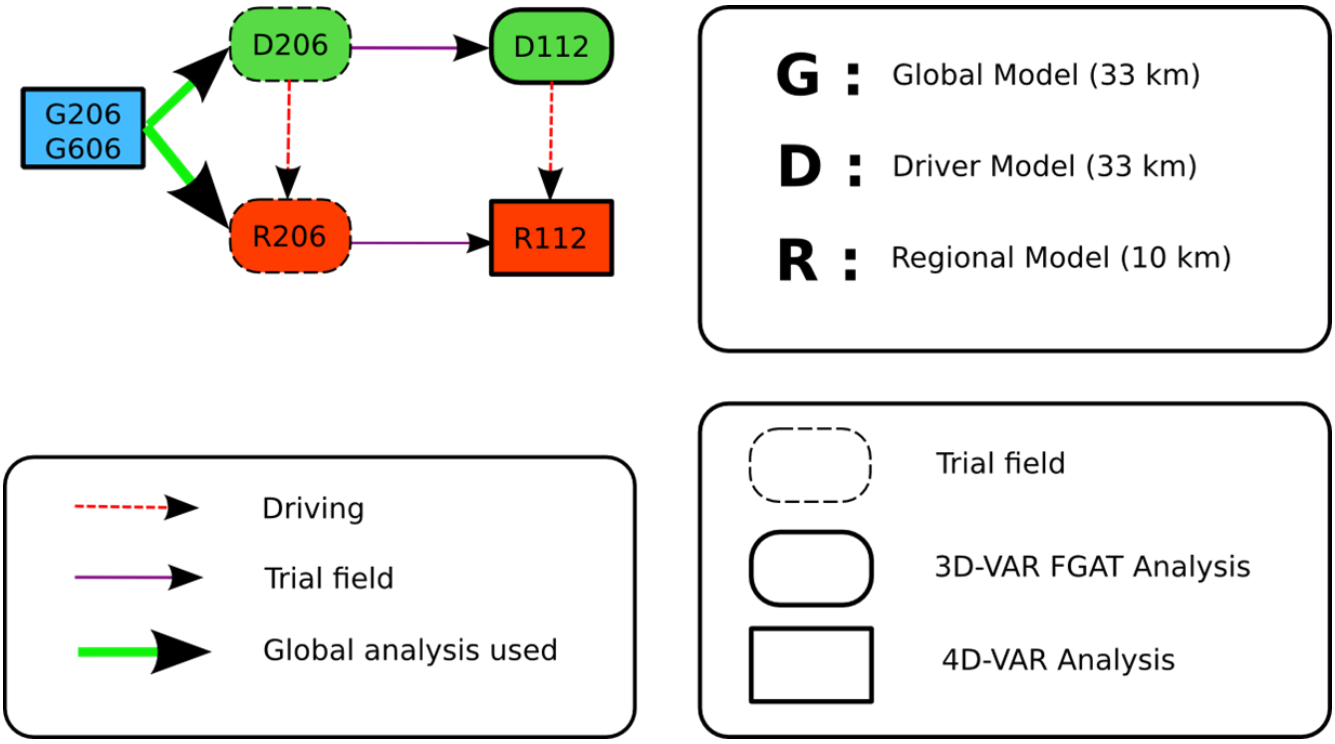

Figure 1 *: Flowchart of the RDPS cycle*

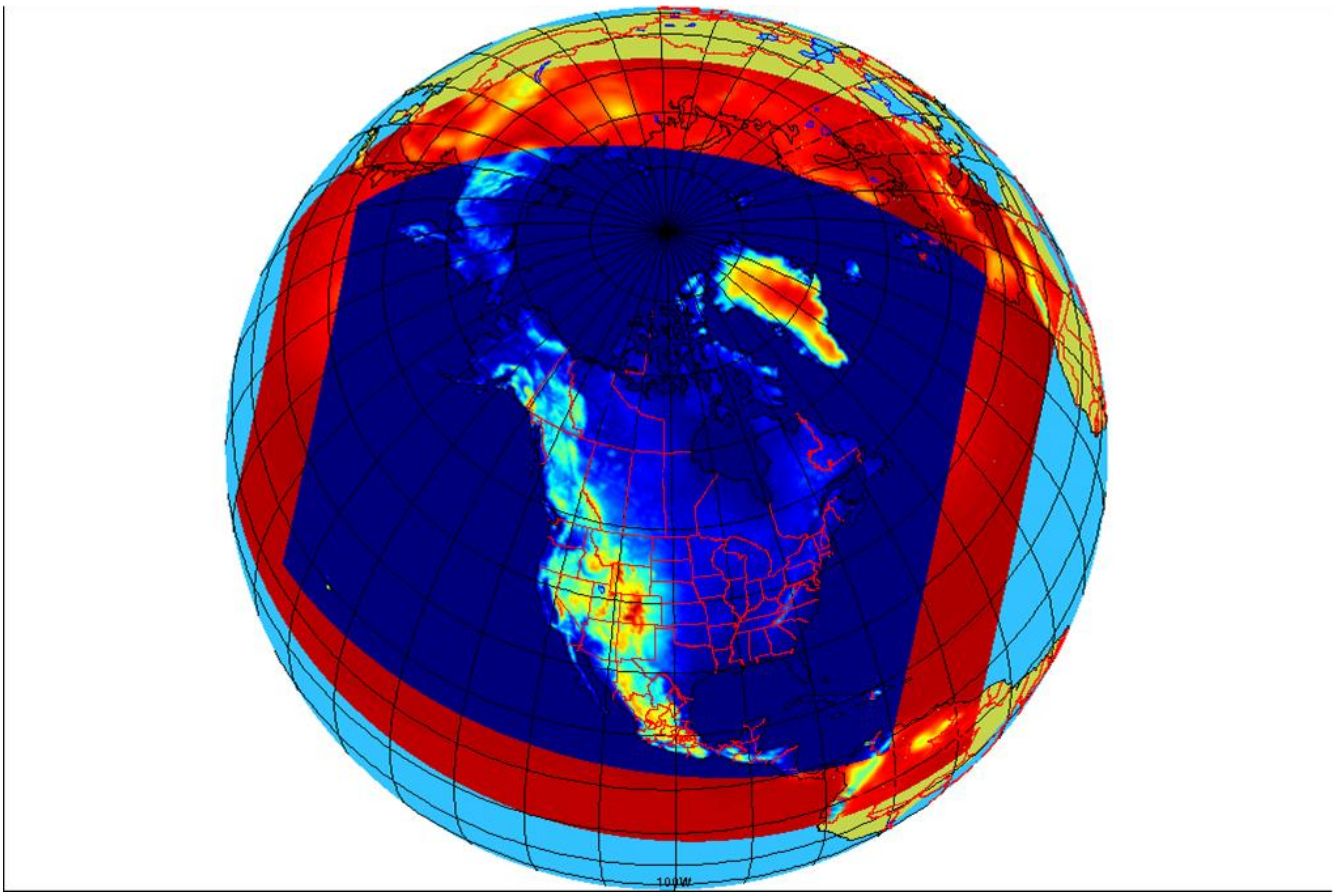

***Figure 2**: 10 km regional model grid (dark blue) and the tangent-linear/adjoint model grid at 100 km horizontal resolution (red)*

a) b)

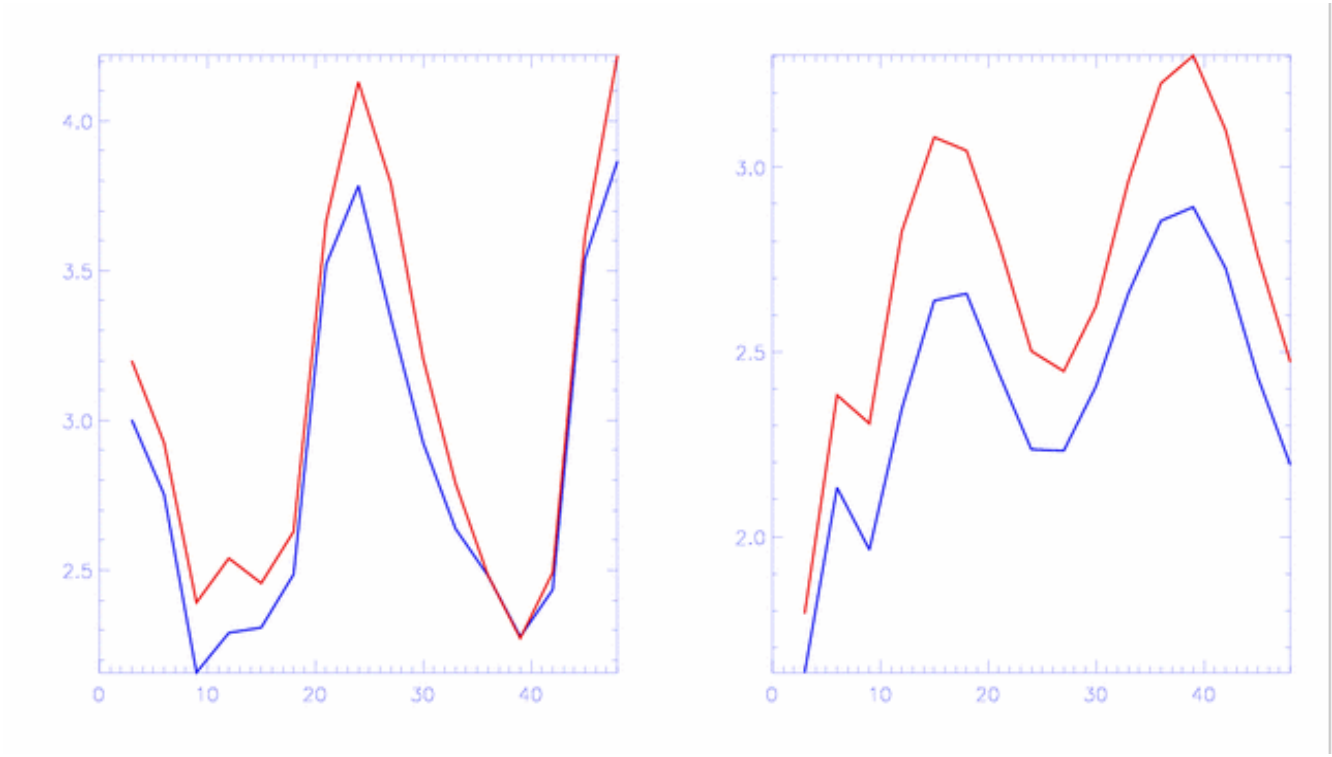

Figure 3*: 1hr averages of precipitation rate in mm/day as a function of lead time up to 48 hrs for summer 2008 0000 UTC cases over land (a) and over water (b). Results for the RDPS-200 are shown in blue and while those of the 10 km RDPS are in red. Note the varying scales on the ordinates.*

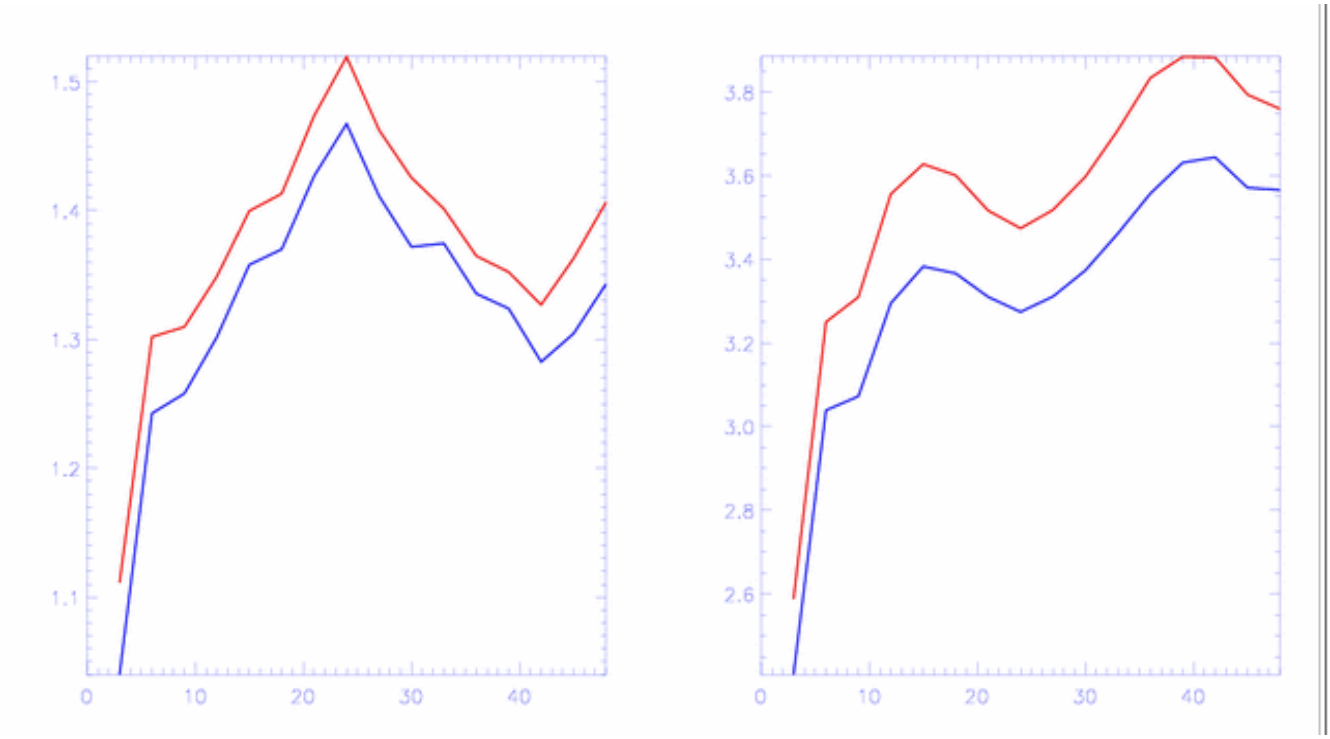

Figure 4*: Same as* ***Figure 3****, except for winter 2009 cases.*

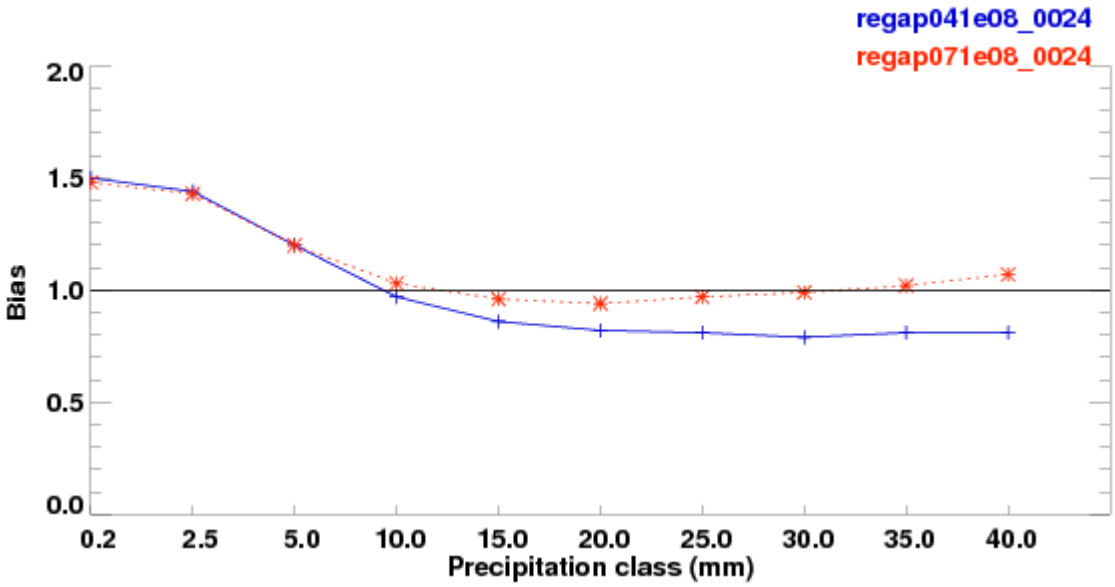

Figure 5: *Day 1 precipitation verification against SHEF network (continental US) for summer 2008, valid at 1200 UTC. The bias of occurrence is shown in function of the precipitation threshold (# of events in model/# of observed events). The blue line is showing results for the RDPS-200 while the red line, the ones of the RDPS-300.*

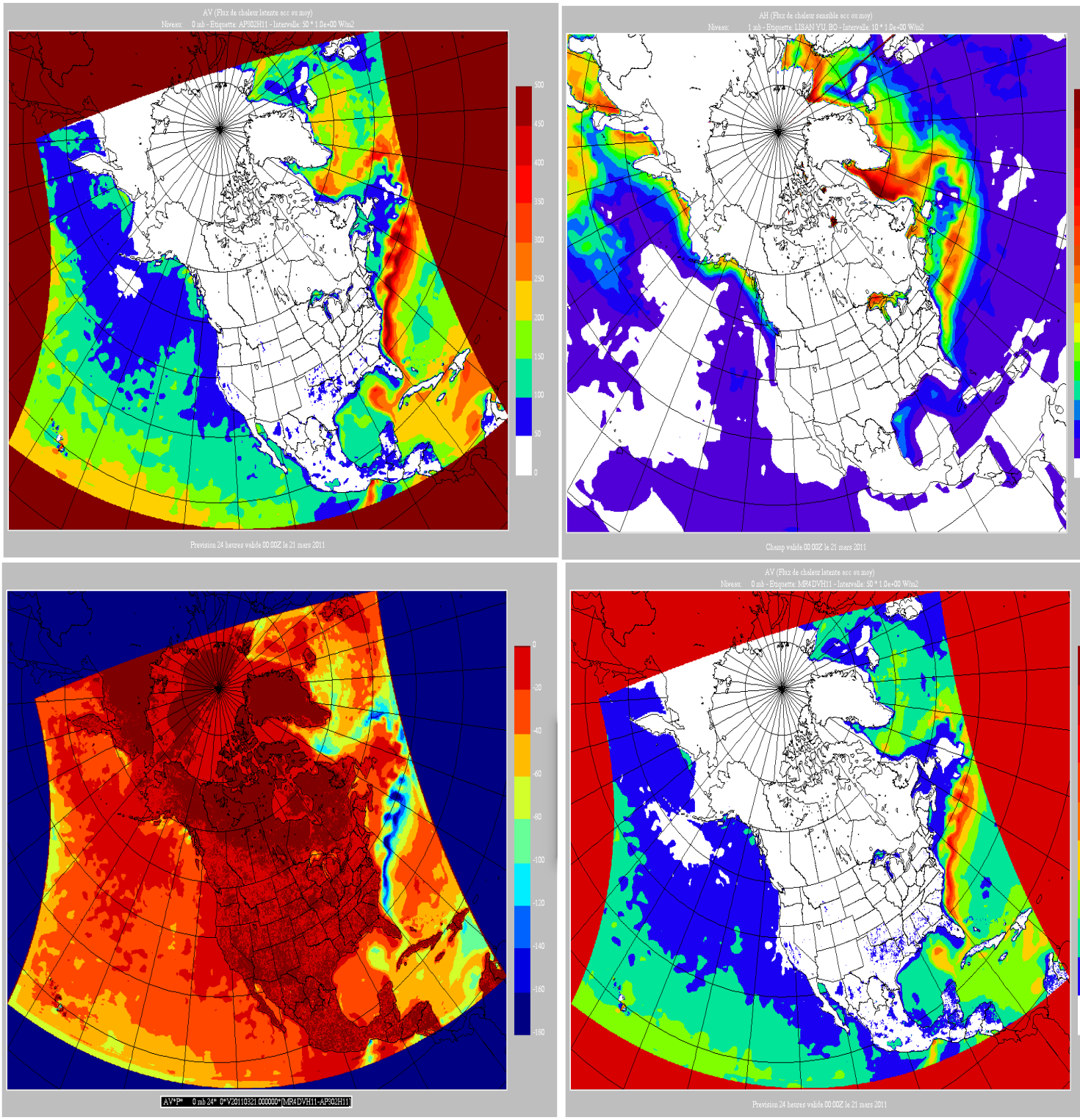

Figure 6*: Average over the winter 2011 season of the latent heat fluxes in W/m2. For the models, the day 1 average fluxes are used for the seasonal averaging. Top left: RDPS-200,. Top right: average of the daily analysis from the Woods Hole Oceanographic Institution "OAFlux" project. Bottom right: RDPS-300. Bottom left: RDPS-300-RDPS-200*

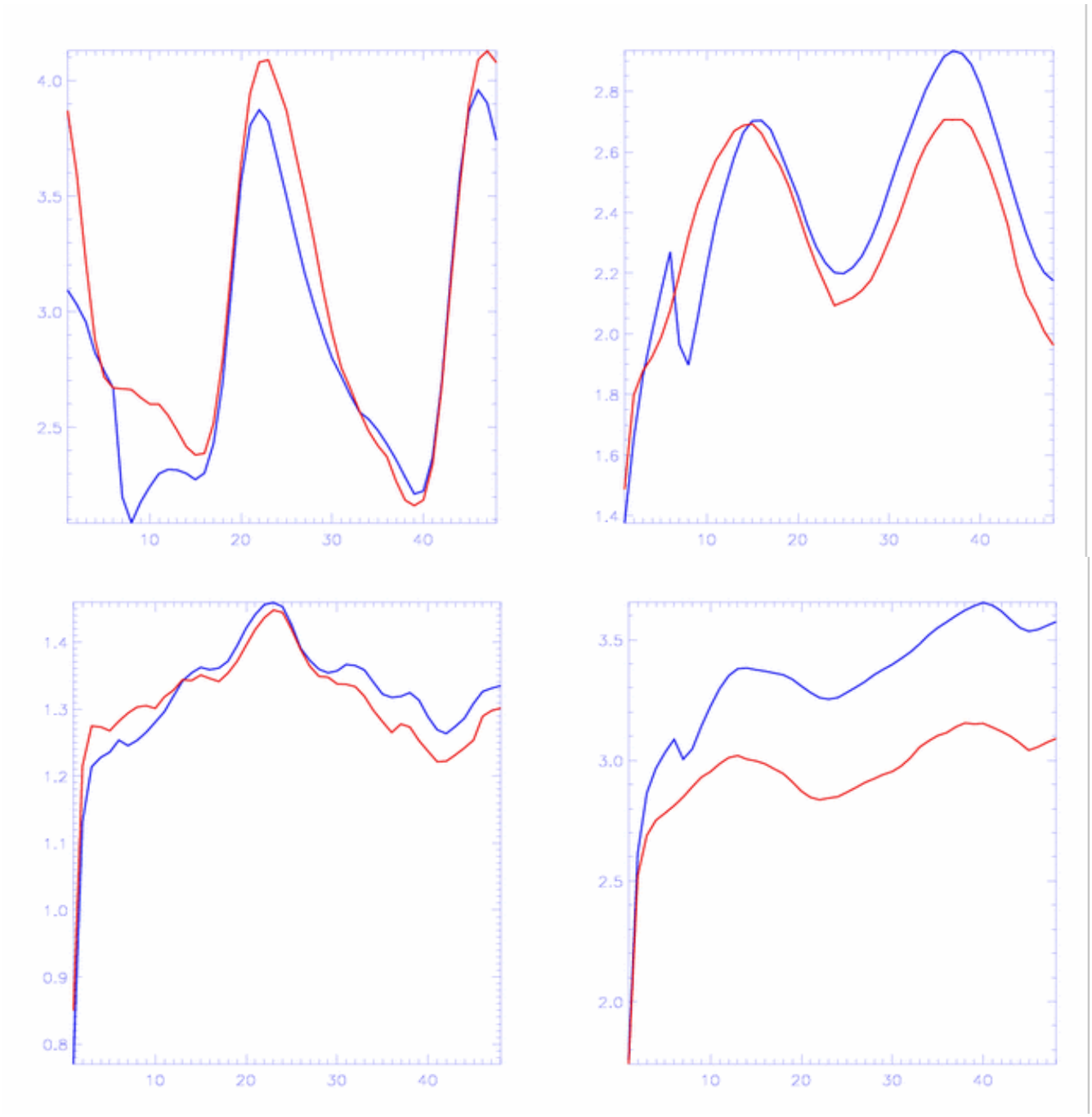

Figure 7*: Same as* ***Figure 3****and* ***Figure 4****, except red curves show results with 10 km RDPS including changes to surface fluxes.*

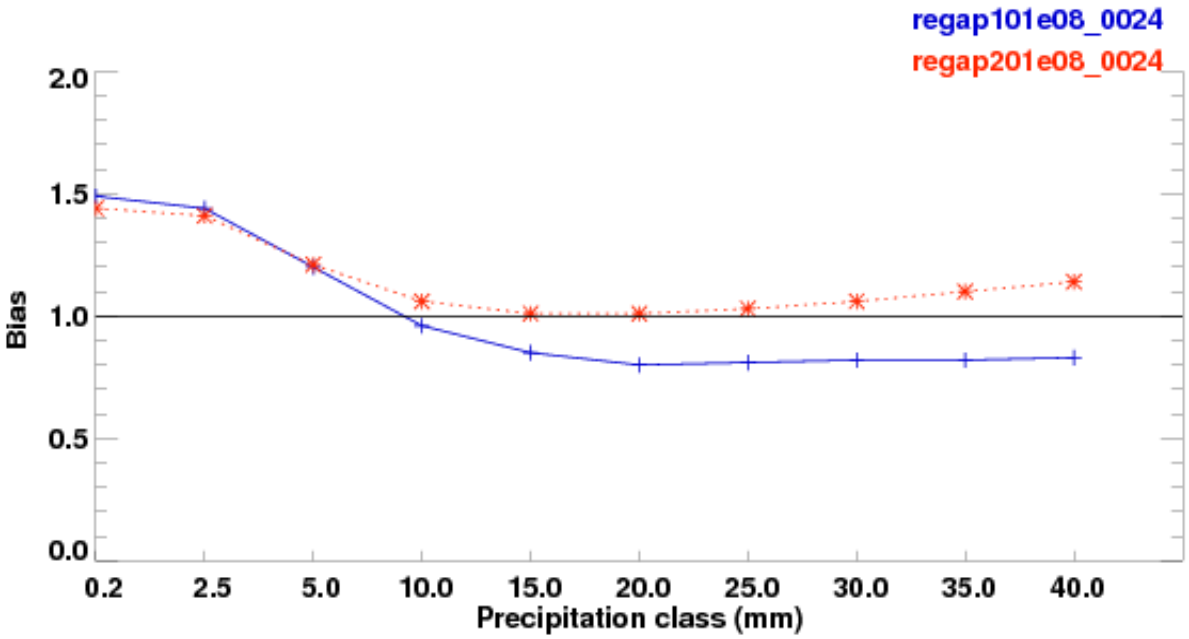

***Figure 8**: Day 1 precipitation verification against SHEF network (continental US) for summer 2008, valid at 1200 UTC. The bias of occurrence is shown in function of the precipitation threshold (# of events in model/# of observed events). The blue line is showing results for the RDPS-200 while the red line, the ones of the RDPS-300 including changes to surface fluxes.*

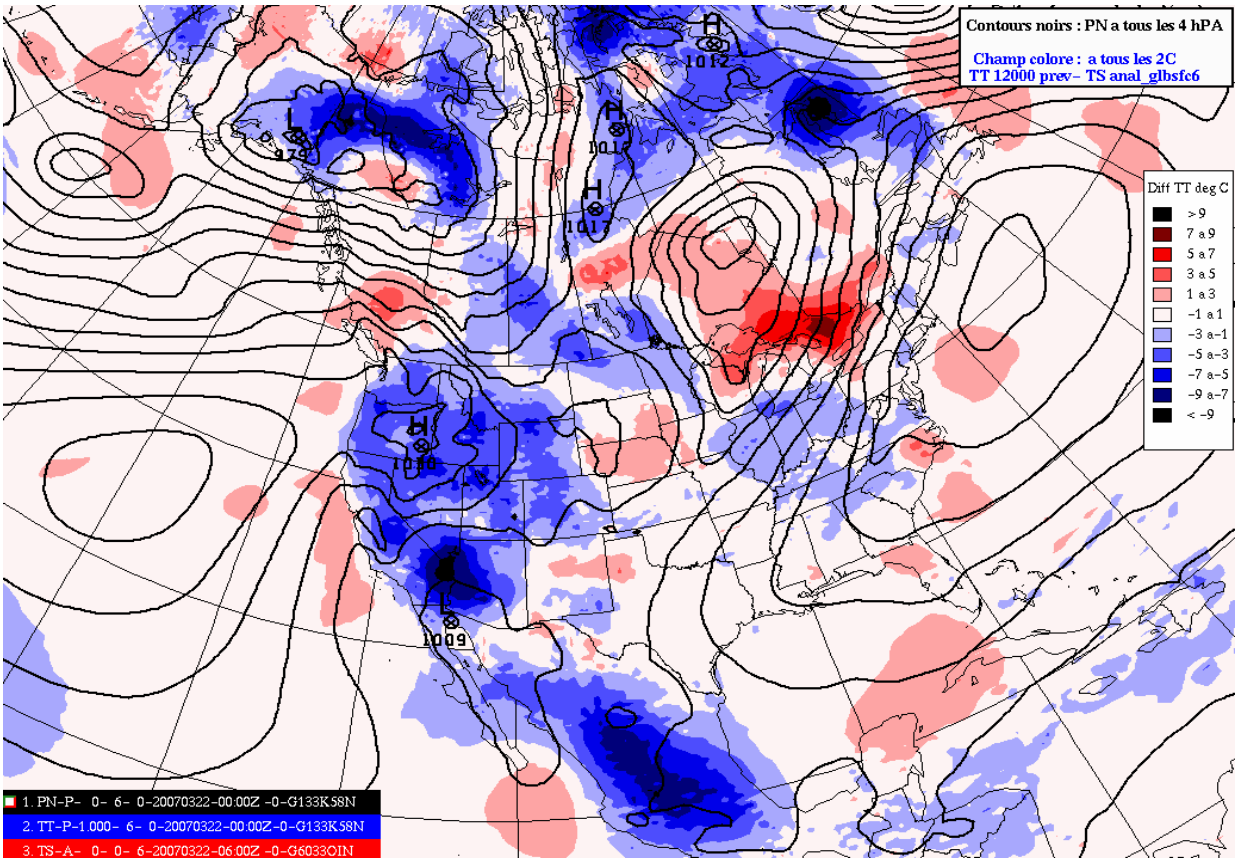

Figure 9: *2m temperature error (forecast – analysis) of 6h forecast for case study of March 22nd 2007. Contours show sea level pressure every 4 hPa.*

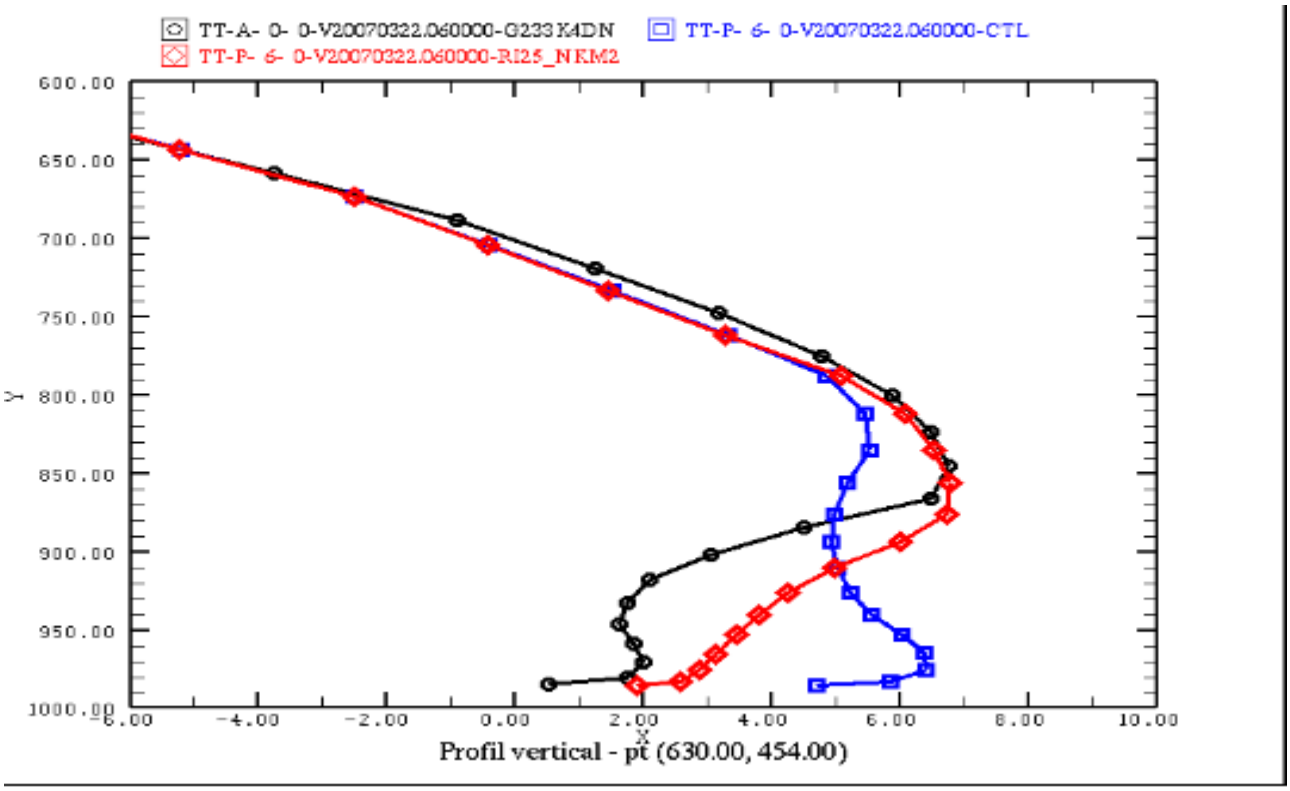

***Figure 10**: Same case study as in **Figure 9**. Temperature profiles ahead of warm front, near Ottawa. In black, verifying analysis at 0600 UTC in blue, 6h control forecast valid at 06UTC, in red, 6h forecast with hysteresis effect, valid at 0600 UTC. Ordinate is in mb, abscissa in Celsius.*

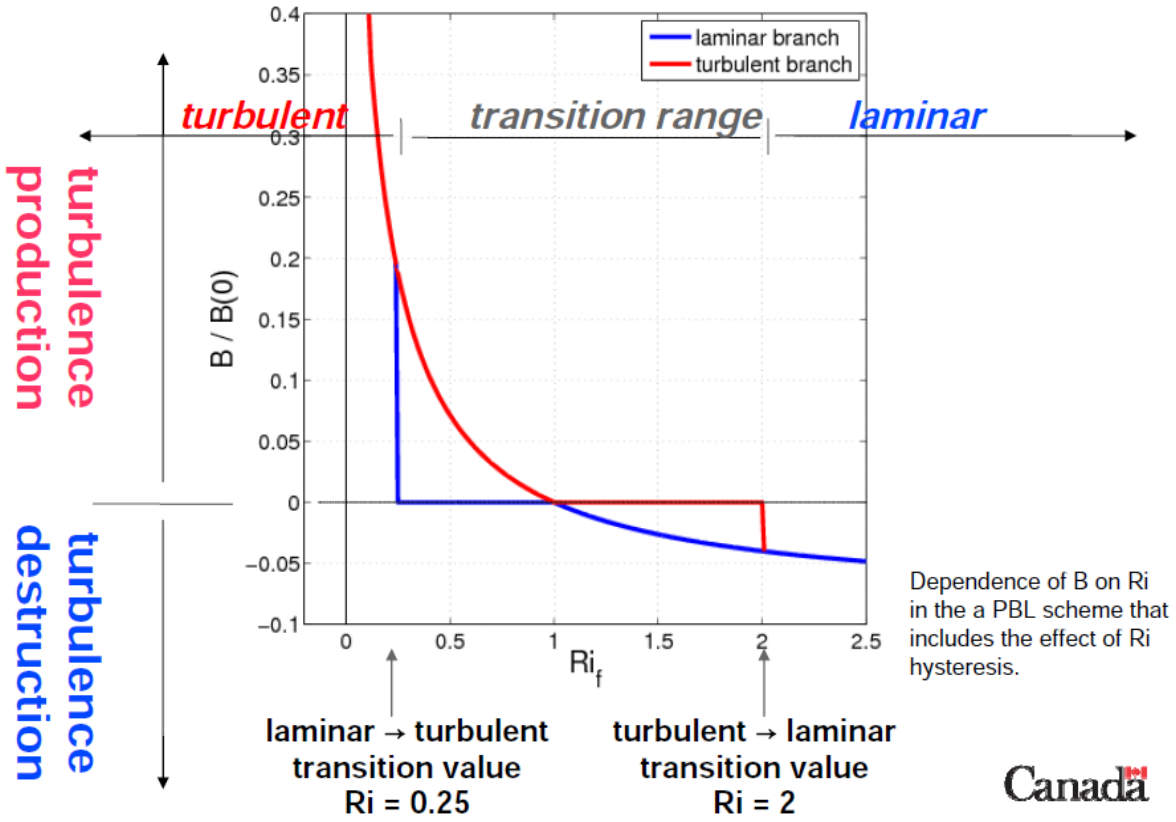

***Figure 11**: Schematic of dependence of B (term in turbulent kinetic energy -TKE - equation that controls the destruction or production of TKE) on the flux Richardson number*

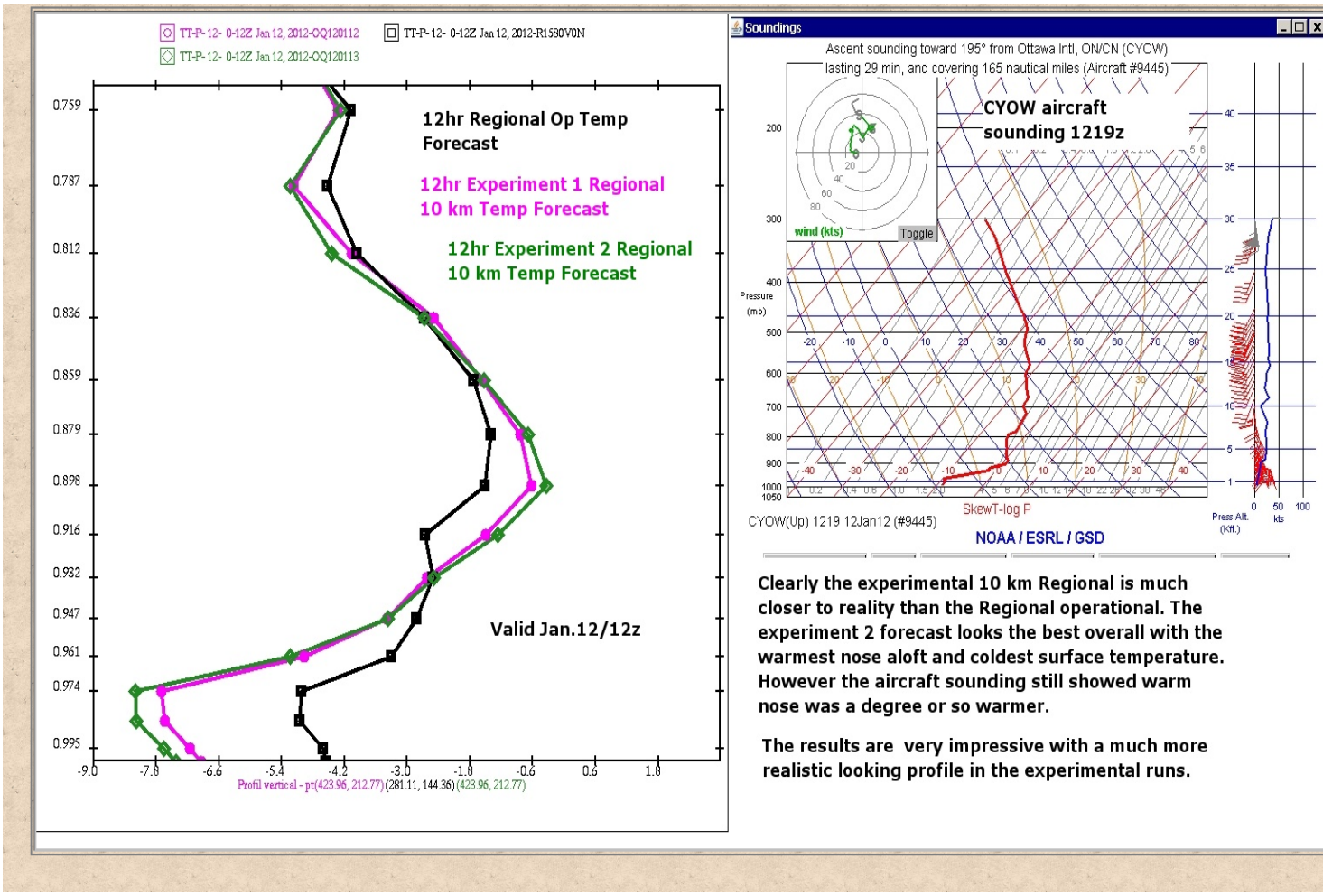

***Figure 12**: Extract from a case study by Victor Thomas on January 12 2012, which shows temperature profiles near Ottawa. Right : aircraft sounding . Left : in black, 12 h forecast of RDPS-200. In pink and green, 12 h forecasts from two experiments including the hysteresis effect (different parameters).*

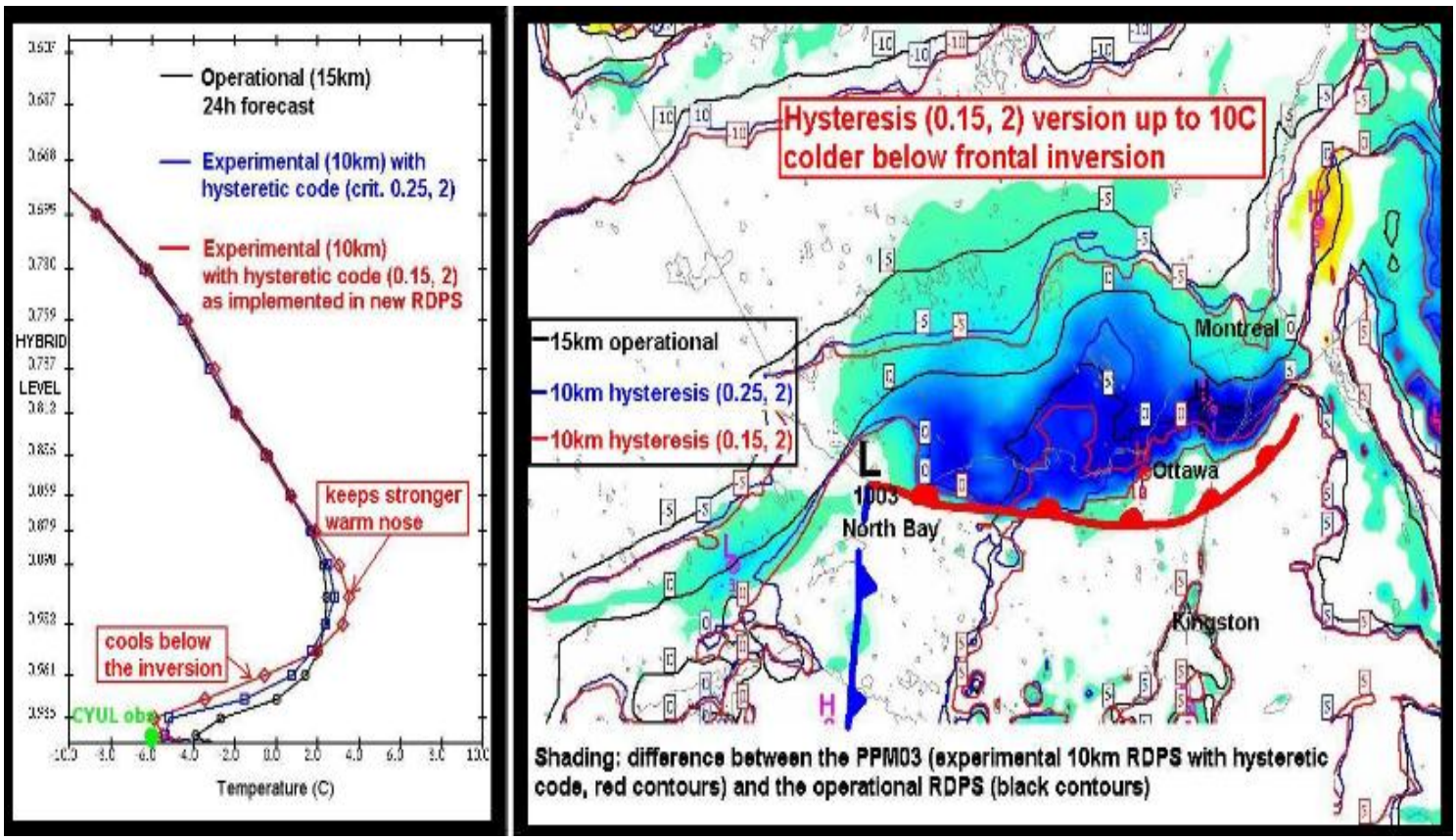

Figure 13*: Extract from Charles Creese CMOS 2012 presentation. February 1st 2012 case. Left : 24hr forecast temperature profiles near Montreal. Right : difference in 2m temperature due to hysteresis effect of 24 h forecasts.*

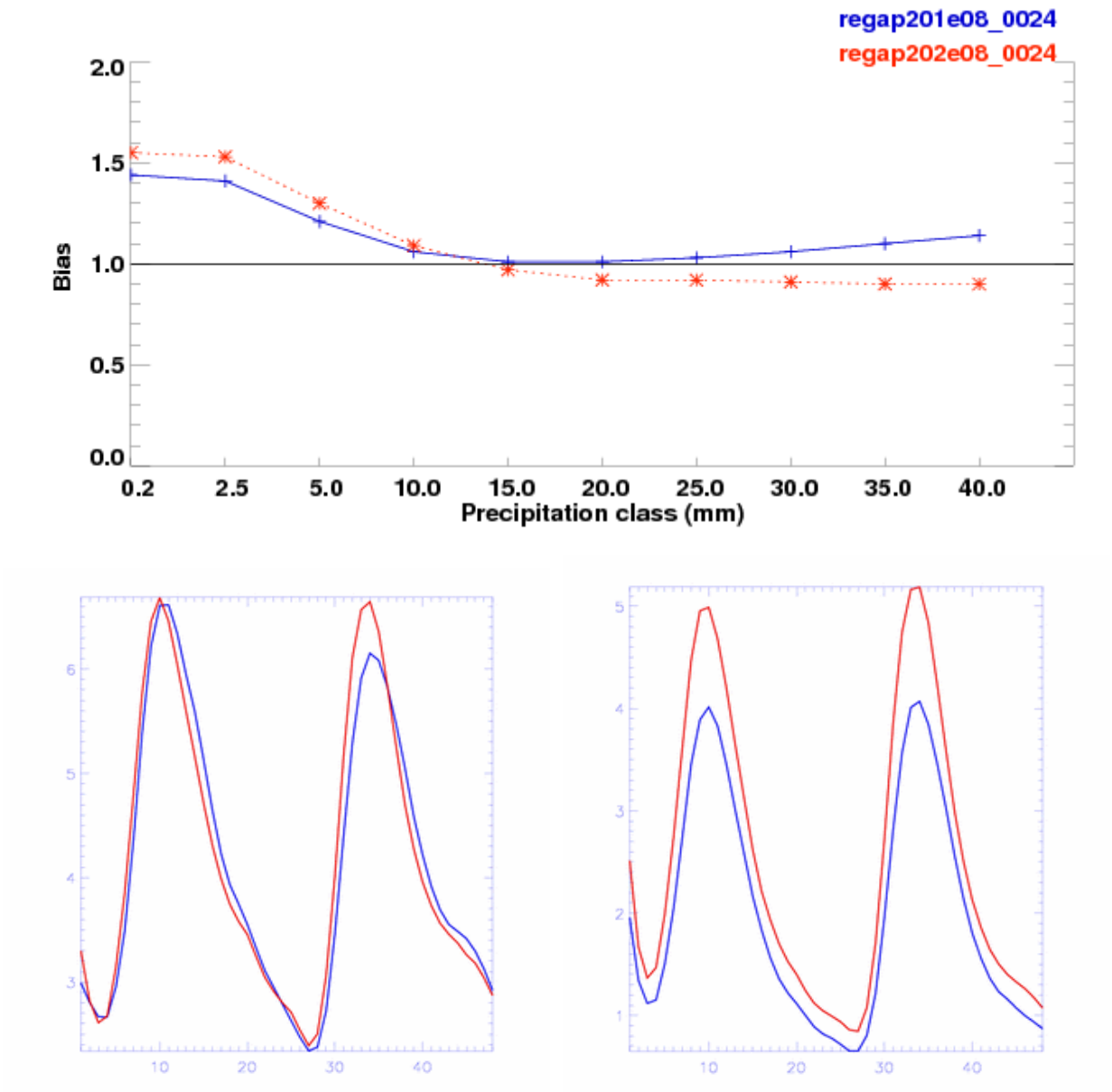

***Figure 14**: Top: Day 1 (0-24hr) precipitation verification against SHEF network (continental US) for summer 2008, valid at 1200 UTC. Bias of occurrence as a function of threshold. In blue, 10 km RDPS with Wt=18cm/s. In red, 10 km RDPS with Wt=12cm/s. Bottom: 1hr averages of precipitation rate in mm/day as a function of lead time up to 48 hrs (only 1200 UTC runs). Average over summer 2008 for the continental US. Bottom left: total precipitation. Bottom right: convective precipitation. Note the varying scales on the ordinates.*

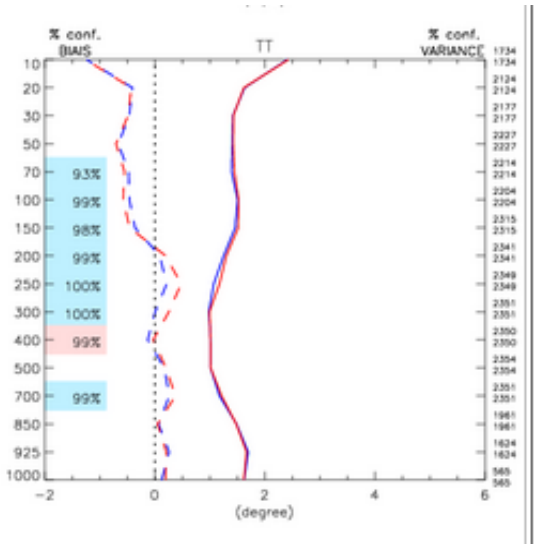

Figure 15*: Bias (dash) and rms errors of temperature against radiosonde network over the continental US. Bias=Model-Obs. In blue, 10 km RDPS with Wt=18cm/s. In red, 10 km RDPS with Wt = 12 cm/s. Ordinate is in mb, abscissa in Celsius*

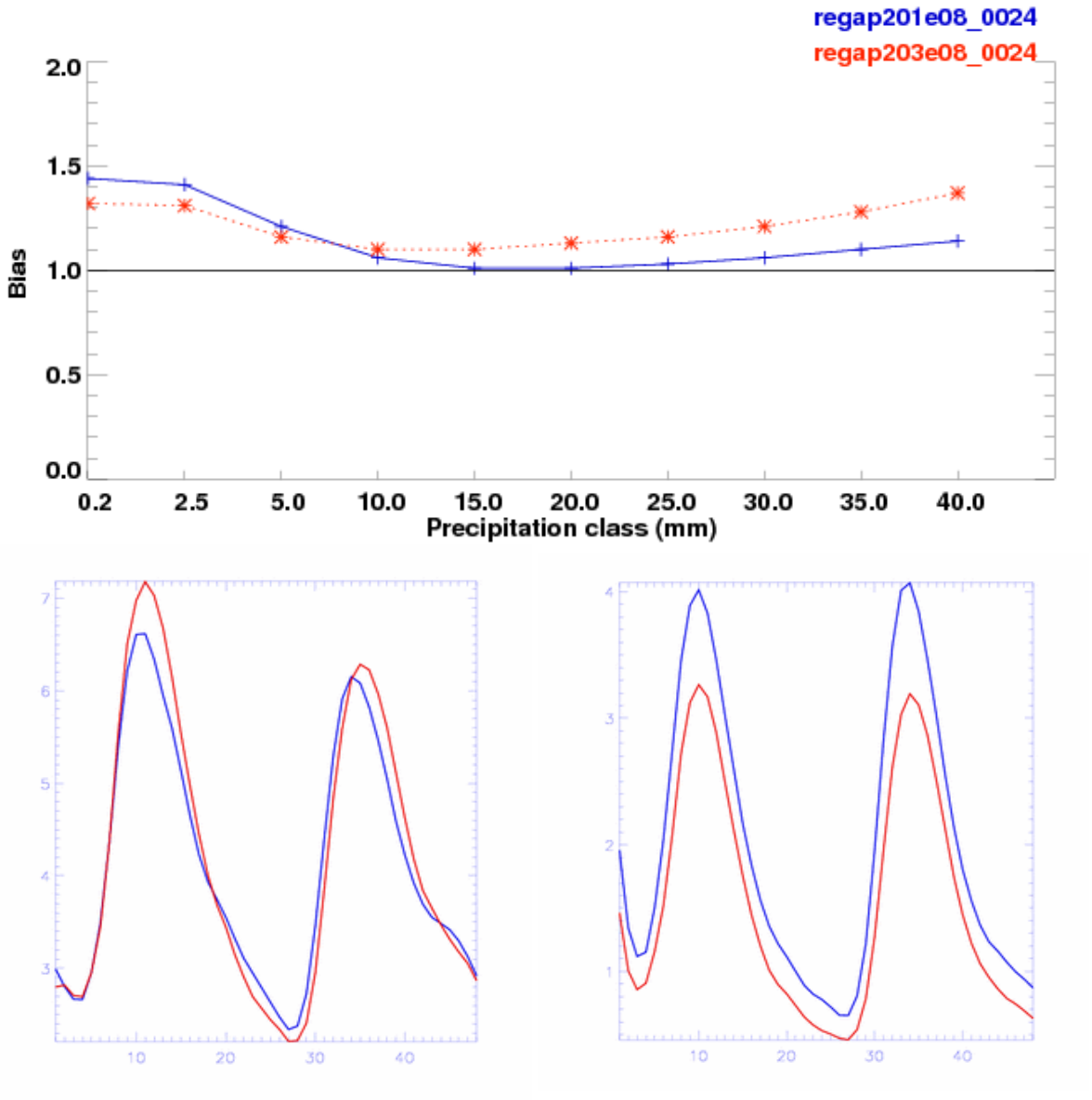

***Figure 16**: Same as **Figure 14**, except red curves are for 10 km RDPS with Wt=27cm/s.*

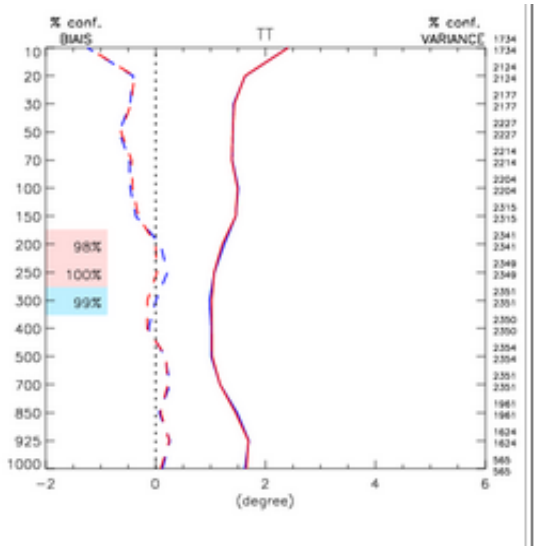

Figure 17*: Same as* ***Figure 15****, except red curves are for 10 km RDPS with Wt=27cm/s.*

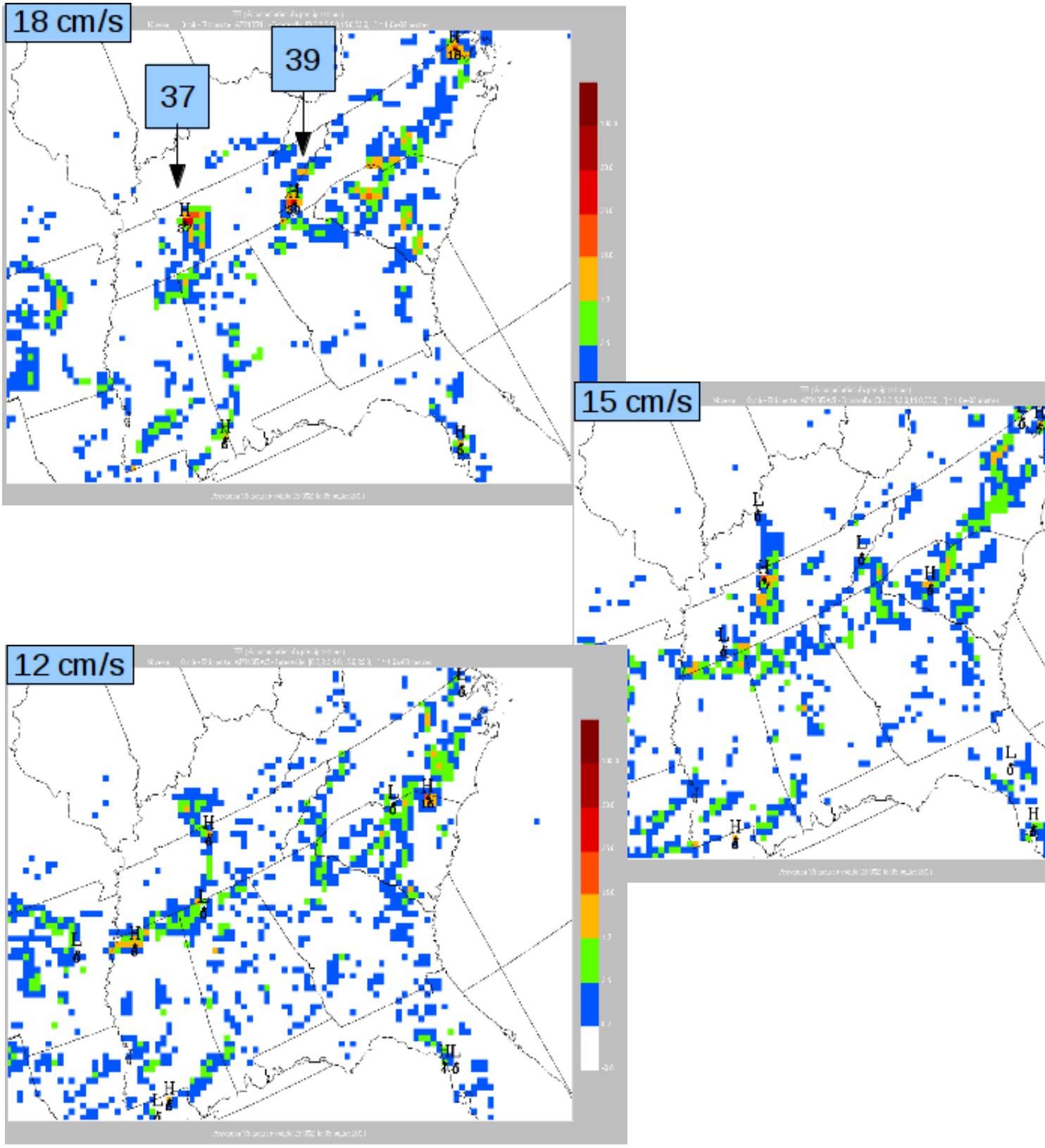

***Figure 18**: Precipitation rate (mm/hr) averaged over 1hr at lead time of 35 hours valid on 20110705-2300 UTC for three values of Wt.*

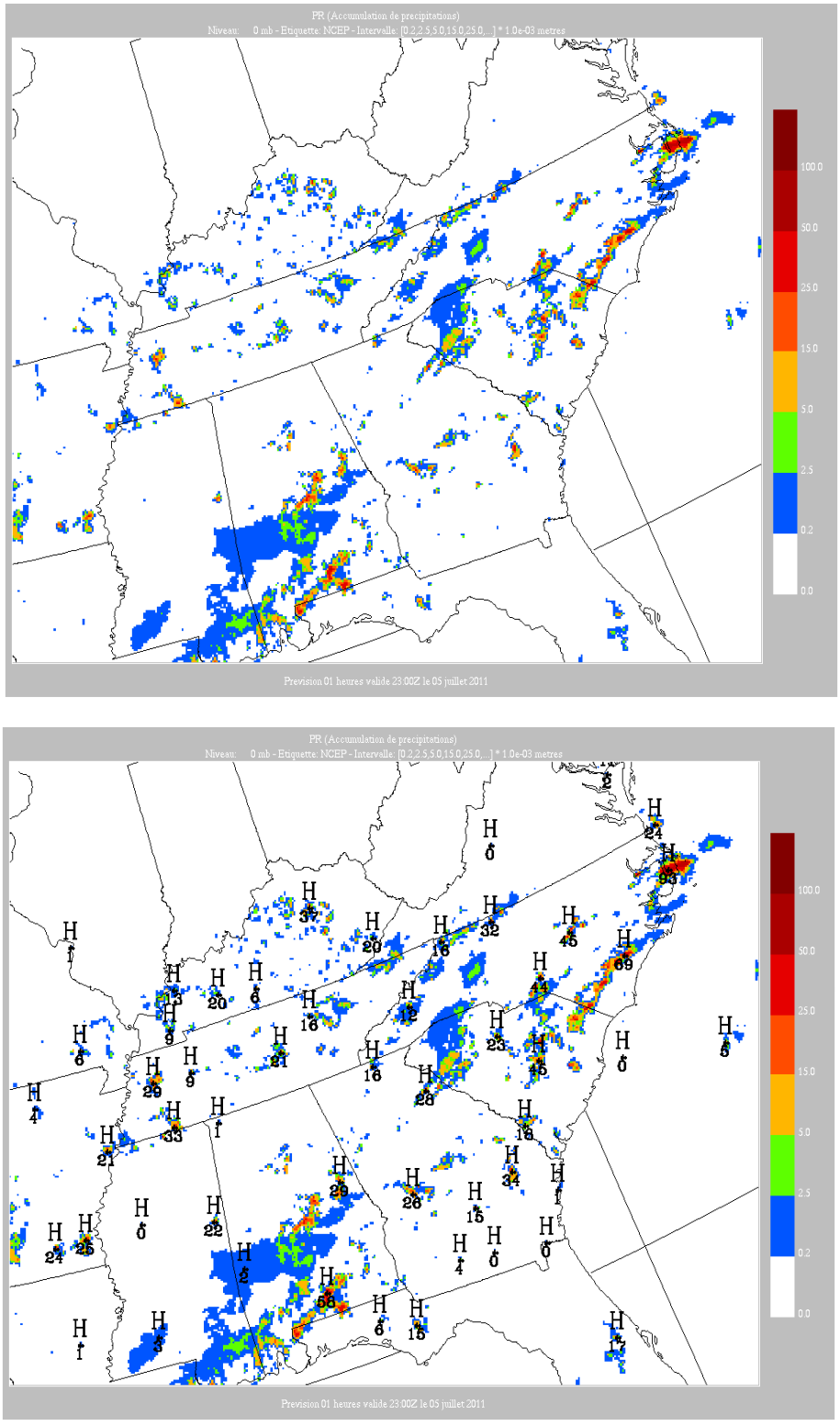

***Figure 19**: Same as for **Figure 18** except based on the precipitation analysis from NCEP`s Stage IV product. Both panels are the same except local extrema are shown on the bottom panel.*

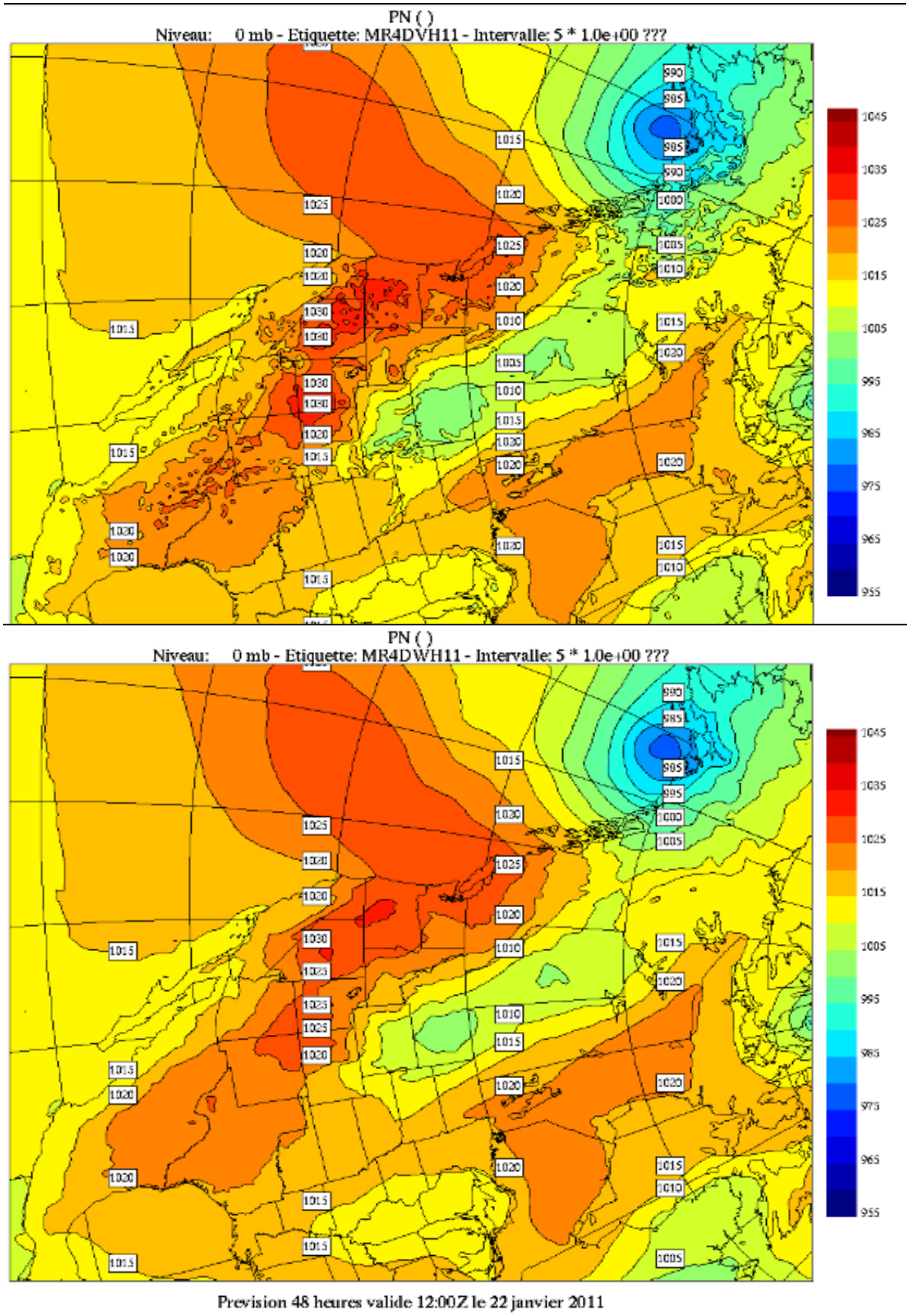

***Figure 20**: Sea level pressure calculated with old algorithm (top) and new algorithm (bottom).*

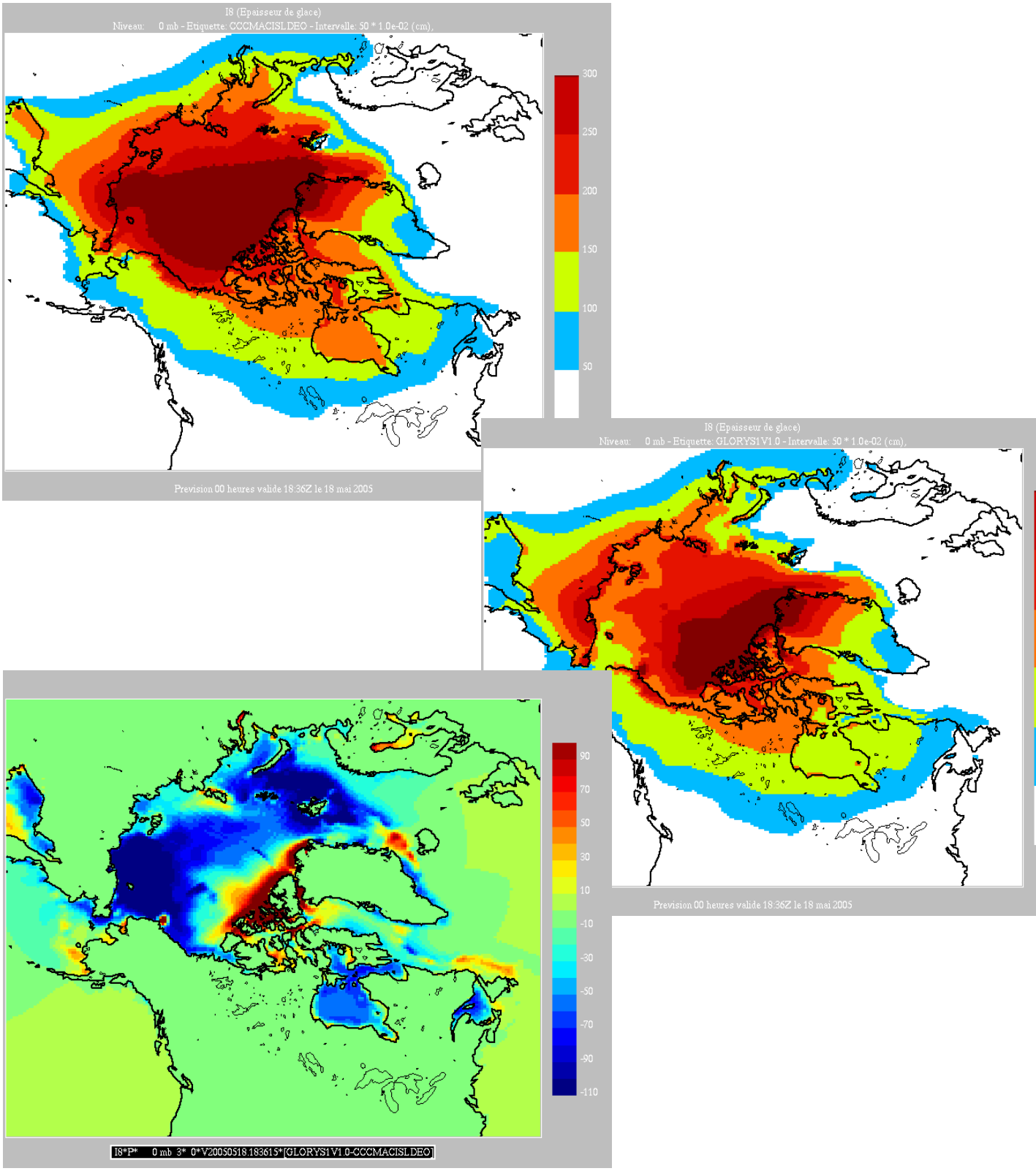

Figure 21*: Climatology of sea ice thickness (cm) for the month of march. Top: RDPS-200. Right: RDPS-300. Bottom: Difference.*

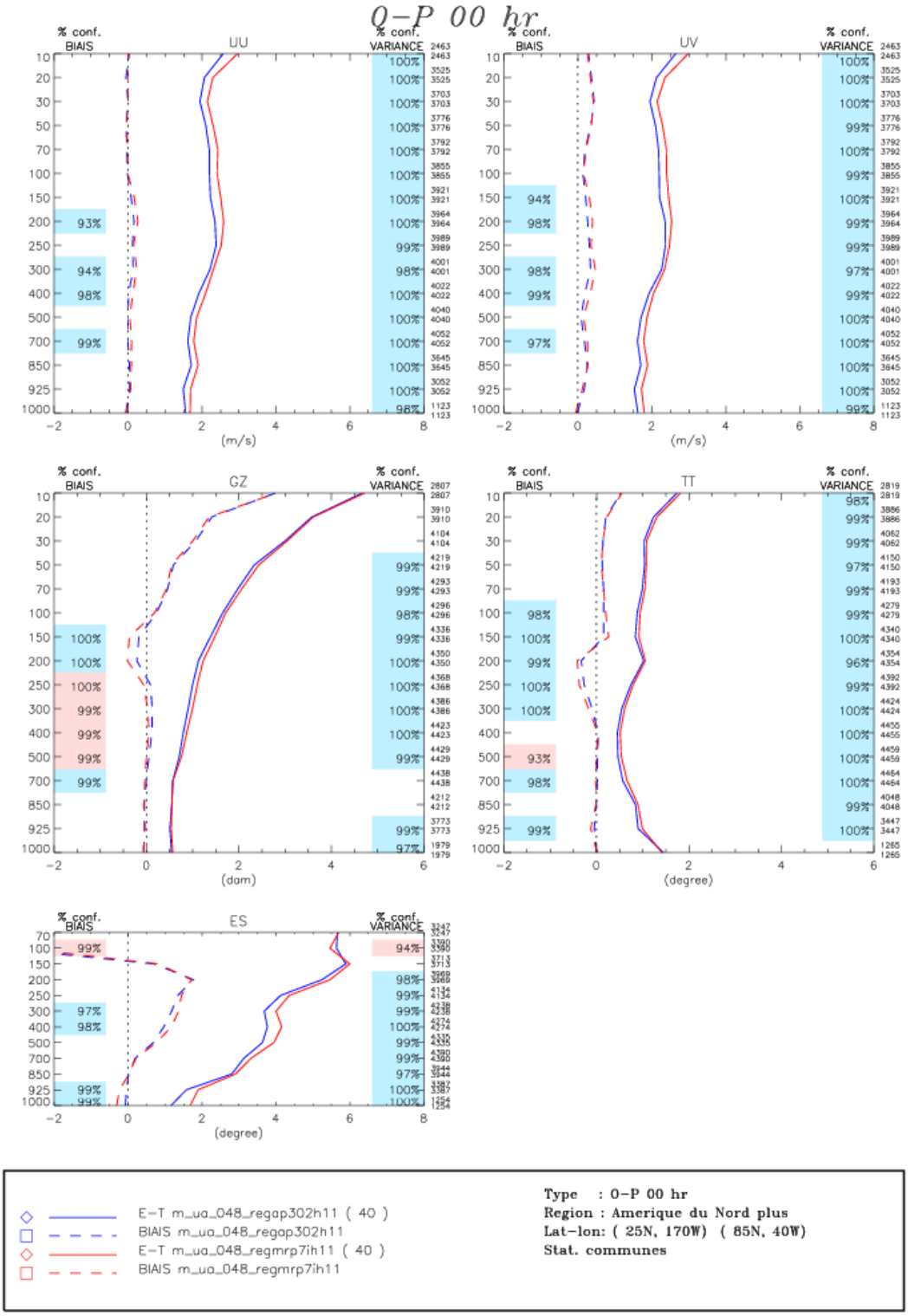

***Figure 22**: Mean forecast verification scores against radiosondes over North America at a lead time of 0 for the period 20 January 2011, 12Z - 20 March 2011, 00Z for the (blue) control and (red) experimental configurations of the RDPS. Plot essentially shows the fit of the analyses to radiosonde observations. Dashed (continuous) curves correspond to bias (standard deviation). Shaded boxes on the left (right) side show the confidence interval, if greater than 90%, for the bias (standard deviation).*

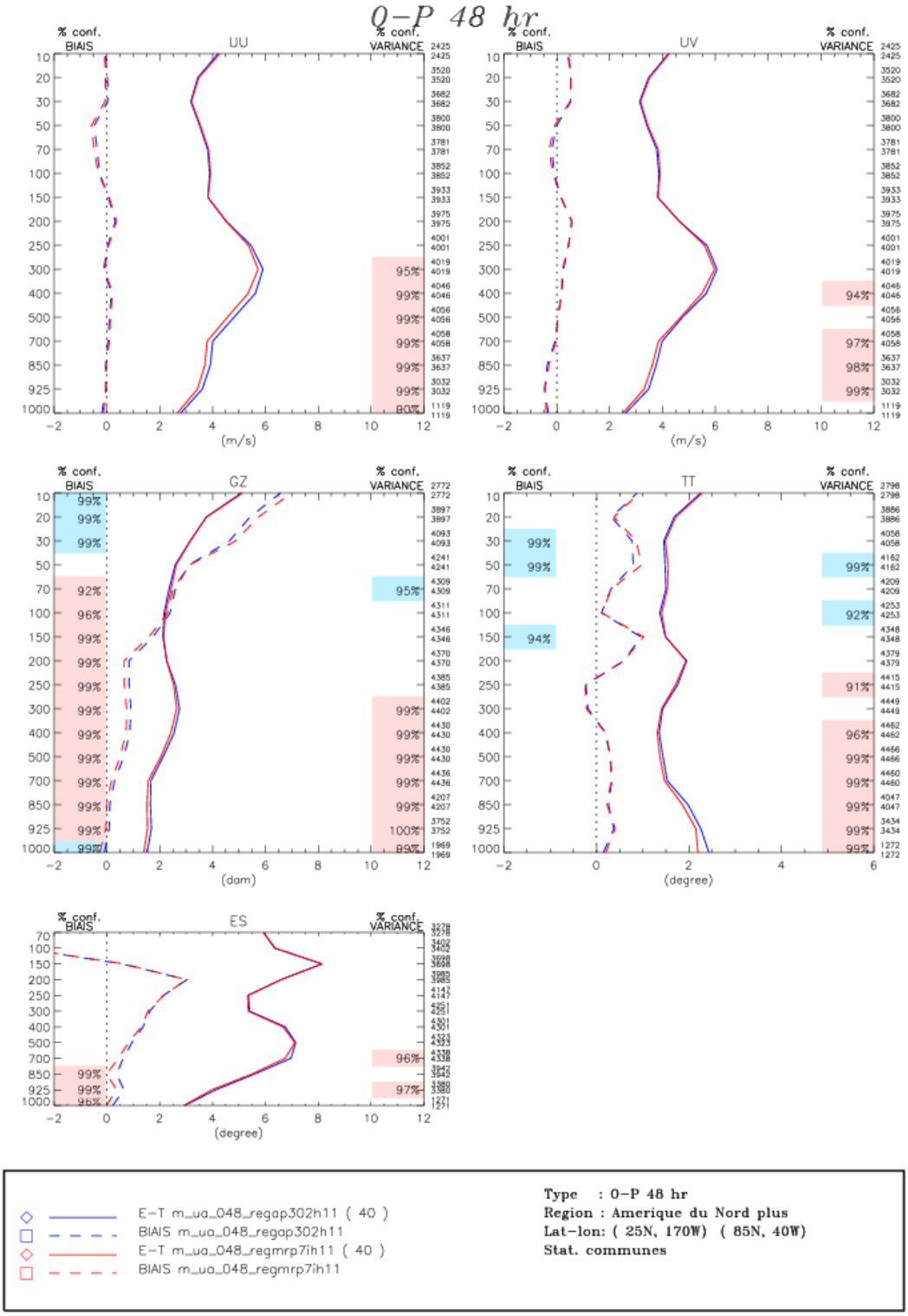

***Figure 23**: Same as **Figure 22** but at a forecast lead time of 48 hours. Plot essentially demonstrates the accuracy of the 48-hour forecasts over North America.*

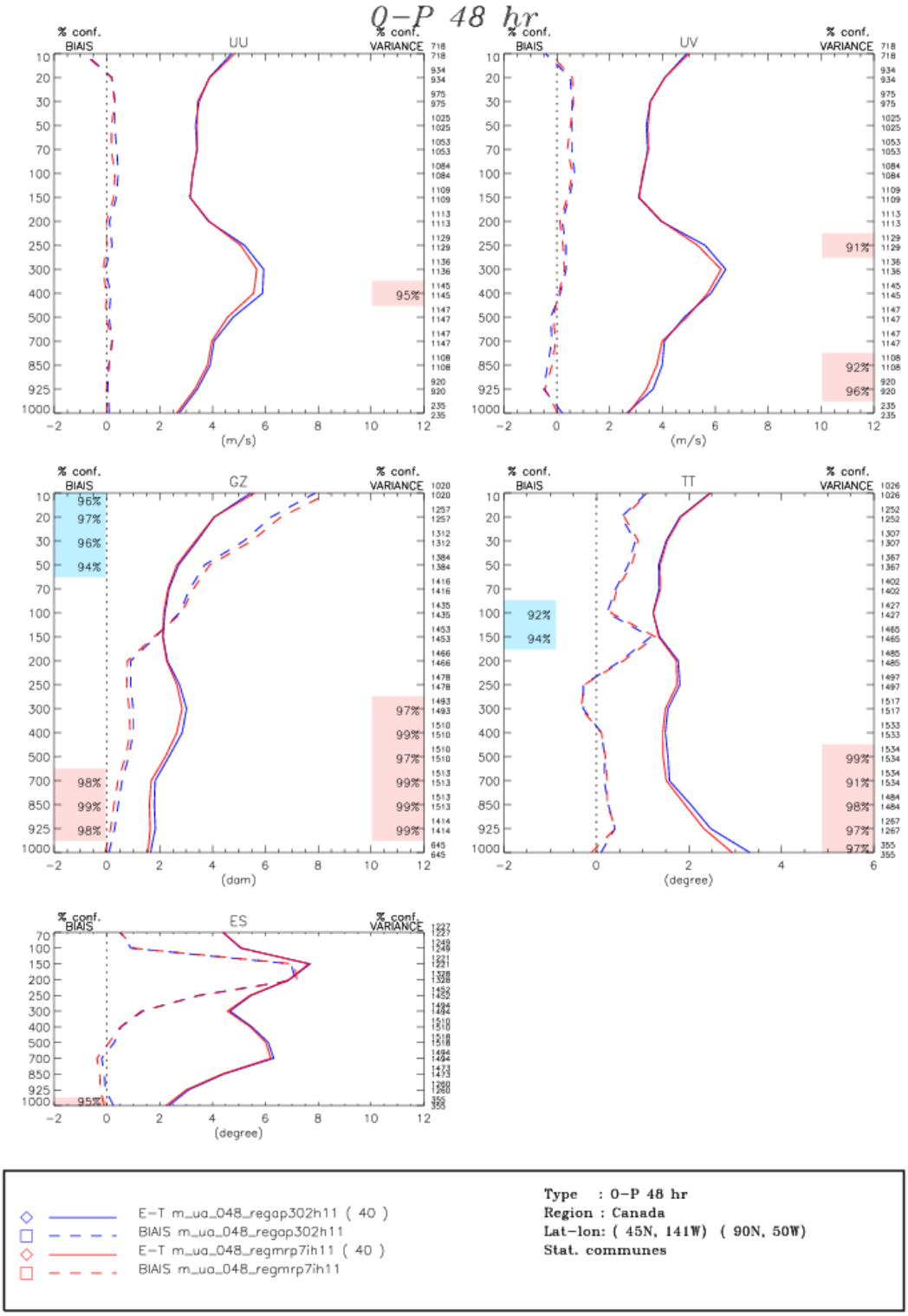

***Figure 24**: Same as **Figure 23** but over Canada.*

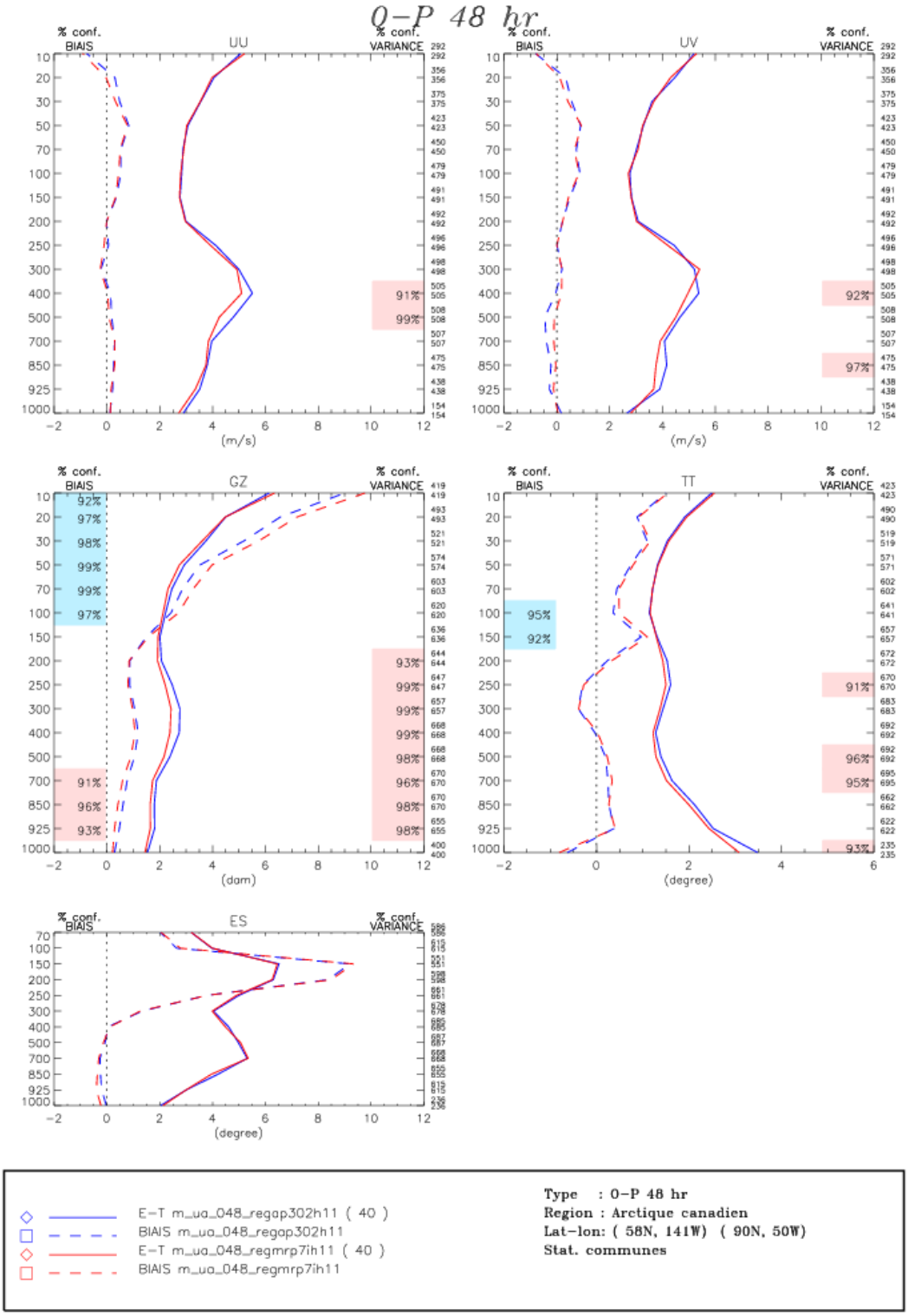

***Figure 25**: Same as **Figure 23** but over the Canadian Arctic.*

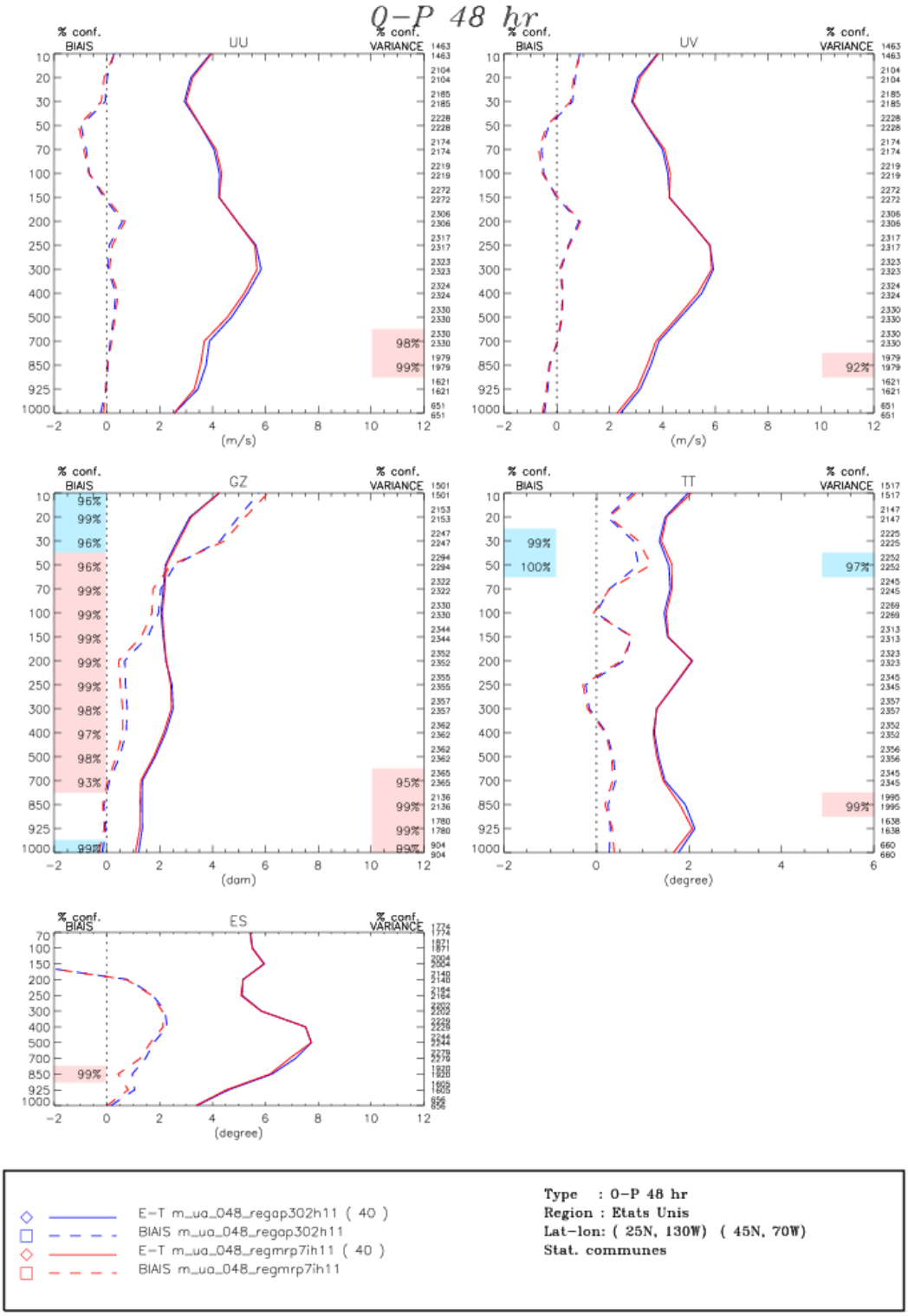

***Figure 26**: Same as **Figure 23** but over the continental United States.*

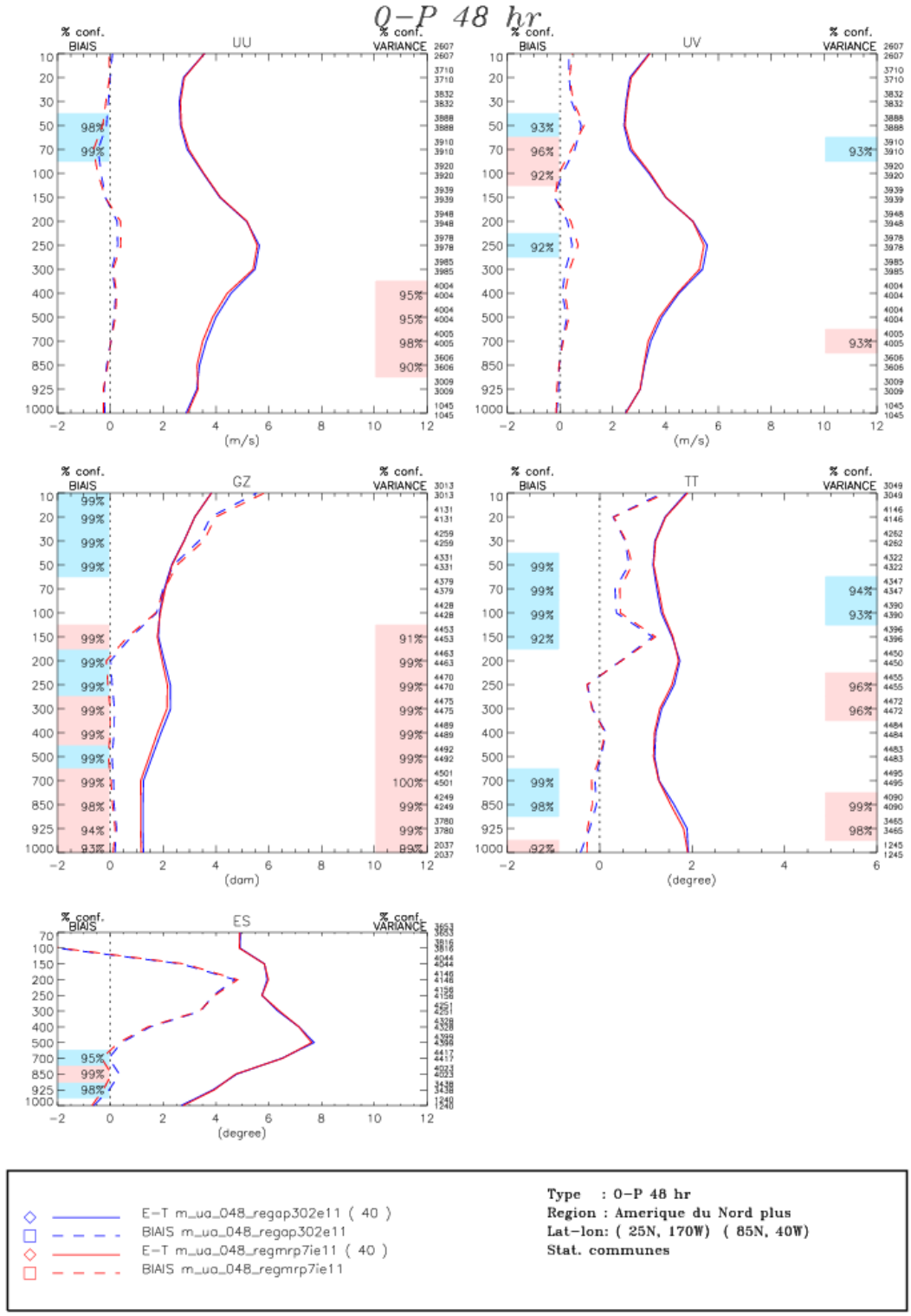

***Figure 27**: Same as **Figure 23** but for the summer period, i.e. 15 May 2011, 12Z - 13 July 2011, 00Z.*

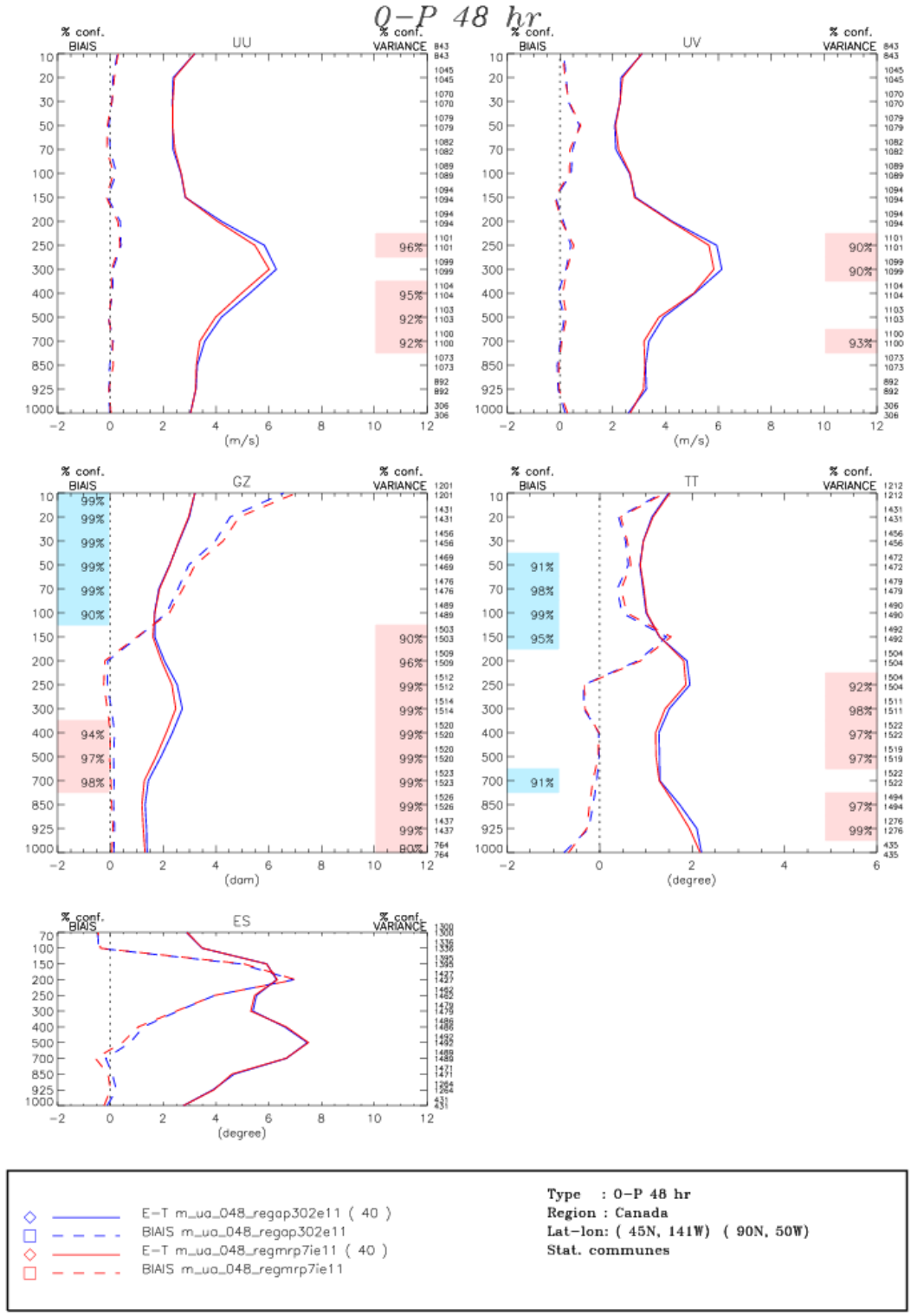

***Figure 28**: Same as **Figure 27** but over Canada.*

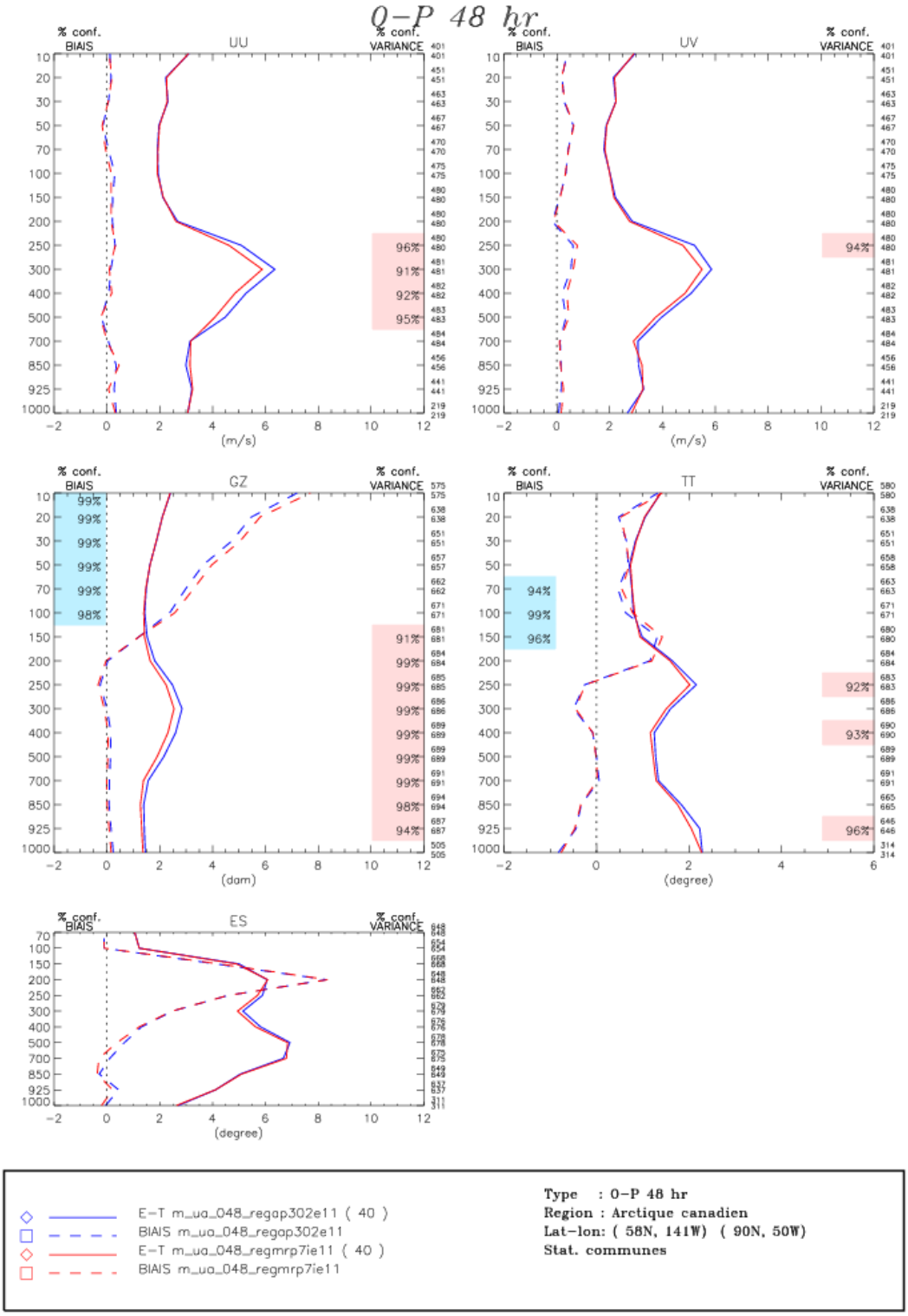

***Figure 29**: Same as **Figure 27** but over the Canadian Arctic.*

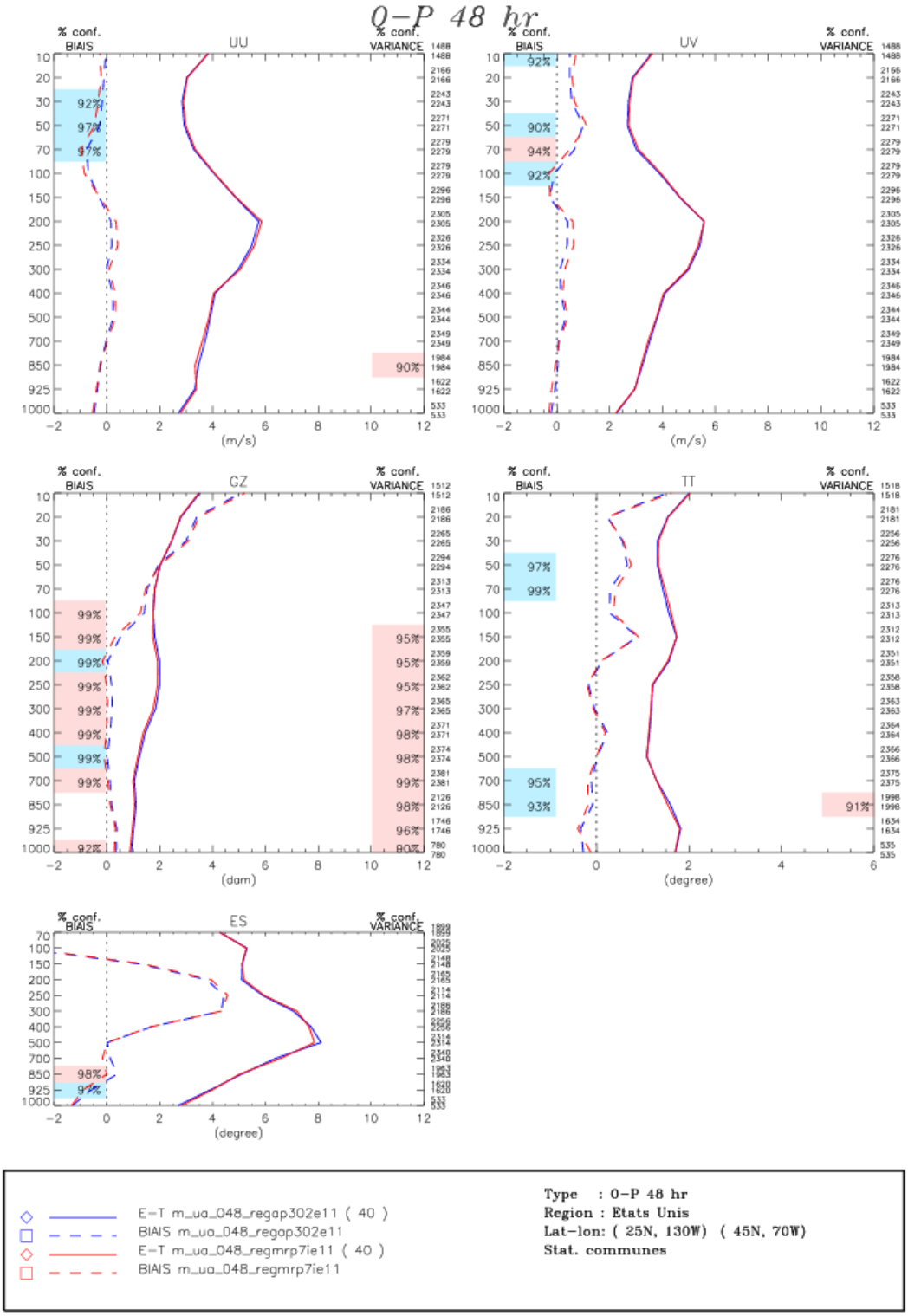

***Figure 30**: Same as **Figure 27** but over the continental United States.*

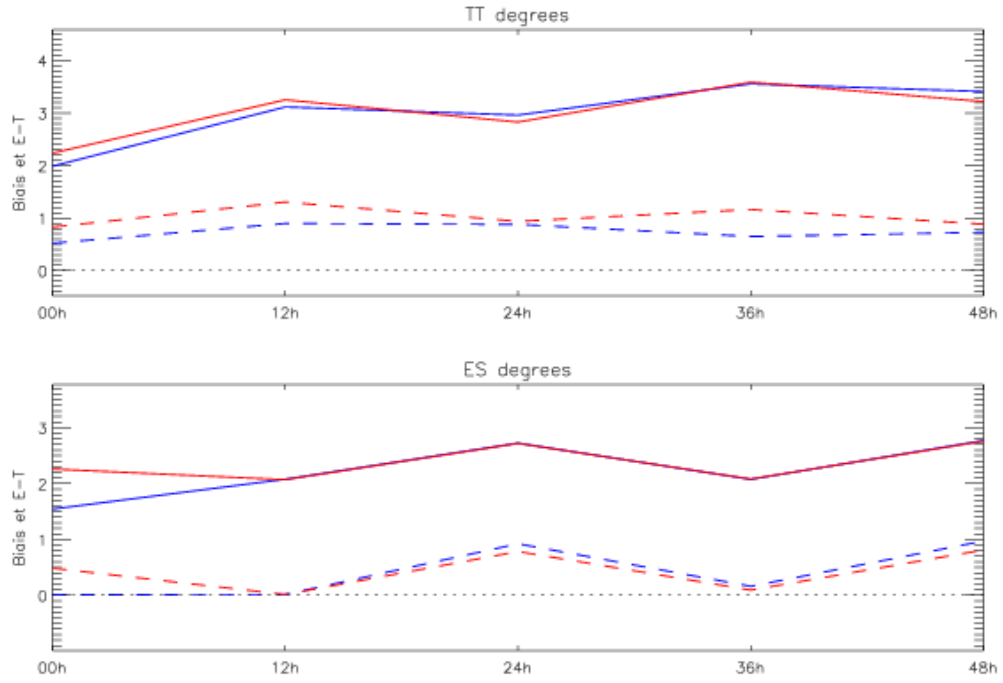

Figure 31**: Mean forecast verification against surface stations over North America as a function of forecast lead time for the period 20 January 2011, 12Z - 20 March 2011, 00Z for the (blue) control and (red) experimental configurations of the Regional forecast system, corresponding to the operational and parallel runs, respectively. **(Dashed (continuous) curves correspond to bias (standard deviation)).

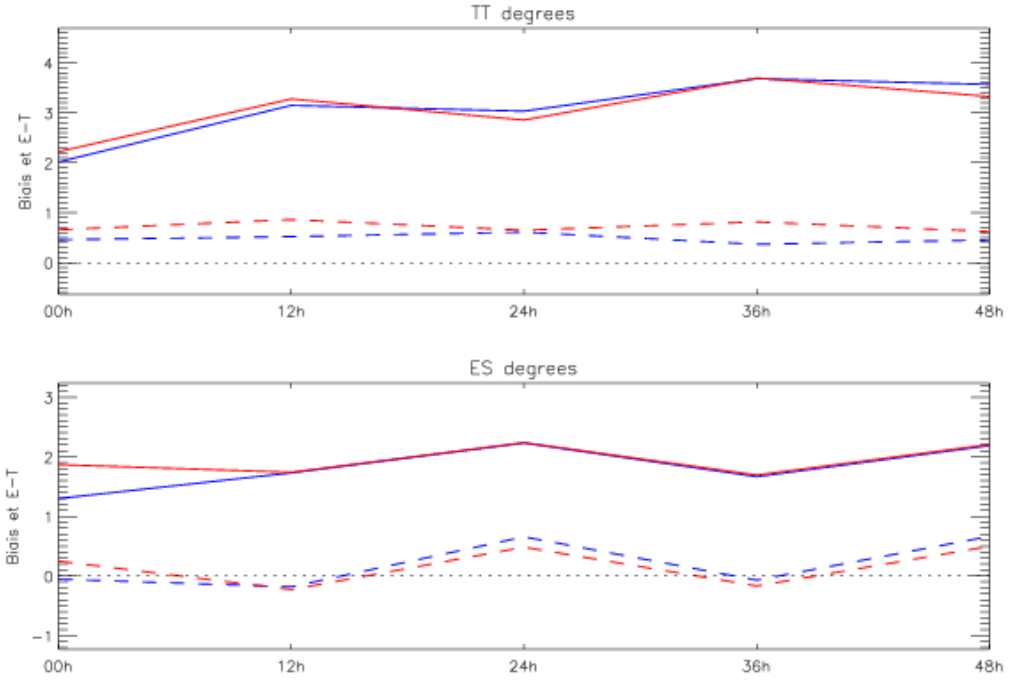

***Figure 32**: Same as **Figure 31** but over Canada.*

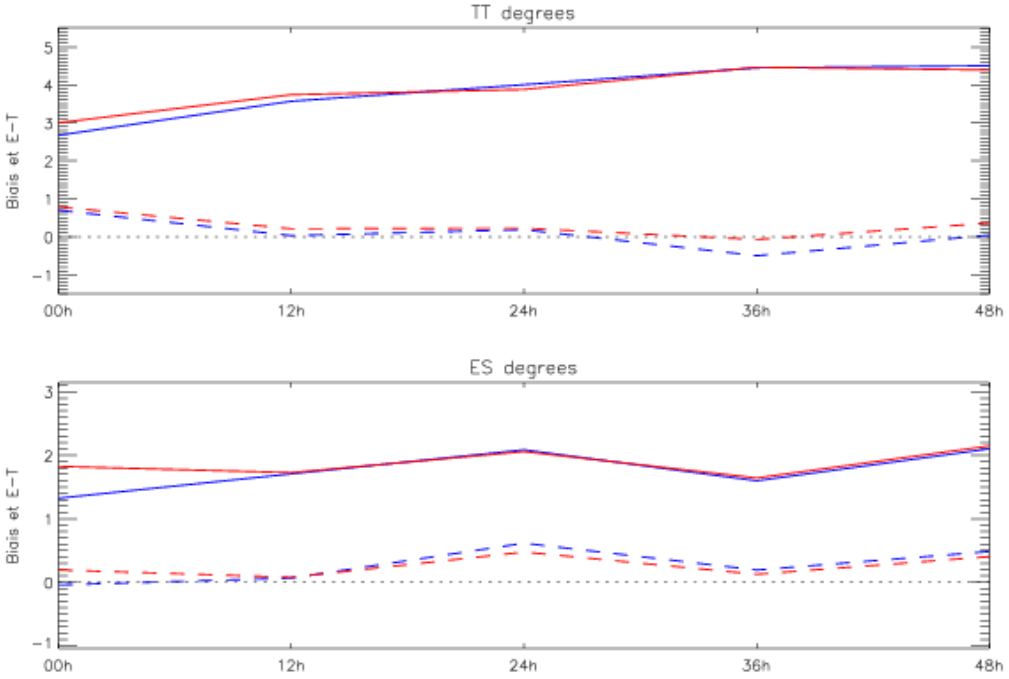

***Figure 33**: Same as **Figure 31** but over the Canadian Arctic.*

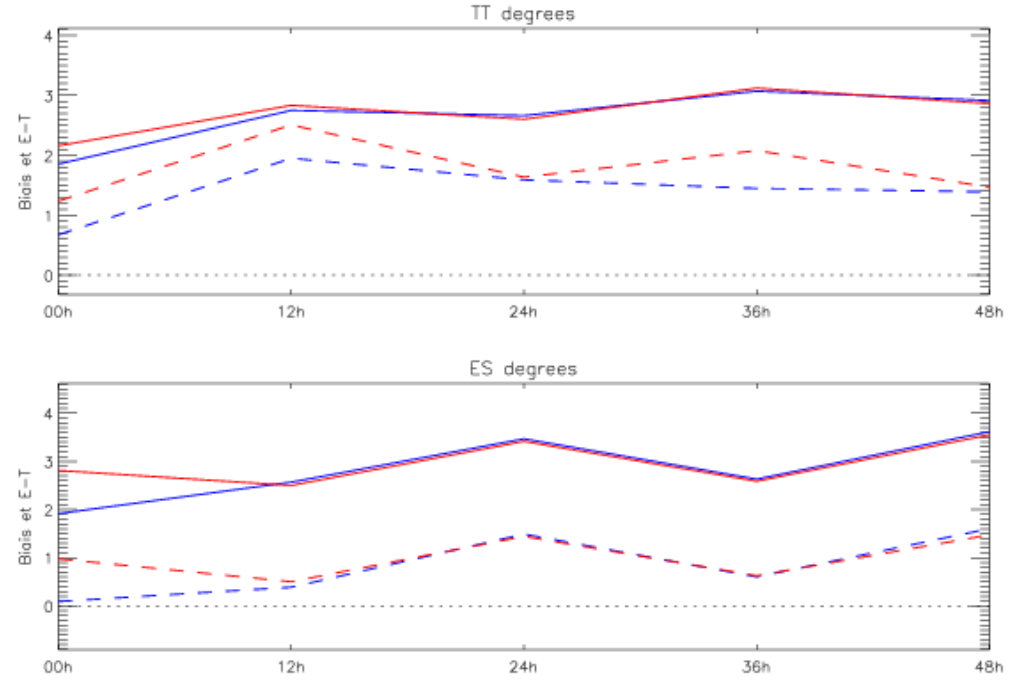

***Figure 34**: Same as **Figure 31** but over the United States.*

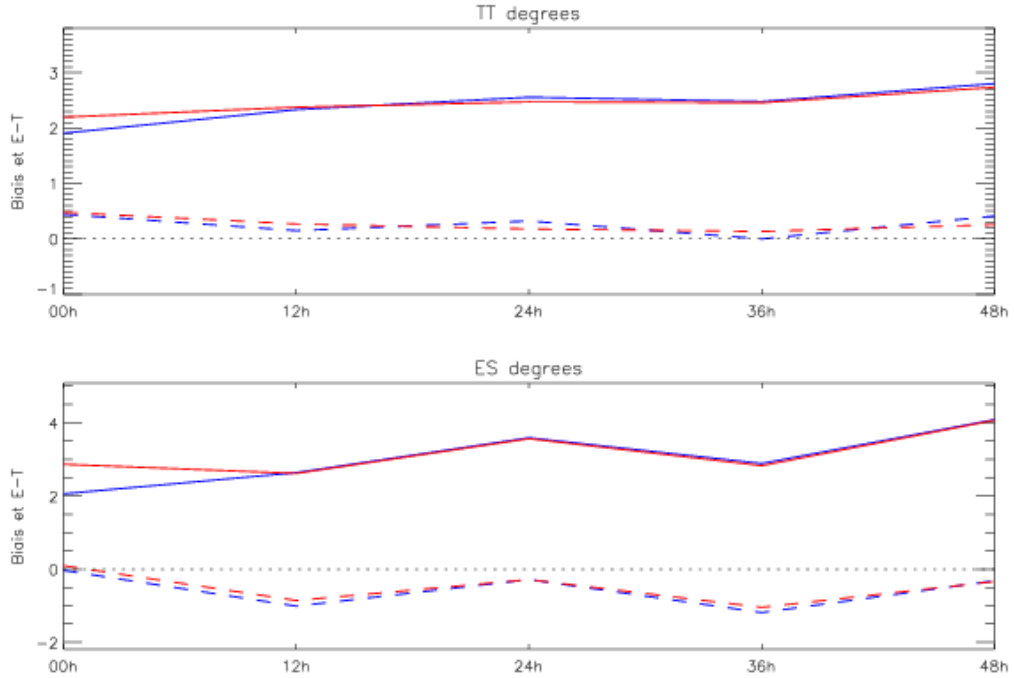

***Figure 35**: Same as **Figure 31** but for the summer period, i.e. 15 May 2011, 12Z - 13 July 2011, 00Z.*

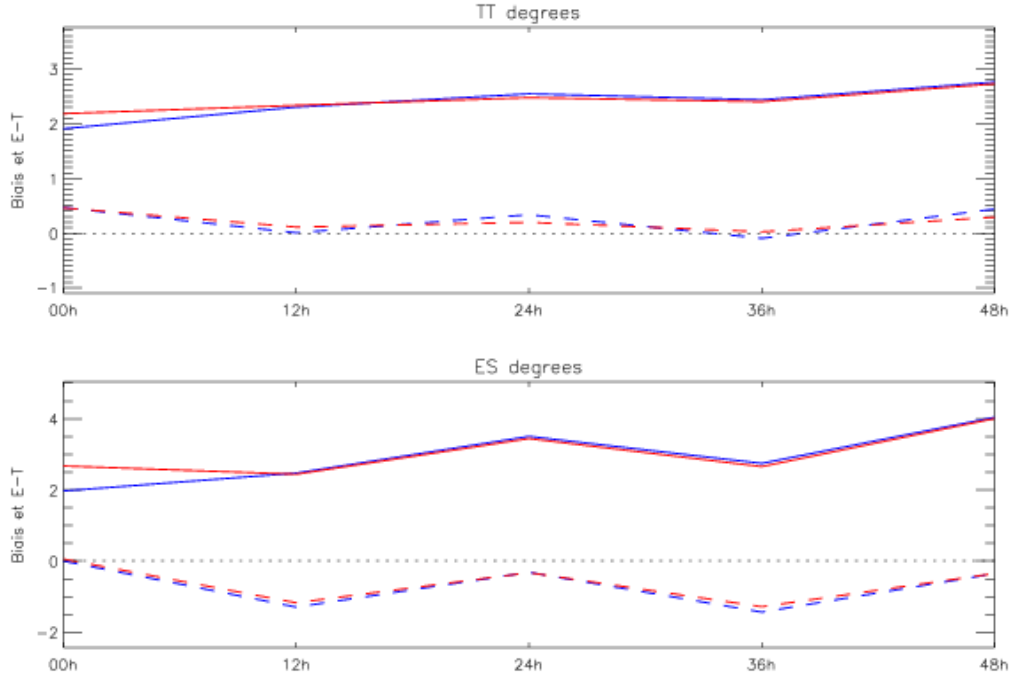

***Figure 36**: Same as **Figure 35** but over Canada.*

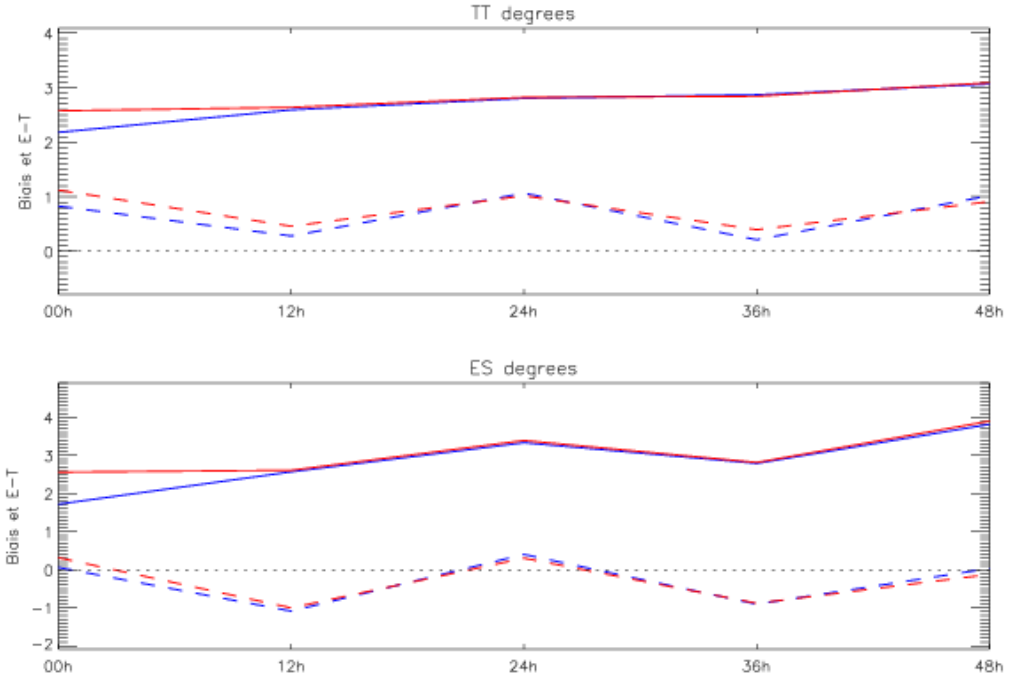

***Figure 37**: Same as **Figure 35** but over the Canadian Arctic.*

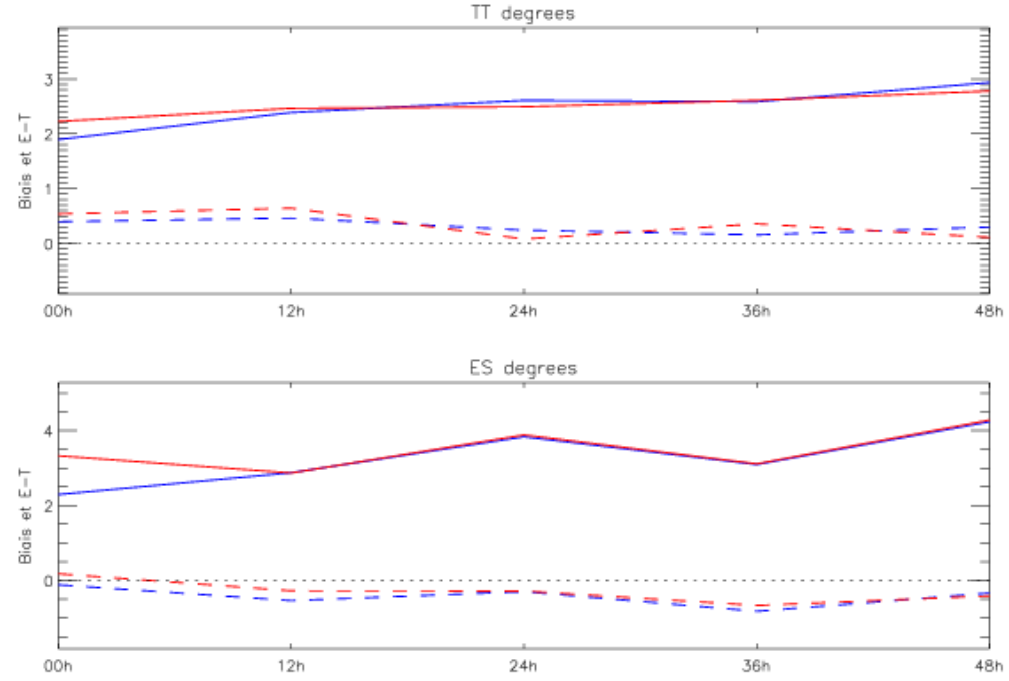

***Figure 38**: Same as **Figure 35** but over the United States.*

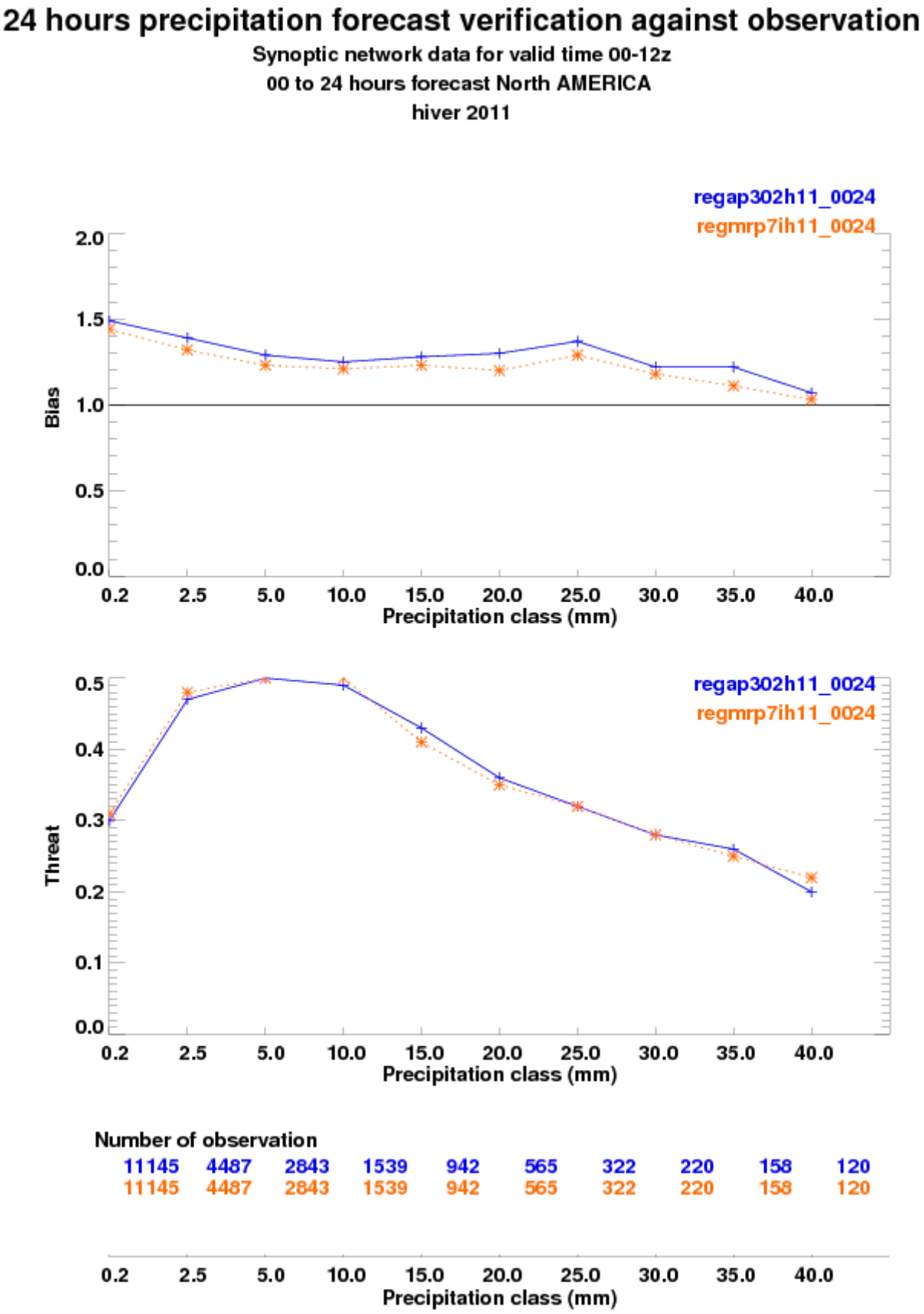

***Figure 39**: Winter precipitation scores against the SYNOP network over North America for 0-24 hours.*

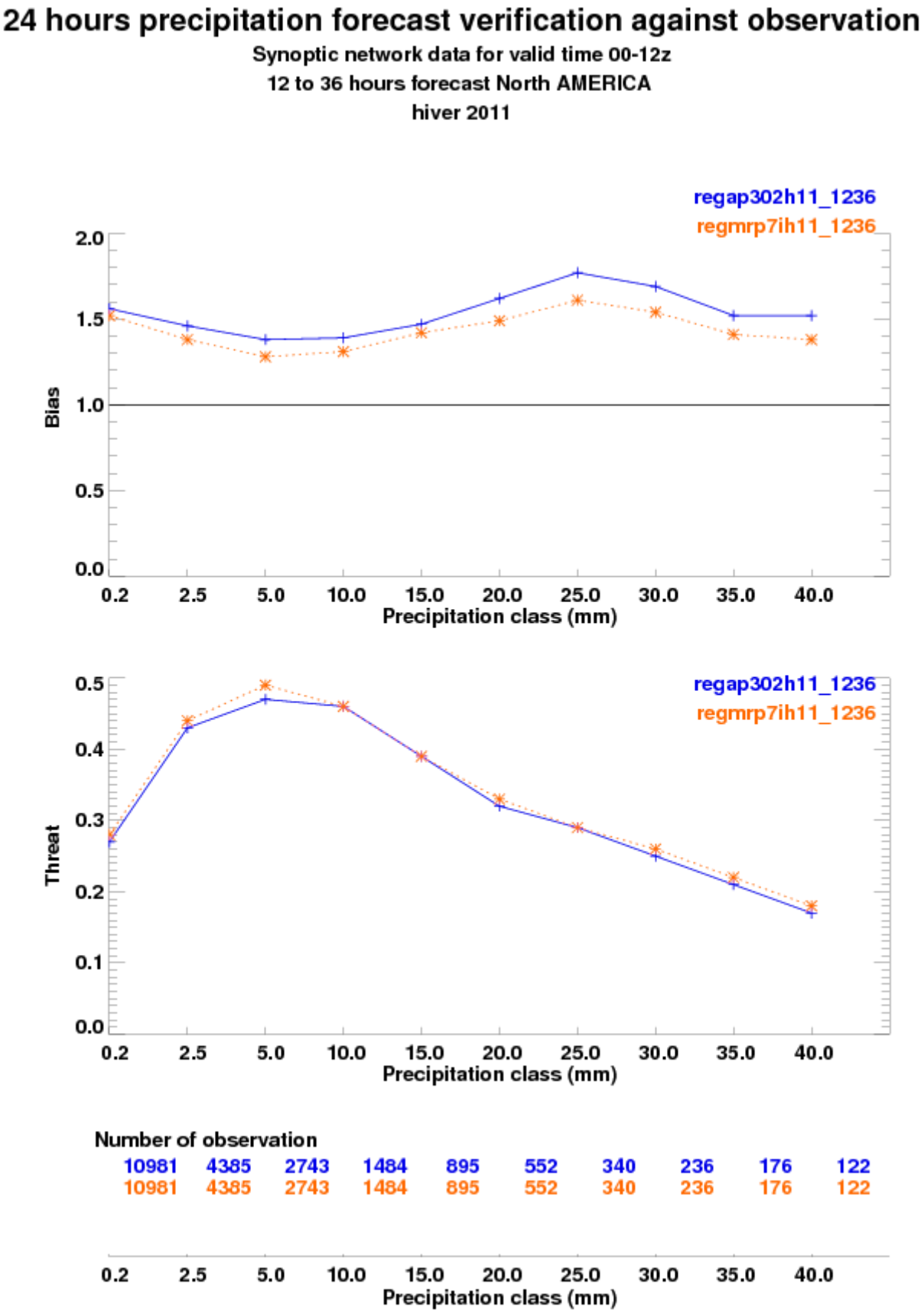

***Figure 40**: Same as **Figure 39** but for 12-36 hours.*

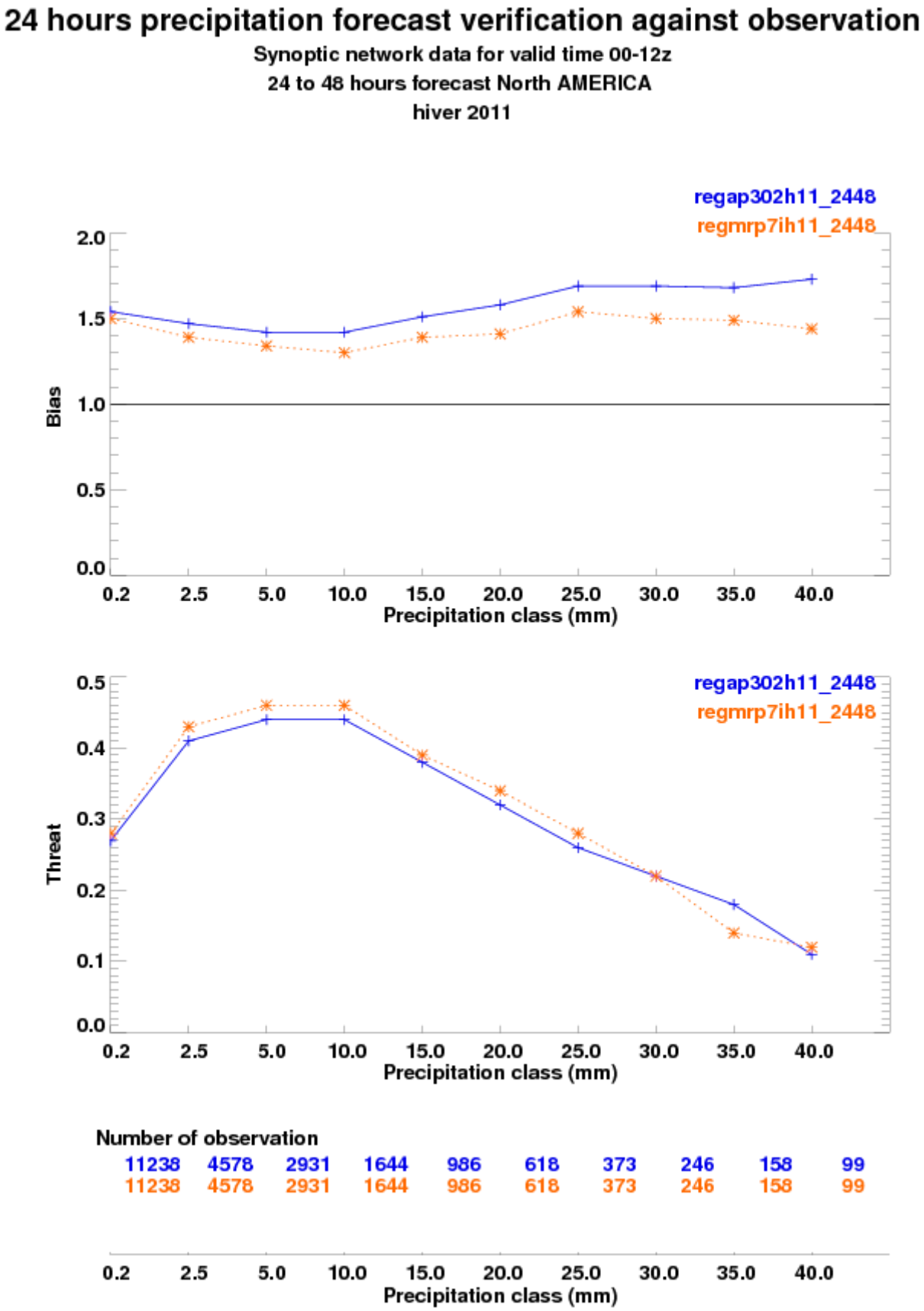

***Figure 41**: Same as **Figure 39** for 24-48 hours.*

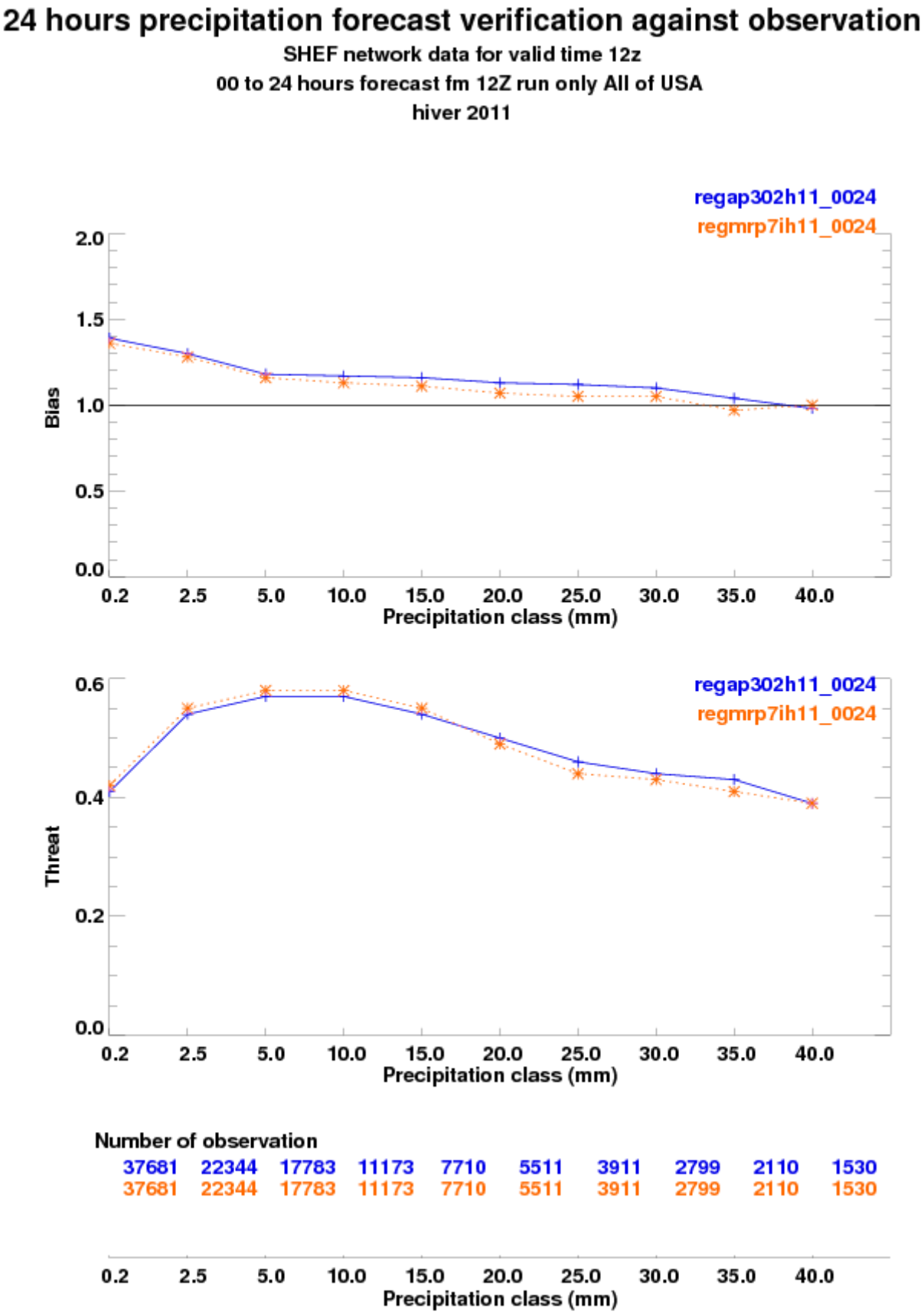

***Figure 42**: Winter precipitation scores against the SHEF network over the United States for 0-24 hours.*

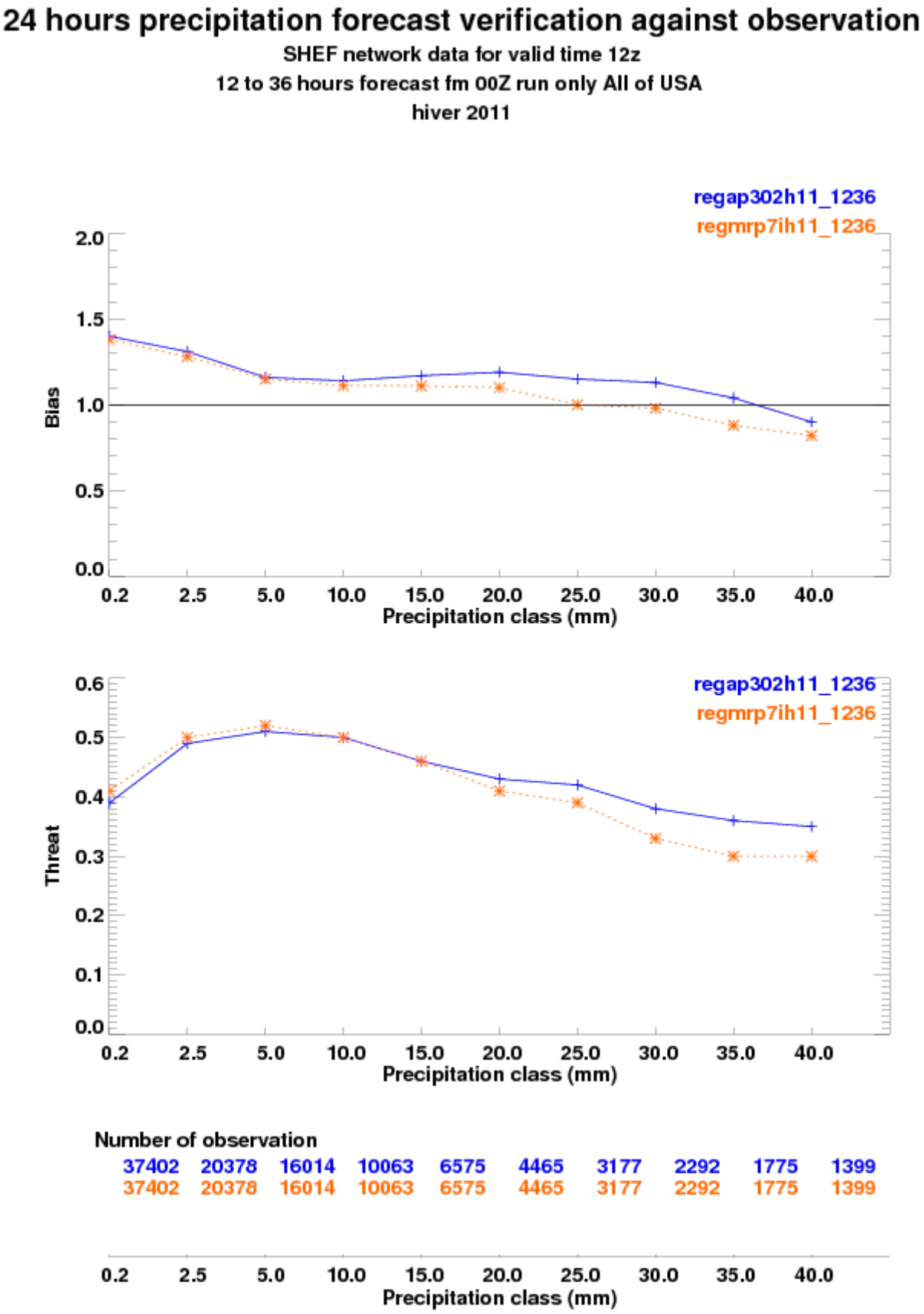

***Figure 43**: Same as **Figure 42** but for 12-36 hours.*

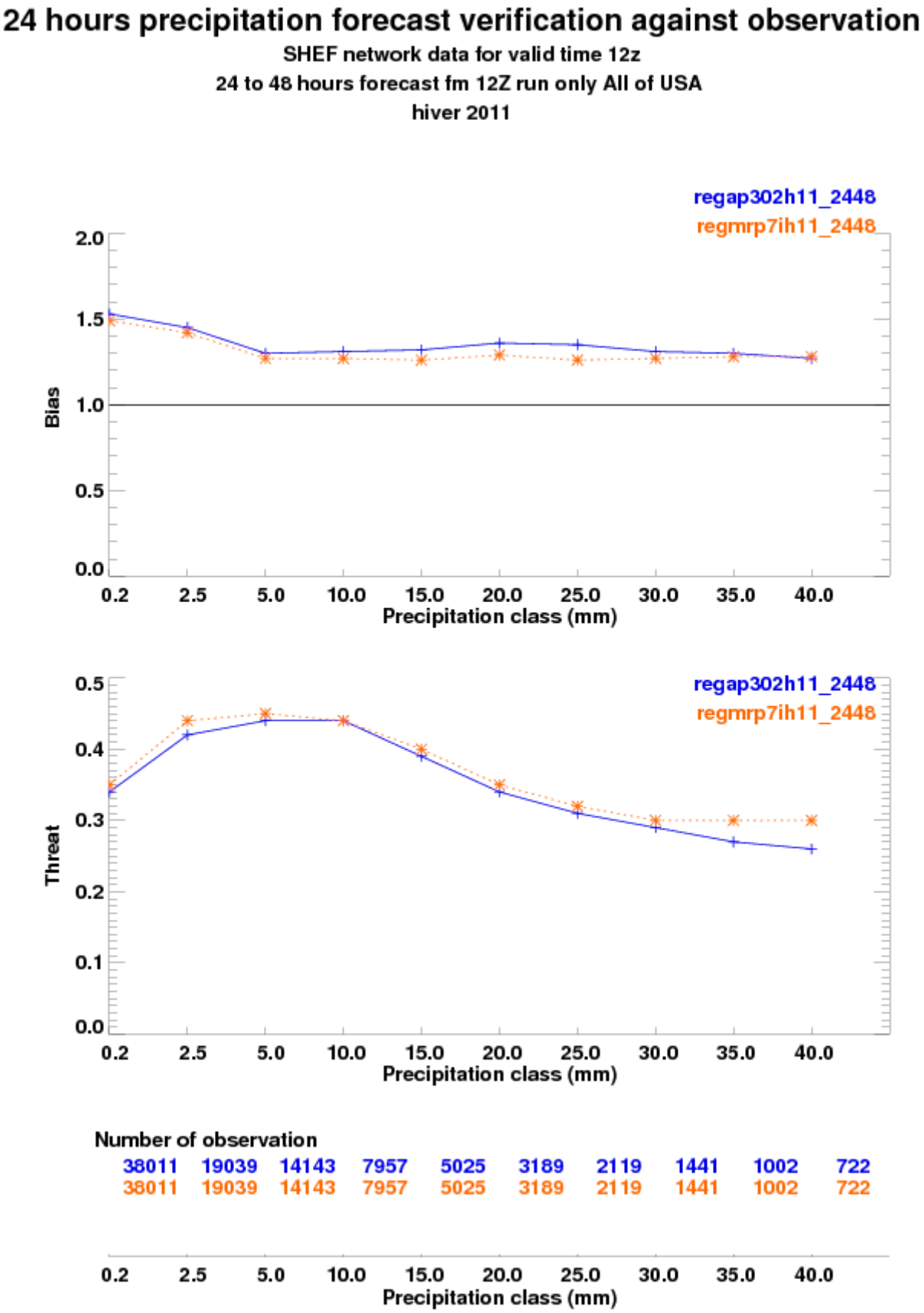

***Figure 44**: Same as **Figure 42** but for 24-48 hours.*

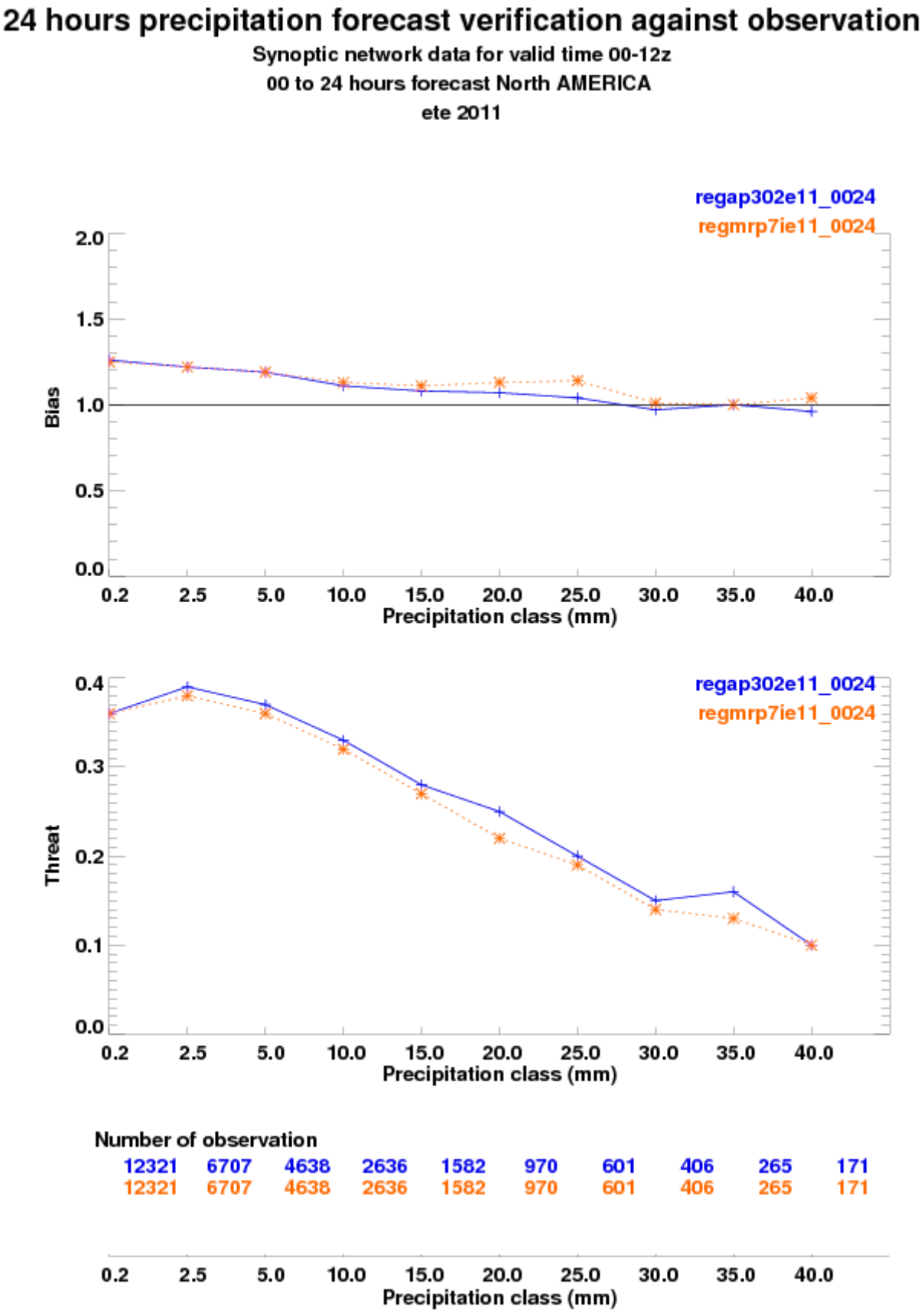

***Figure 45**: Summer precipitation scores against the SYNOP network over North America for 0-24 h.*

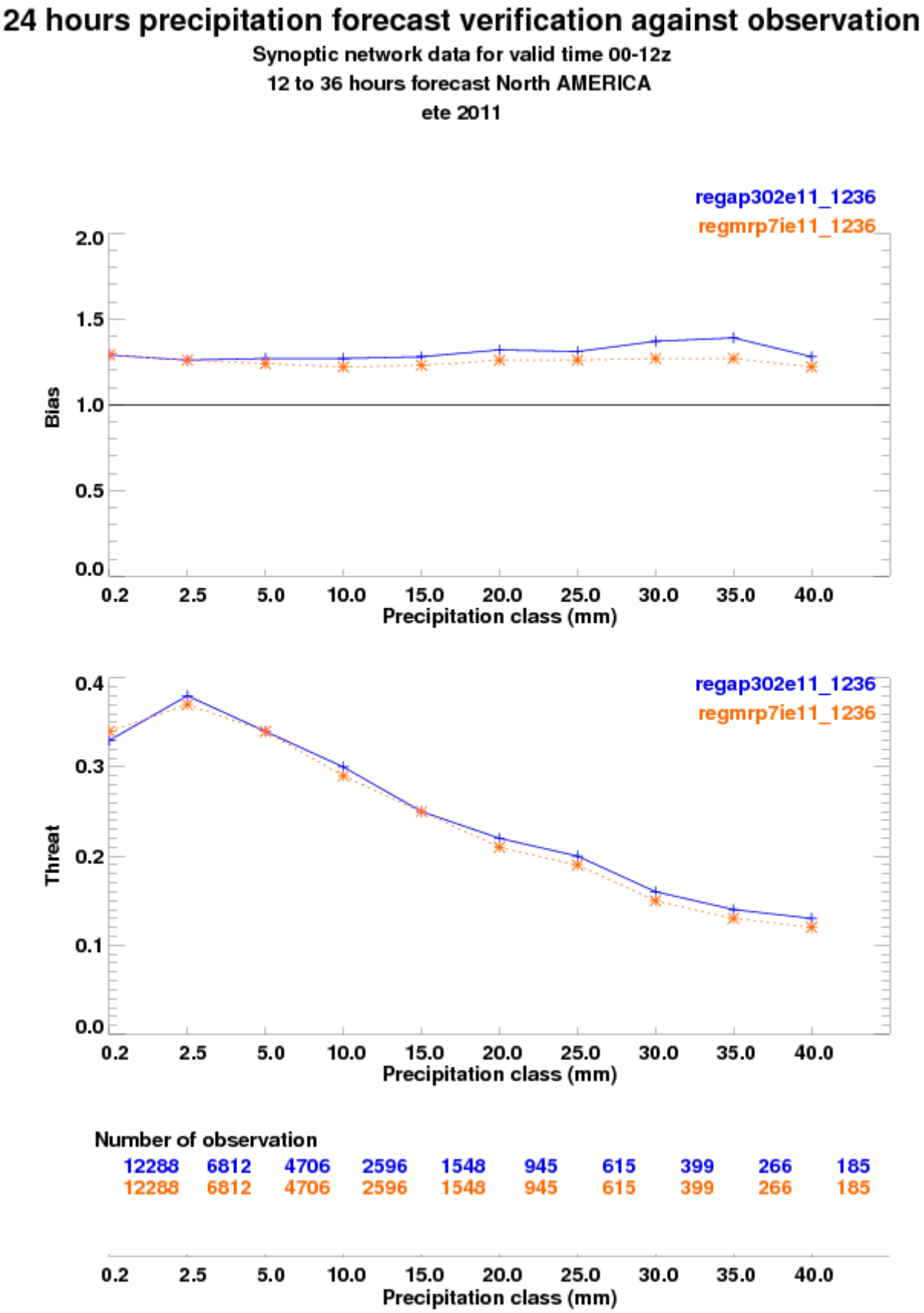

***Figure 46**: Same as **Figure 45** but for 12-36 h.*

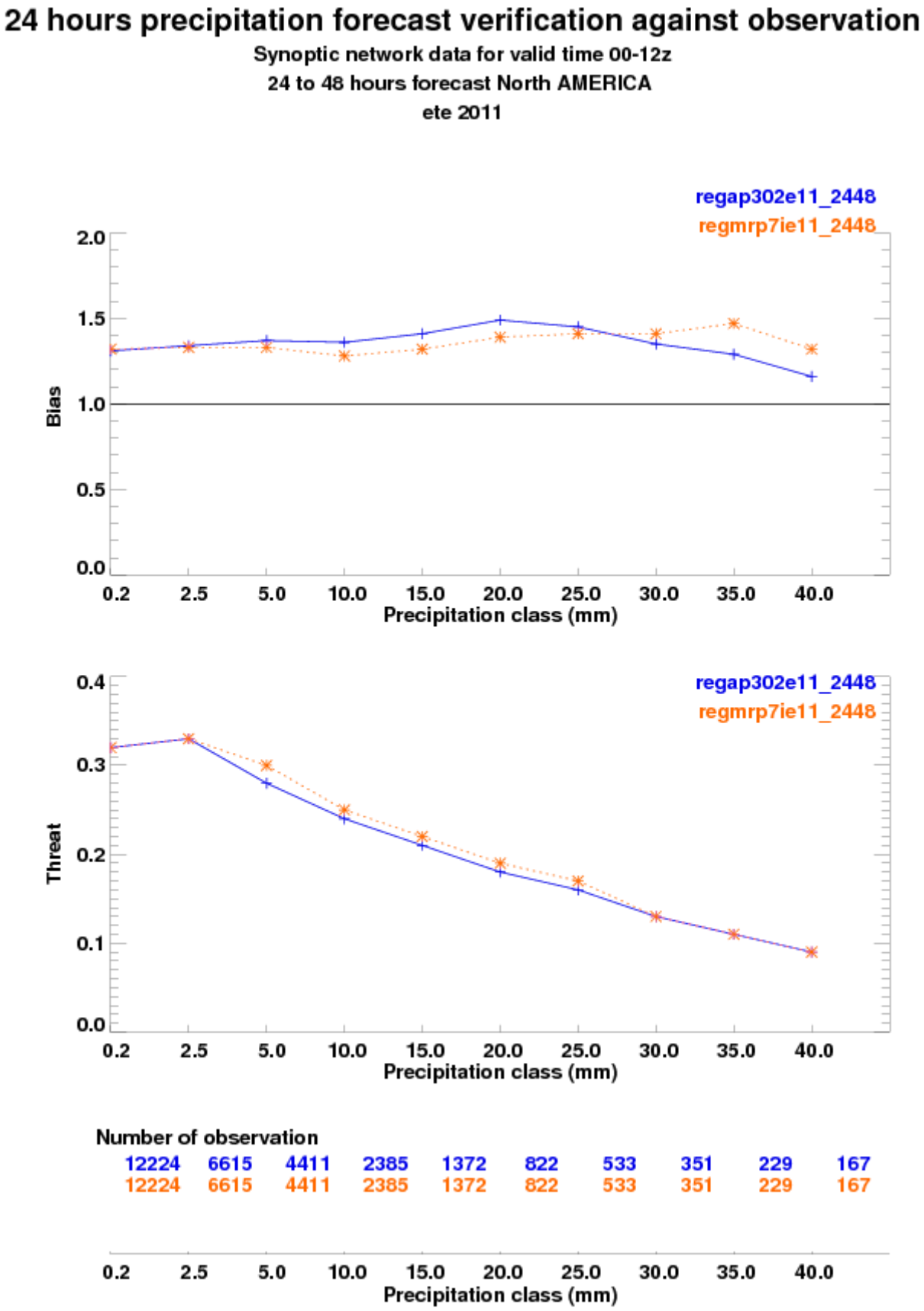

***Figure 47**: Same as **Figure 45** but for 24-48 h.*

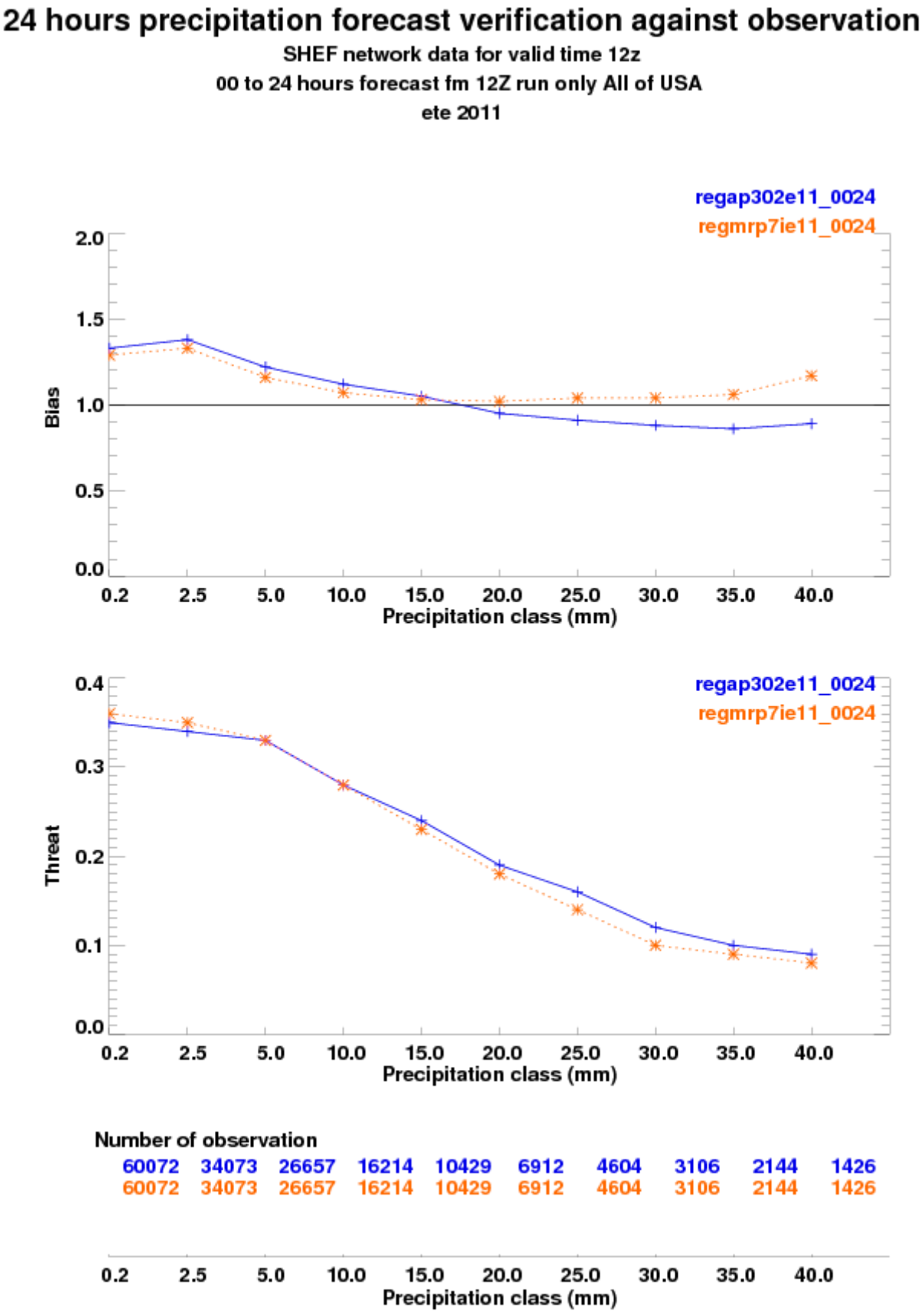

Figure 48: *Summer precipitation scores against the SHEF network of the United States for 0-24 h.*

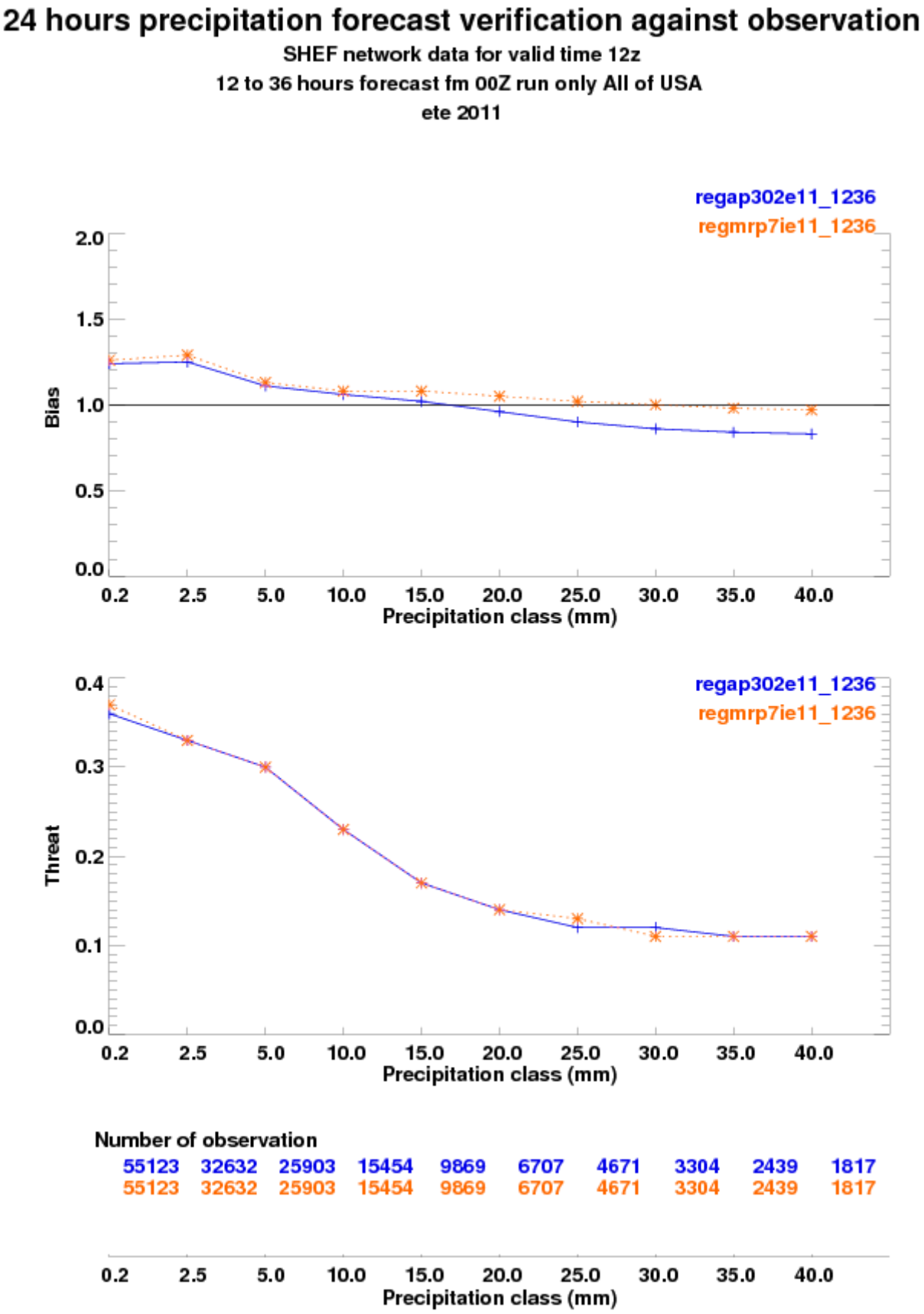

***Figure 49**: Same as **Figure 48** but for 12-36 h.*

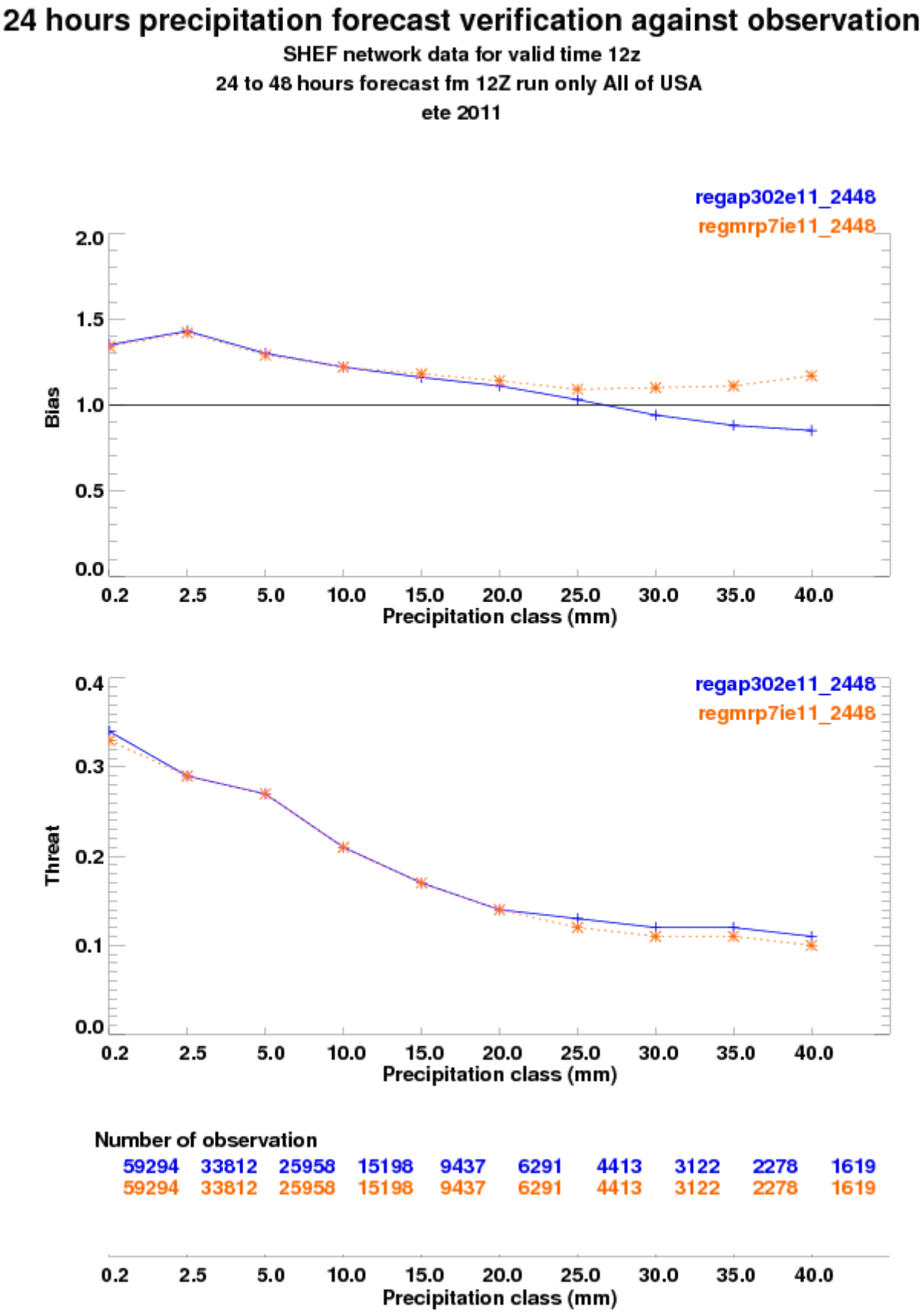

Figure 50: *Same as* ***Figure 48*** *but for 24-48 h.*

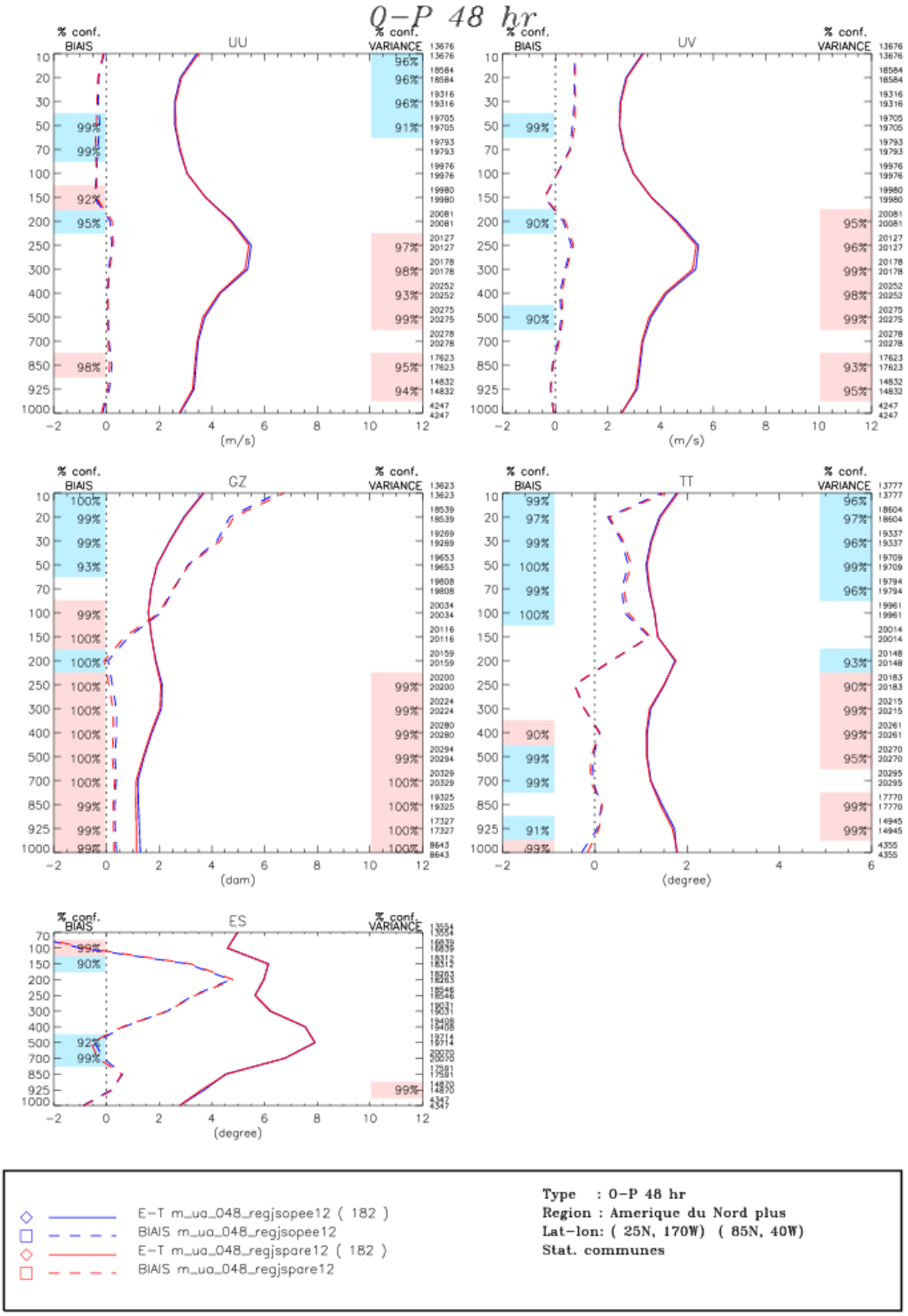

Figure 51: *Mean forecast verification scores against radiosondes over North America at a lead time of 48 hours for the period 20 June 2012 – 18 September 2012 for the (blue) operationnal and (red) parallel configurations of the RDPS. Plot essentially shows the fit of the analyses to radiosonde observations. Dashed (continuous) curves correspond to bias (standard deviation). Shaded boxes on the left (right) side show the confidence interval, if greater than 90%, for the bias (standard deviation).*

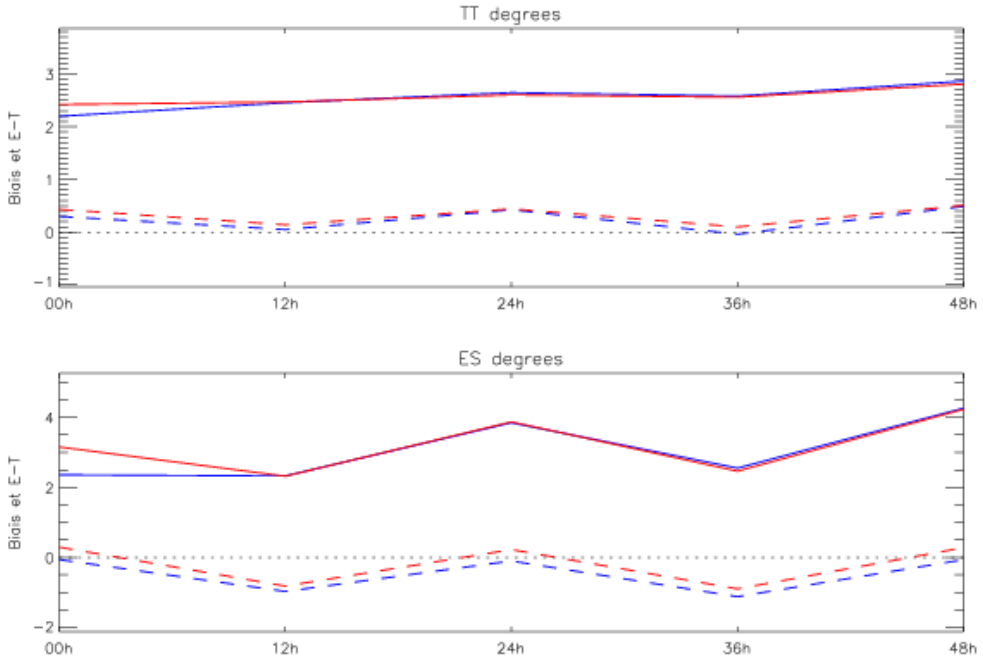

***Figure 52**: Mean forecast verification against surface stations over North America as a function of forecast lead time for the period 20 June 2012 – 19 September 2012 for cases launched at 00Z only. The blue (red) curves corresponds to the operational (parallel) RDPS respectively. Dashed (continuous) curves correspond to bias (standard deviation).*

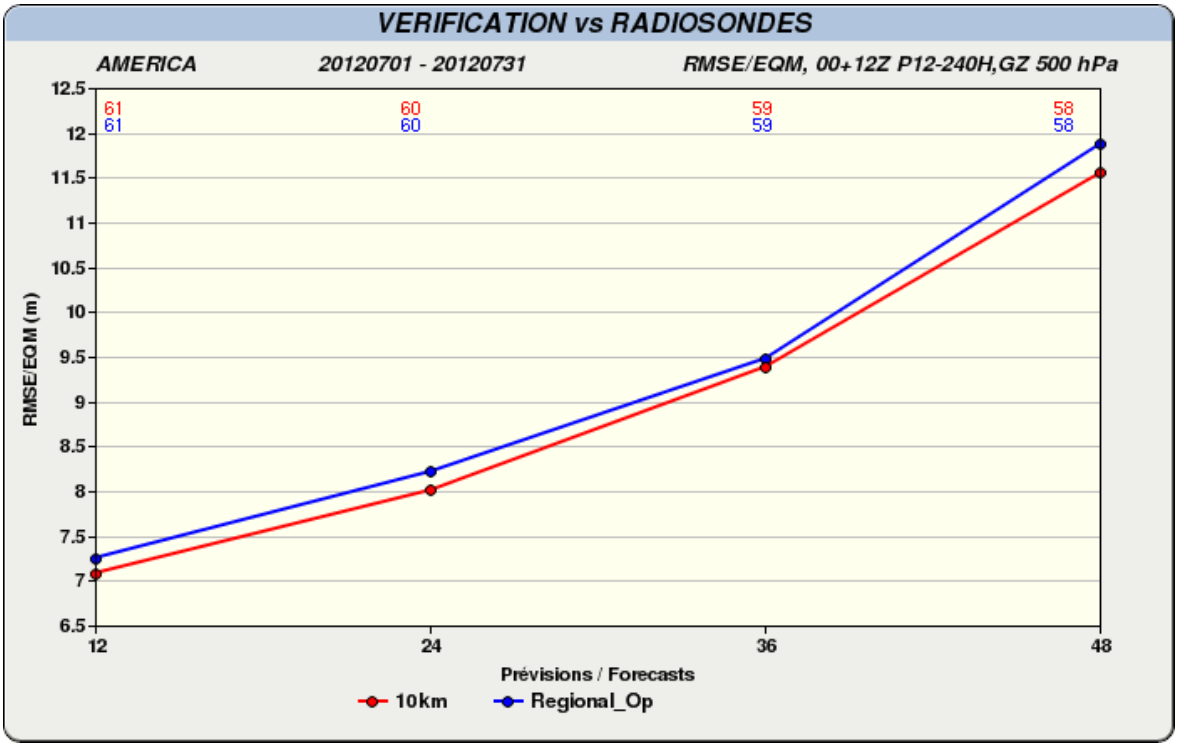

***Figure 53**: Growth in 500 hPa geopotential height root mean square error as a function of forecast time for the operational (blue) and parallel (red) RDPS for the month of July 2012.*

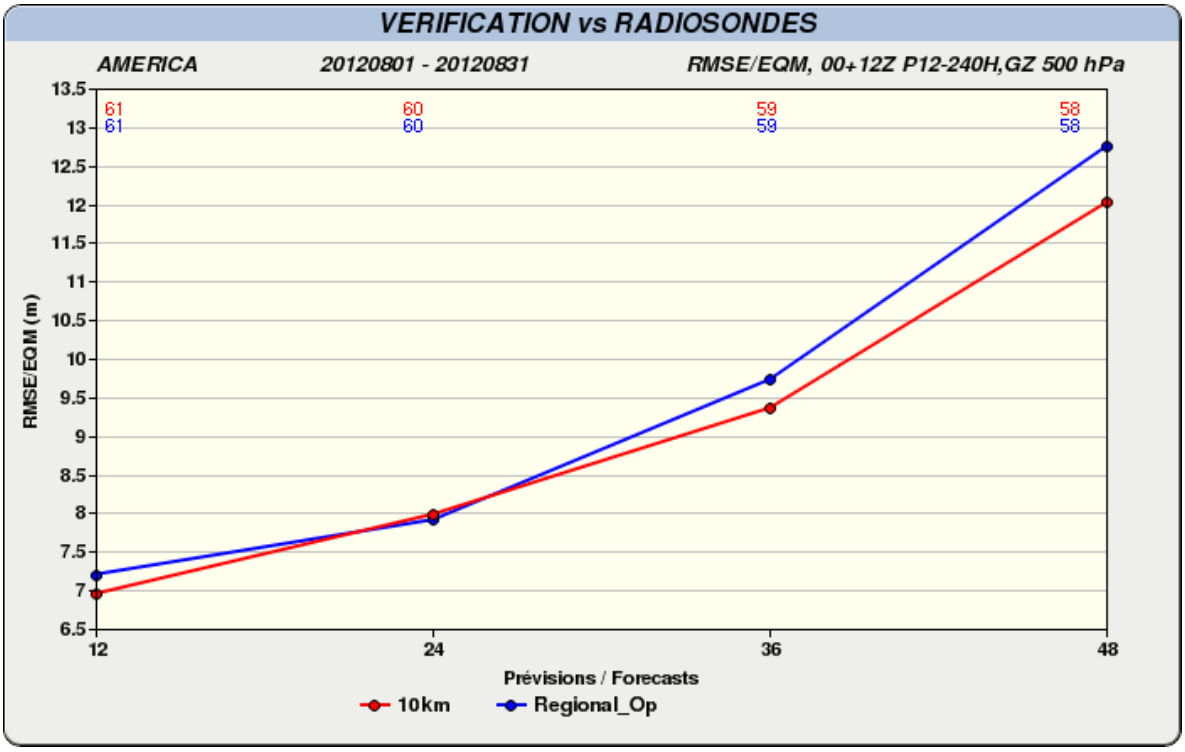

Figure 54: *Growth in 500 hPa geopotential height root mean square error as a function of forecast time for the operational (blue) and parallel (red) RDPS for the month of August 2012.*

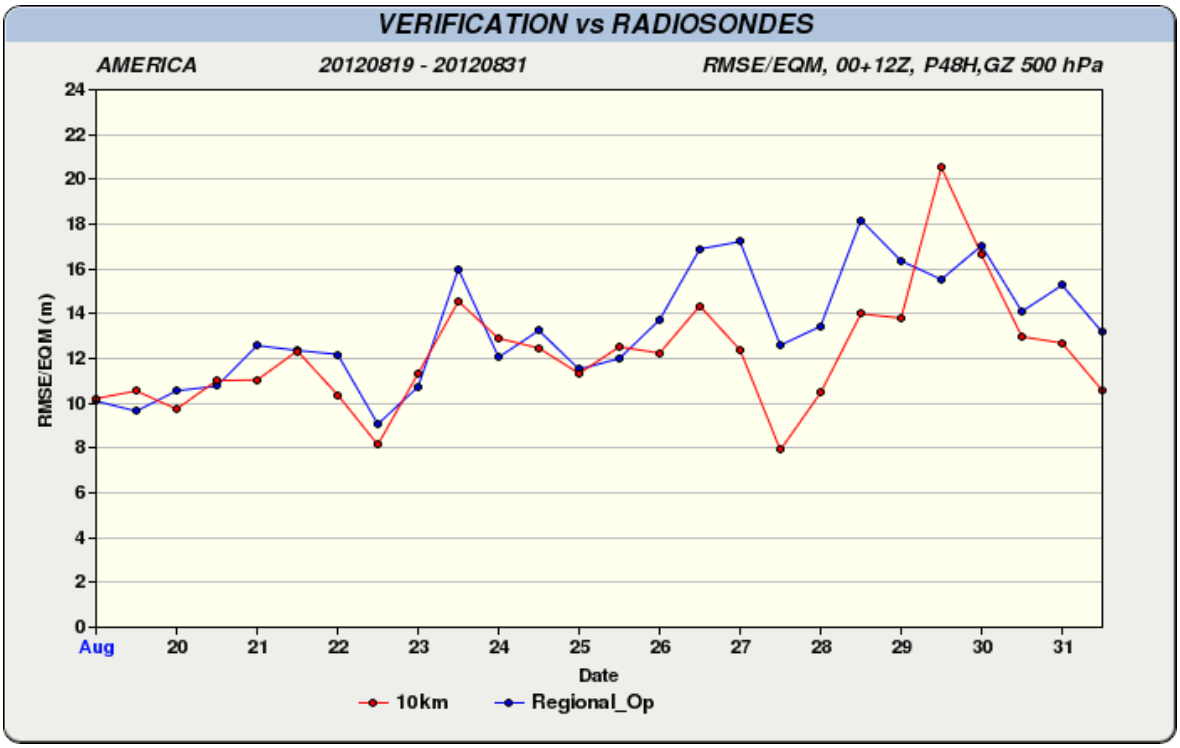

Figure 55*: Daily root mean square errors of the 48-hour 500 hPa geopotential height errors for the operational (blue) and parallel run (red) RDPS during the month of August 2012.*

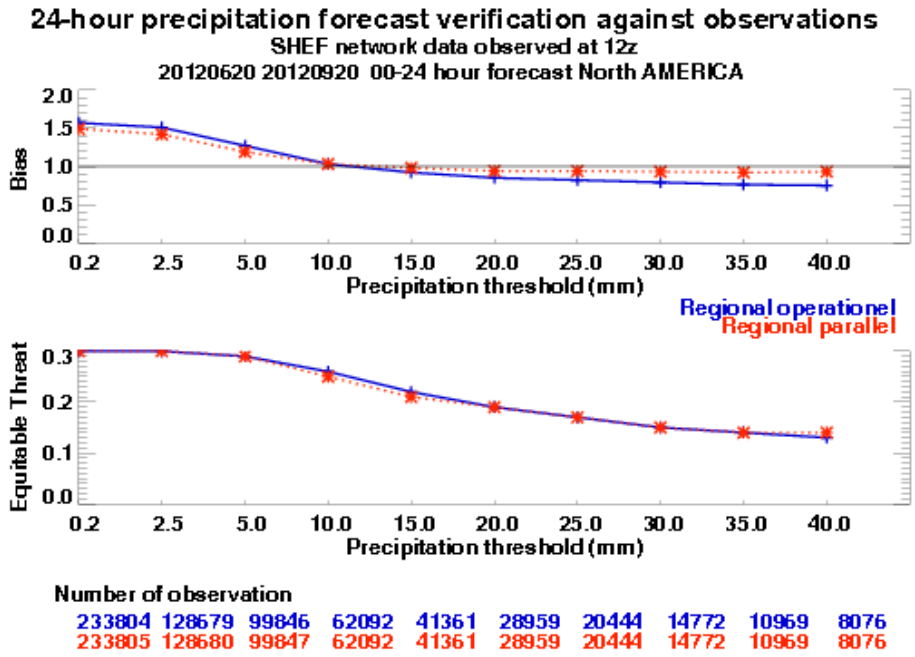

***Figure 56**: Equitable Threat and Bias for the operational (blue) and parallel (red) 00-24 hour RDPS QPF, scored against U.S. SHEF observation network, by threshold.*

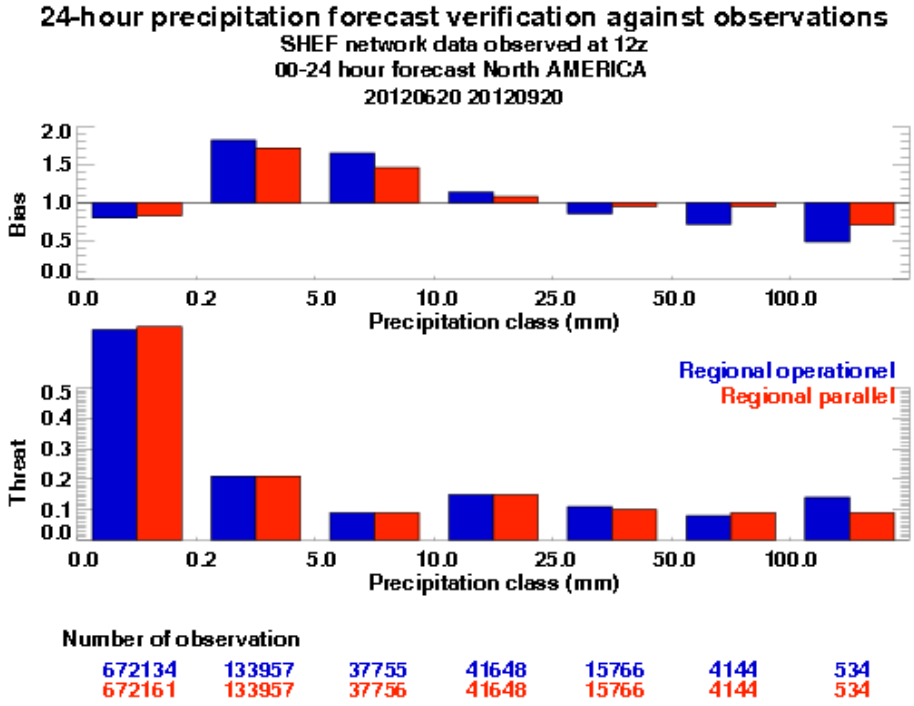

***Figure 57**: Equitable Threat and Bias for the operational (blue) and parallel (red) 00-24 hour RDPS QPF, scored against the North American synoptic observation network, by precipitation class.*

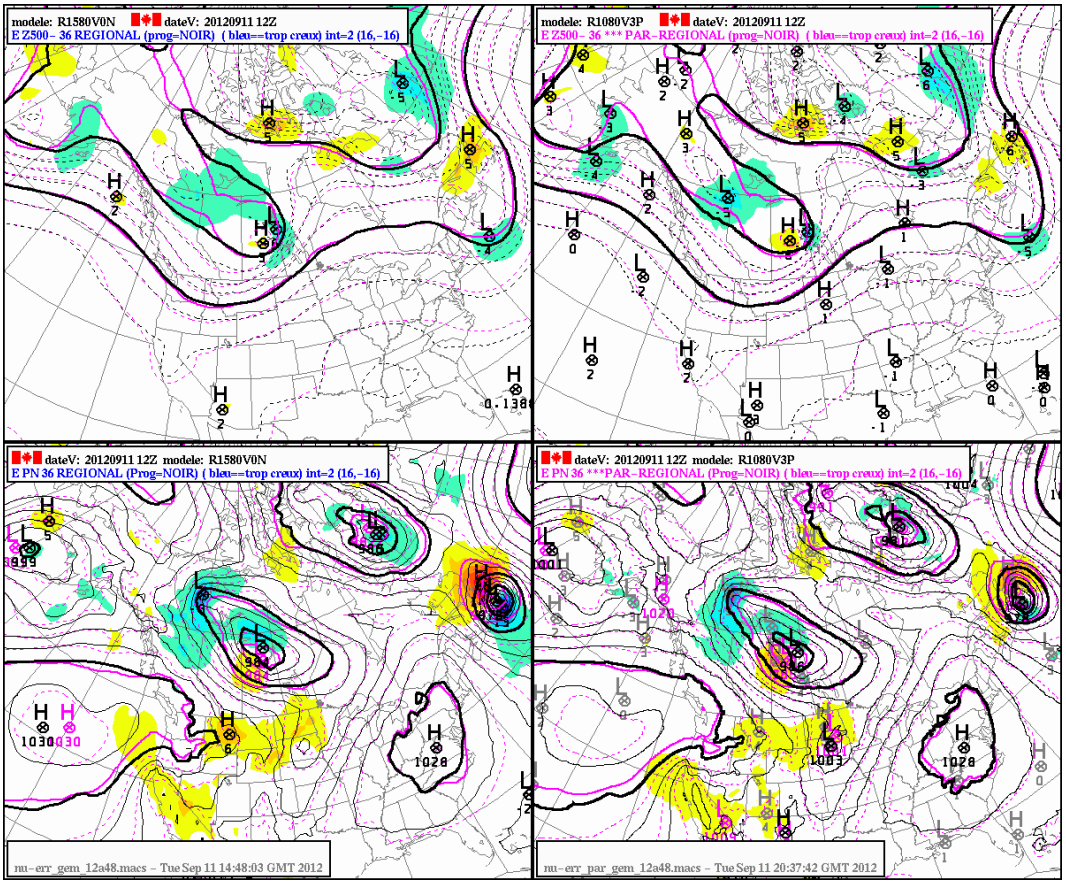

Figure 58: *Difference between the forecast from one system and its respective analysis, for 11 September 2012 at 1200 UTC (hurricane Leslie). The operational system is at left, parallel (RDPS-300) at right, GZ500 at top, and PNM at bottom. Positive errors are in yellowish shades, negative errors in bluish shades.*

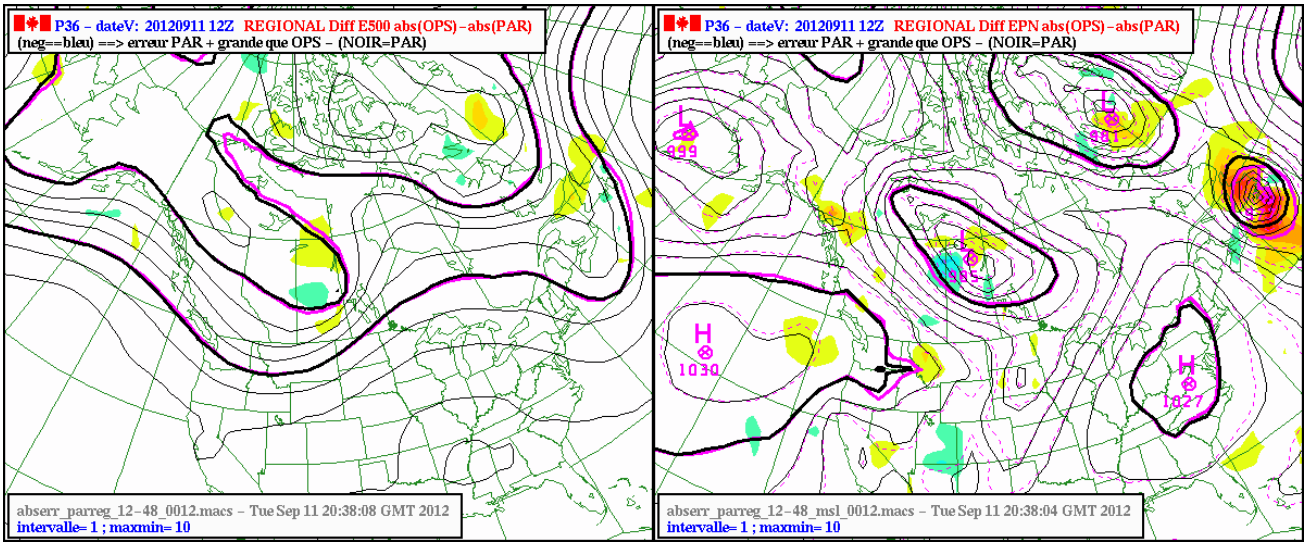

Figure 59: *Difference between the absolute values of the errors (as seen in Figure 59) of the two system, for 11 September 2012 at 1200 UTC (hurricane Leslie). Yellowish shades indicate greater errors from the operational system, bluish shades larger errors from the parallel (RDPS-300) system.*

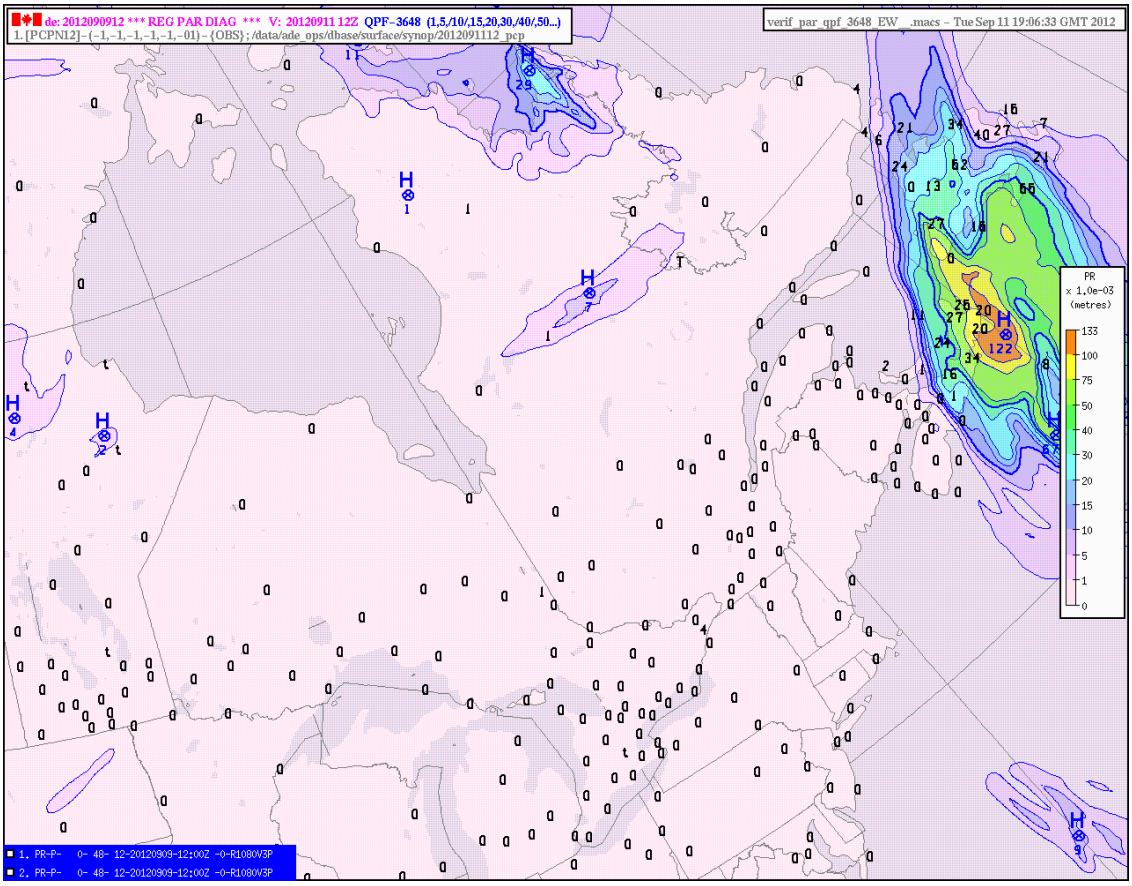

***Figure 60**: Quantitative precipitation forecast from the RDPS-300, for the 36 to 48 hour lead time over Eastern Canada, at 1200 UTC on September 11 2012, showing approaching hurricane Leslie. Similar images from the operational system were used for comparison.*

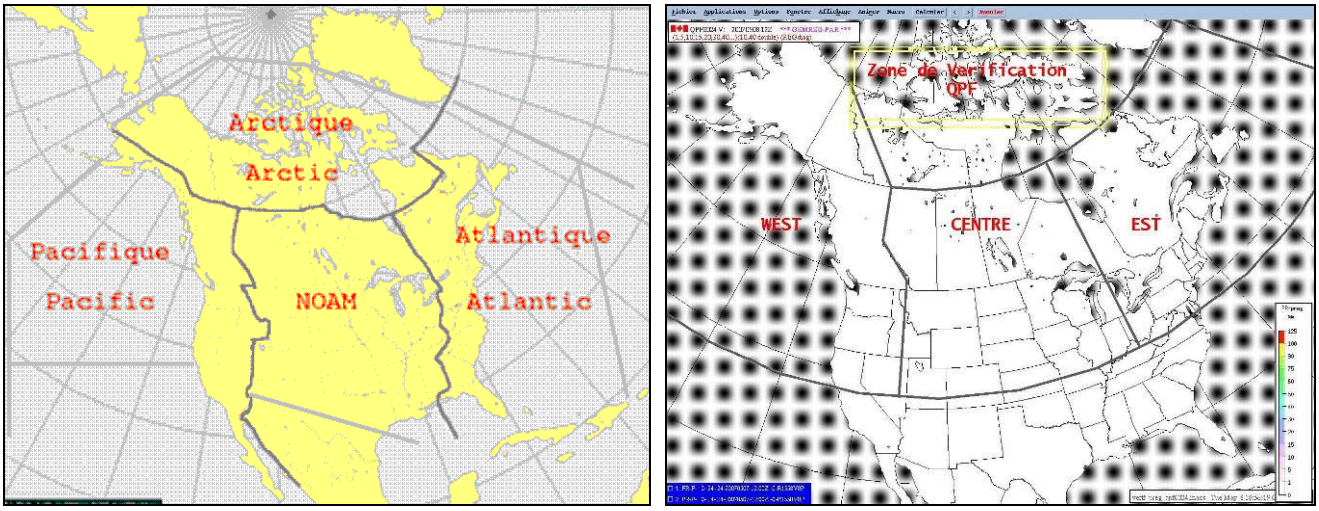

***Figure 61**: Evaluation regions for the CMC subjective evaluation, for mass files (left) and QPF (right)*

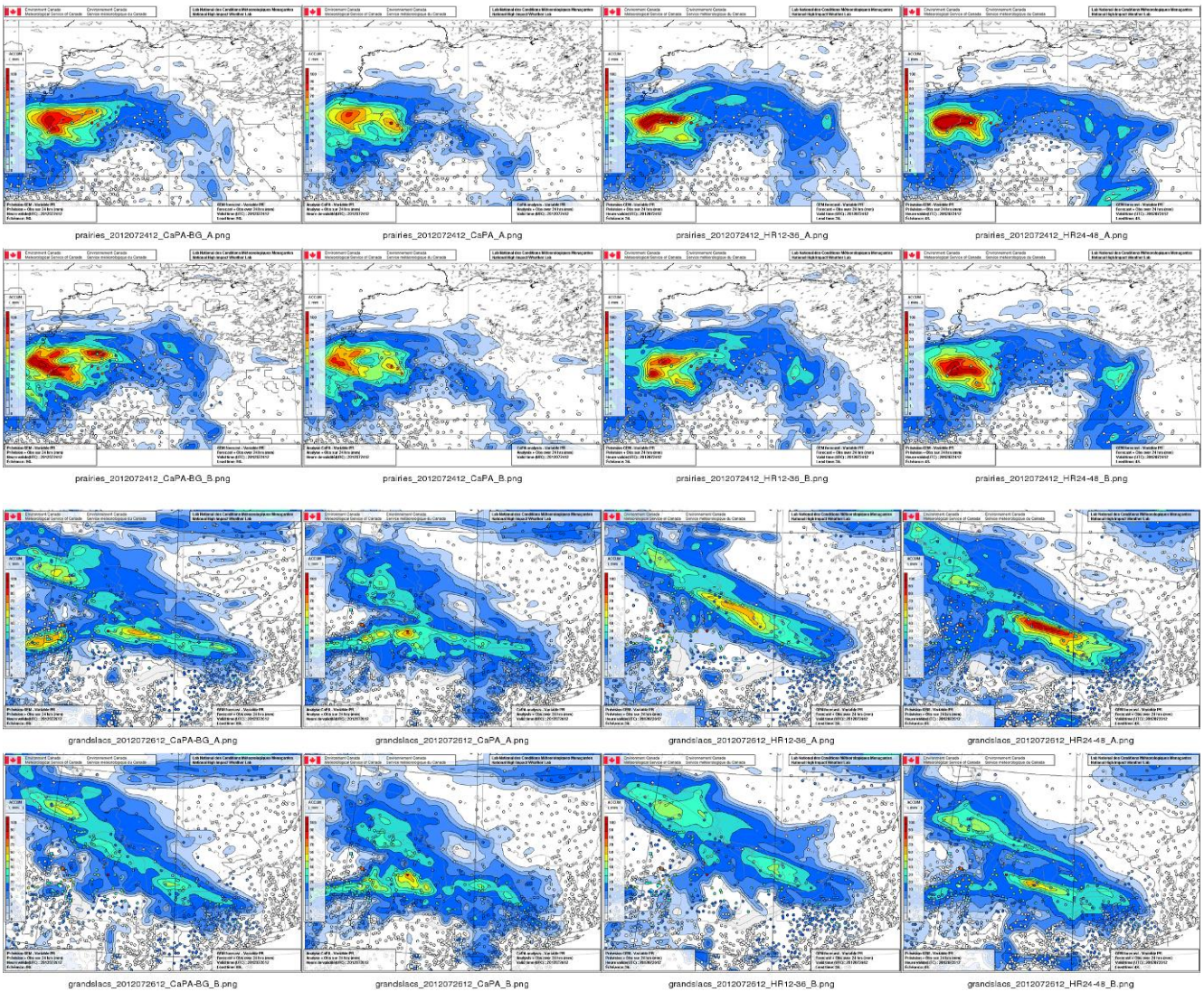

***Figure 62**: Example of the images used for the blind evaluation of the QPF, for two domains, Prairies (top two rows) and Great Lakes (bottom two rows). From the leftmost to the rightmost column one finds the guess field for the Regional Deterministic Precipitation Analysis system (CaPA), the analysis itself, then the forecast of the 12 to 36 hour lead-time period and the 24 to 48 hour lead-time period. For each domain top row is model "A" and bottom row is model "B", which can be either the operational (RDPS-200) or parallel system (RDPS-300). These were visually compared by evaluators who did not have knowledge of the actual corresponding system.*